CO-OFDM Elastic Optical Networks - Issues on Transmission, Routing, and Bandwidth Allocation

by

Bo Wang

A thesis
presented to the University of Waterloo
in fulfillment of the
thesis requirement for the degree of
Doctor of Philosophy
in
Electrical and Computer Engineering

Waterloo, Ontario, Canada, 2015

I hereby declare that I am the sole author of this thesis. This is a true copy of the thesis, including any required final revisions, as accepted by my examiners.

I understand that my thesis may be made electronically available to the public.

Abstract

The use of orthogonal frequency division multiplexing (OFDM) technology helps an optical transmission system to break the limitation of wavelength grids by wavelength division multiplexing (WDM), in which a flexible and elastic transmission paradigm is created, so as to achieve better energy and spectrum efficiency and flexibility of the fiber resource. By jointly considering the nonlinear effect of Mach-Zehnder modulator (MZM) and amplified spontaneous emission (ASE) noise, we first provide an analytical model on the bit error rate (BER) performance for a single elastic optical transmission line. A novel adaptive transmission strategy in OFDM-based elastic optical transmission systems is proposed. Based on the adaptive transmission strategy, an optimization problem is formulated and solved via mathematical programming. By using proposed adaptive transmission strategy, the routing and bandwidth allocation (RBA) problem is formulated in elastic optical networks and numerically solved to route a set of lightpaths into a network according to the static or dynamic traffic demands with the best energy efficiency, where the laser transmit power, modulation level, number of subcarriers, and routing path of each node pair, are jointly determined. Case studies via extensive numerical experiments are conducted to verify the proposed strategy and gain better understanding on the solutions of formulated optimization problem. By further extending proposed adaptive transmission strategy, we propose a novel adaptive radio-over-fiber (RoF) transmission system for next-generation cloud radio access network (C-RAN). By considering nonlinear distortion from both MZM and high power amplifier (HPA), a 2×2 MIMO-OFDM baseband model for simulating the required ESNR of end-to-end RoF transmission system is developed. The RoF system for current C-RAN and proposed RoF system for future C-RAN are presented. We also propose a model to analyze the power consumption for the optical part of RoF transmission system. By performing case studies, proposed RoF system is demonstrated to be more energy efficient than current RoF system.

Acknowledgements

I would like to thank my beloved family for their spiritual and financial support throughout my student career.

I would like to thank my supervisor, Prof. Pin-Han Ho, for his guidance and great help during the past 4 years, and also his suggestions for my future career.

I also would like to thank other research collaborators for their help to my research and study.

Contents

List of Tables

List of Figures

Abbreviations and Symbols

Abbreviations

CD	Chromatic dispersion
PMD	Polarization mode dispersion
OFDM	Orthogonal frequency division multiplexing
RF	Radio frequency
IFFT	Inverse fast Fourier transformation
DAG	Digital-to-analog
MZM	Mach-Zehnder modulator
PAPR	Peak-to-average power ratio
BER	Bit-error-rate
WDM	Wavelength division multiplexed
QoT	Quality of transmission
BVT	Bandwidth-variable OFDM transponder
SNS	Simplified null-switching
PTS-SA	Partial transmit sequence-simulated annealing
RBA	Routing and bandwidth allocation

SA	Simulated annealing
KSP	K-shortest paths
FWM	Inter-channel four wave mixing
XPM	Cross phase modulation
SPM	Self phase modulation
CO-OFDM	Coherent optical OFDM
HPA	High power amplifier
SLM	Selective mapping
EDFA	Erbium doped fiber amplifiers
ASE	Amplified spontaneous emission
AWGN	Additive white Gaussian noise
ESNR	Electrical signal-to-noise ratio
QAM	Quadrature amplitude modulation
ISI	Inter symbol interference
OSNR	Optical signal-to-noise ratio
QPSK	Quadrature phase-shift keying
CSI	Channel side information
W	Watt
CW	Continuous wave
OEO	Optical-electrical-optical
DSP	Digital signal processing
DAC	Digital-to-analog convertor
ADC	Analog-to-digital convertor
FEC	Forward-error-correction
BV-WXCs	Bandwidth variable wavelength cross-connects

NLP	Nonlinear programming
NP	Non-deterministic Polynomial-time
Iter	Iteration
NSFNet	National science foundation network
OXC	Optical cross-connect
IF	Iterative flipping
ES	Exhaustive search
QoP	Quality of protection
BPSK	Binary phase-shift keying
ROF	Radio-over-fiber
PON	Passive optical network
OLT	Optical line terminal
LTE	Long-term evolution
C-RAN	Cloud radio access network
CU	Central unit
CoMP	Co-operative multi-point
MIMO	Multiple-input multiple-output
OFDMA	Orthogonal frequency-division multiple access
CPRI	Common public radio interface
LR-PON	Long-reach passive optical network
SVD	Singular value decomposition
STTC	Space-time trellis codes
STBC	Space-time block codes
NRZ	Non-return-to-zero
PDM	Polarization division multiplexing

DAS Distributed antenna systems

RRH Remote radio head

RAU Remote antenna unit

FDM Frequency division multiplexing

SCM Sub-carrier multiplexing

SSMF Standard single mode fiber

PHY Physical layer

MAC Media access control

APD Avalanche photodiode

PIN Intrinsic region between a p-type semiconductor and an n-type semiconductor

BS Base station

RF Radio frequency

BPF Band pass filter

OSSB Optical single sideband

AWG Array waveguide grating

LE Local exchange

ODSB Optical double sideband

IFFT Inverse fast Fourier transformation

TS Training symbol

CP Cyclic prefix

LO Local oscillator

PMF Polarization maintaining fiber

PBS Polarization beam splitter

IQ In-phase and quadrature

DFB Distributed feedback laser

Symbols

P Variance of independent and identically distributed OFDM data symbols

L Number of subcarriers

N_0 Variance of the AWGN noise

H Number of null-subcarriers for PAPR reduction

B in GHz, consumed spectrum bandwidth

m Modulation level parameter, $2^{2m} = M$ for M-ary QAM

D in Gbps, required transmission rate of single transmission line

P_{out} in dBm, fiber input power or output power of laser source

P_k in Watt, input power consumption of EDFA

P_{CW} in Watt, laser continuous wave (CW) output power

P_{SC}^{m} in Watt, power consumption of variable part in OFDM transponder

P_{TOEO} in Watt, power consumption of OEO conversion in optical transceiver (per Gbps)

N_{span} Total number of spans per transmission line

P_{OEO} : power consumption of OEO conversion at intermediate nodes due to electronic switching

P_{OT} : power consumption at optical transceiver

P_{FT} : power consumption of fixed part in OFDM-based optical transponder

P_{AMP} : power consumption of an in-line EDFA per 80KM fiber span

P_{SC} : power consumption of variable part in transponder

P_{CW}^{up} : upper bound of laser continuous wave (CW) output power

BER_{th} : BER threshold without using forward-error-correction (FEC) for all lightpaths

BW : spectrum bandwidth on each fiber

$[D_{s,d}$]: traffic matrix with traffic demands $D_{s,d}$ between a source to destination (s, d) pair

P_W : power consumption of wavelength converter, and it equals to 1.65W per wavelength

F : channel width of each subcarrier

NF_{max} : maximum number of fibers available in each physical link

$NP_{s,d}$: number of possible paths for groomed traffic flow between (s, d)

$H_{s,d,r}$: number of hops in r_{th} routing path of groomed traffic flow between (s, d)

GB : guard-band for each optical channel (default value as 20 GHz) [61]

R_{TP} : transmission bit rate of each transponder

$N_{WC}^{s,d,k}$: number of wavelength conversions for k_{th} segment of groomed traffic flow between (s, d)

$NF^{a,b}$: number of fibers lighted up for physical link (a, b)

m : Modulation level parameter, $2^{2m} = M$ for M-ary QAM

R : Rate of each subcarrier based on different modulation level m

$P_{CW}^{s,d,k}$: required laser continuous wave (CW) output power on k_{th} lightpath of groomed traffic flow between (s, d)

$BER_{s,d,k}^{m}$: BER adopting modulation level m on k_{th} lightpath of groomed traffic flow between (s, d)

$N_{span}^{a,b}$: the total number of spans on physical lightpath (a, b)

$K_{s,d}$: total number of traffic segments of groomed traffic flow between (s, d)

$D'_{s,d}$: total groomed traffic flow between a source to destination (s, d) pair

$D'_{s,d,k}$: traffic demand on k_{th} segment of groomed traffic flow between (s, d)

$T_{s,d,b}$: partition of traffic flow $D_{s,d}$ to be delivered through lightpaths (s, b) and (b, d) with electronic switching at node b

$\sigma_{s,d,k}^{a,b,n}$: equal to 1 if the k_{th} lightpath of groomed traffic flow between (s, d) is routed through fiber number n in physical link (a, b), and 0 otherwise

$\delta_{s,d}^{k,r}$: equal to 1 if the r_{th} routing path is chosen for k_{th} lightpath of groomed traffic flow between (s, d), and 0 otherwise

$t_{1,sdk}$: lower subcarrier index allocated to k_{th} lightpath of groomed traffic flow between (s, d)

$t_{2,sdk}$: upper subcarrier index allocated to k_{th} lightpath of groomed traffic flow between (s, d)

P_{in} : the average power of the input signal

$E_{in}(t)$: the input of MZM in optical field

$E_{out}(t)$: the output of MZM in optical field

$V(t)$: voltage of electrical OFDM signal

V_{π} : the required voltage difference applied to a single electrode

x_k : discrete vector of the applied voltage at the MZM

y_k : discrete vector of the output voltage at the MZM

q : the order of nonlinearity

α_q : the odd coefficient of the MZM nonlinear transfer function

B_{ref} : reference bandwidth used for OSNR measurement

m_{sys} : optical transmission system margin

L_{MZM} : optical excess loss of MZM

L_{Cir} : circulator loss

L_{Pol} : polarization control loss

L_{AWG} : the AWG loss

L_{Split} : passive splitter loss

L_{OBPF} : optical bandpass filter loss

L_{TOF} : tunable optical filter

α_{span} : loss of SSMF span

F_{EDFA} : EDFA noise figure

G_{EDFA} : EDFA gain

G_{Rx} : receiver sensitivity for the APD

P_{LO} : output power of LO at coherent receiver

G_{Co-Rx} : sensitivity of coherent receiver without amplification

L_{PDM} : PDM loss

γ_{DC} : power conversion efficiency

P_{map} : power consumption for signal mapping

$P_{P/S}$: power consumption for parallel-to-serial (or serial-to-parallel) conversion

P_{DAC} : power consumption for a single digital-to-analog converter (DAC)

P_{MZM} : power consumption for a single-drive MZM

$P_{IFFT-CP-TS}$: power consumption for the IFFT, CP and TS modules

n_{DAC} : the number of required DACs

n_{MZM} : the number of required MZMs

P_{LO} : power consumption for the local oscillator at coherent receiver

P_{TIA} : power consumption of trans-impedance amplifier with automatic gain control for current-to-voltage conversion

P_{PD} : power consumption for a single photodiode

P_{ADC} : power consumption for a single analog-to-digital converter (ADC)

P_{Rx-DSP} : power consumption for the DSP module of signal post-processing at receiver

n_{ADC} : number of required ADCs

n_{PD} : number of required photodiodes

D_{down} : downstream data rate

E_{Laser} : the laser energy consumption

D_{up} : upstream data rate

$E_{LaserDr}$: energy consumption of laser equipped with driver

γ_{EDFA} : conversion efficiency of EDFA power

P_{EDFAoh} : power consumption of EDFA overhead

h : the Plancks constant

ν : the optical frequency constant

M : constellation size of M-ary quadrature amplitude modulation (QAM)

Chapter 1

Introduction

Thanks to the partially overlapped subcarriers and high-tolerance to chromatic dispersion (CD) and polarization mode dispersion (PMD), an orthogonal frequency division multiplexing (OFDM) based coherent optical transmission system demonstrates superb spectrum efficiency and bandwidth slicing flexibility, and is expected to play an important role in the emerging backbone and metro applications such as data center networks and cloud radio access network (C-RAN).

1.1 Background

In current optical backbone networks, data center and cloud computing require very high data rate corresponding to very high bandwidth that could even reach the bandwidth limit of a fiber segment. The use of OFDM technology enables an optical transmission system to break the limitation of wavelength grids due to the legacy of wavelength division multiplexing (WDM). Compared with a fixed-grid WDM system, an elastic coherent optical OFDM (CO-OFDM) system improves its flexibility and granularity by using a

variable number of low-rate OFDM subcarriers. To generate optical OFDM signals, a fixed number of bits are firstly modulated into a symbol in the radio frequency (RF) domain and mapped onto individual subcarrier. Each subcarrier of modulated signal is then converted to the electrical baseband OFDM signal through inverse fast Fourier transformation (IFFT) and digital-to-analog (DAG) conversion. Then the baseband OFDM signal in the RF domain is up-converted to the optical domain by using a wavelength-tunable laser and Mach-Zehnder modulator (MZM) [1]-[2]. Ref. [3] presented an example of elastic bandwidth provisioning in the spectrum domain of fiber optics by controlling the number of subcarriers, in which the transmission rate is linearly proportional to the number of subcarriers under a constant modulation level. Alternatively, the choice of the modulation level can be jointly taken into consideration according to the required quality of transmission (QoT). With constant channel spacing of subcarriers, the capacity of an individual subcarrier is defined by the selected modulation level. Thus, a transmission requesting for a specific rate can be provisioned by elastically and adaptively allocating spectrum bandwidth using a proper number of OFDM subcarriers and a modulation level. Other parameters related to the transceiver and channel characteristics, such as linear and non-linear physical layer impairments, can also affect the modulation level choice [4]. Meanwhile, compared with the limits of transmission reach by an OFDM-based dense WDM system with little or no frequency guard band studied in [5], elastic CO-OFDM systems with sufficient guard bands can support higher modulation level and further transmission reach, due to its resistance to cross phase modulation (XPM) and interchannel four wave mixing (FWM).

Similar to optical backbone traffic, today's wireless traffic is dominated by IP based multimedia services and applications, which have caused significant data growth in wireless system. Especially, the increase of peak to average load ratio on base stations (BSs) leads to poor equipment utilization and low energy efficiency. Not only the higher capacity

and wider bandwidth, but also smaller cell and better spectral efficiency are required for next generation wireless standards such as advanced long term evolution (LTE-Advance) and those under the banner of 5G [6]. As the goal of next generation radio cells, LTE-Advance with data rates up to 1 Gbps will unavoidably require higher density of BS deployment and increased spectral efficiency. In consequence, higher bandwidth and cost-effective back-haul links are needed to support connections between each BS to a common central unit (CU). Featured by link transparency and lower bandwidth requirement per BS comparing to current digital transmission approaches [7], RoF schemes collaborating with MIMO-OFDM technique are expected to be a solution for centralized wireless equipments of C-RAN in next generation wireless communications [8].

In spite of its numerous merits, the design of OFDM based optical transmission systems is subject to some challenges. One of the major problems is a possibly high instantaneous peak-to-average power ratio (PAPR) of the transmitted electrical OFDM signals due to the superposition of many individual sinusoidal subcarriers, which may render high amplitude when these sinusoids are in-phase at the IFFT input, and are thus added constructively to generate large amplitude corresponding to a high PAPR at the IFFT output. Since PAPR is proportional to the number of used subcarriers [9], the peak amplitude of the electrical OFDM signal could be L times that of a single-carrier system, where L denotes the number of subcarriers. When the peak amplitudes of the electrical OFDM signals with high PAPR reach or exceed the linear transformation region of Mach-Zehnder modulator (MZM) or high power amplifier (HPA), the optical OFDM signals will suffer from nonlinear distortion that causes bit-error-rate (BER) degradation at the receiver.

1.2 Contribution

The contribution of this thesis is listed as follows

- develop an analytical model of end-to-end BER performance for OFDM-based adaptive optical transmission systems by considering nonlinear effect of Mach-Zehnder modulator and optical amplified spontaneous emission (ASE) noise, where the effect of high PAPR in both electrical and optical domains is jointly considered.

- propose a PAPR reduction scheme to the scenario of optical transmission, namely simplified null shifting (SNS), which is featured as subject to less dependence on CSI and better performance.

- investigate the performance improvement when a PAPR reduction mechanism is equipped.

- formulate an optimization framework for adaptive transmission by jointly determining laser transmit power, bandwidth, and modulation level of a single transmission line under a given transmission data rate.

- embed proposed adaptive transmission model in routing and bandwidth allocation (RBA) problem for energy saving corresponding to a set of connection requests upon network node pairs.

- solve the formulated RBA problem via a heuristic method based on simulated annealing (SA) and K shortest paths.

- propose an iterative flipping (IF) method to solve the RBA problem, which maintains better power saving performance than SA scheme while keeping very low computational complexity.

- introduce a 2×2 MIMO-OFDM baseband model for simulating the required ESNR of end-to-end RoF transmission system by considering nonlinear distortion from both Mach-Zehnder modulator (MZM) and high power amplifier (HPA).

- propose a novel adaptive radio-over-fiber (RoF) transmission system for next-generation cloud radio access network (C-RAN), aiming to minimize the system operation cost in terms of power consumption for a required data rate.

- propose a model to analyze the power consumption for the optical part of RoF transmission system.

1.3 Organization

This thesis is organized as follows: in Chapter 2, by jointly considering the nonlinear effects of Mach-Zehnder modulator (MZM) and optical amplified spontaneous emission (ASE) noise, as well as the performance impairment due to high peak-to-average-power ratio (PAPR) in the electronic domain, we first provide an analytical model on the bit error rate (BER) performance for a single elastic optical transmission line. Based on the model, we consider using proposed strategy in a single transmission line for determining laser transmit power, spectrum, and modulation level under a given transmission data rate. To achieve an efficient PAPR reduction, we introduce a new method called simplified null switching (SNS), which is considered very suitable in the elastic optical transmission systems due to lower computation complexity and little dependence on the channel side information (CSI). Based on the analytical model and PAPR reduction method, an optimization framework for achieving a least-cost transmission is formulated by manipulating a number of parameters at the transmitter side, including the number of subcarriers allocated for the transmission, the optical signal power at the bandwidth-

variable OFDM transponder (BVT), as well as the modulation level that determines the rate of the transmission. Case studies were performed, where the mathematical formulation was numerically solved to achieve least-cost, in order to gain better understanding of the proposed approach. We demonstrated that by adaptively choosing coupled laser power, spectrum width, and modulation scheme, the proposed mathematical model can accurately capture the BER performance of a transmission in the considered elastic CO-OFDM optical systems, where a superb performance compared with other counterparts can be achieved.

In Chapter 3, to taking a step further on the routing problem in elastic OFDM optical networks, we investigate routing and bandwidth allocation (RBA) problem corresponding to a set of connection requests upon network node pairs, where the total energy consumption is minimized. By assuming one or multiple concatenated transmission segments form a single connection, the three parameters (laser output power, number of subcarriers, and modulation level) of each transmission segment along the connection are jointly determined in order to satisfy the rate requirement of the connection request. Since the optimization problem with a large search space is NP-Complete, we first solve the formulated problem via a heuristic method based on simulated annealing (SA) and K shortest paths. It is demonstrated that the proposed strategy can achieve better performance than that using a single modulation level with shortest path routing only. By exploring the unique feature of the problem, we propose to using an iterative flipping method to solve the problem, which flips the candidate modulation levels and routing paths for each lightpath one by one to reach a suboptimal solution. The proposed method maintains better power saving performance than SA scheme while keeping very low computational complexity.

In Chapter 4, we propose a novel adaptive radio-over-fiber (RoF) transmission system for next-generation cloud radio access network (C-RAN), aiming to minimize the system

operation cost in terms of power consumption for a required data rate. By jointly considering the nonlinear distortion from Mach-Zehnder modulator (MZM) and high power amplifier (HPA) due to high peak-to-average-power ratio (PAPR) in the electronic domain, we first provide a 2×2 MIMO-OFDM baseband model on electrical SNR (ESNR) with given bit error rate (BER) requirement for a single RoF transmission line. Then, we introduce the RoF system for current C-RAN, and proposed RoF system for future C-RAN. To relate the candidate modulation levels with system power consumption, we provide the OSNR analysis and its relation with ESNR, which are used in the following power consumption analysis for both the downlink and uplink of the RoF transmission system. Case studies via simulation and numerical experiments are conducted to verify the proposed RoF system can not only reach the lowest power and spectrum consumptions at same time, but also consumes considerably less power than current RoF system.

In Chapter 5, we conclude this thesis and discuss future work.

Chapter 2

Adaptive CO-OFDM Transmission Scheme

The use of Orthogonal Frequency Division Multiplexing (OFDM) technology enables an optical transmission system to break the limitation of wavelength grids due to legacy of Wavelength Division Multiplexing (WDM). This constructs a flexible and elastic transmission paradigm so as to achieve high spectrum efficiency and flexibility of fiber resource usage. This chapter introduces a novel adaptive transmission strategy in elastic coherent optical OFDM (CO-OFDM) transmission systems, aiming to optimize the system operation in terms of energy and spectrum consumptions for a transmission demand with a required data rate. By jointly considering the nonlinear effects of Mach-Zehnder modulator (MZM) and optical amplified spontaneous emission (ASE) noise, as well as the performance impairment due to high peak-to-average-power ratio (PAPR) in the electronic domain, we first provide an analytical model on the bit error rate (BER) performance for a single elastic optical transmission line. To achieve an efficient PAPR reduction, we introduce a new method called simplified null switching (SNS), which is considered very suitable in the elastic optical transmission systems due to lower compu-

tation complexity and little dependence on the channel side information (CSI). Based on the proposed analytical model, an optimization problem is formulated and solved via mathematical programming. Case studies via extensive numerical experiments are conducted to verify the proposed analytical model and gain better understanding on the solutions of formulated optimization problem.

2.1 Enabling Technology

The study is mainly related to two topics, which are energy-efficient design for optical transmission system and peak-to-average power ratio (PAPR) problem in optical OFDM systems. These topics are reviewed in the following subsections.

2.1.1 PAPR Reduction in Optical OFDM Systems

OFDM as an attractive multicarrier transmission technology for wire line, provides greater bandwidth efficiently, immunity to multi-path fading and impulse noise, resistance to frequency selective fading, and also exempts the need for complex equalizers and digital signal-processor hardware implementation. Nevertheless, some challenging issues remain unresolved in designing the OFDM systems. One of the major drawbacks is a possibly high instantaneous Peak-to-Average Power Ratio (PAPR) of transmitted OFDM signals. The OFDM signal, which superposes many individual sinusoidal subcarriers, would have a high amplitude when these sinusoids are in-phase at the IFFT input, and are thus added constructively to generate a large amplitude corresponding to a high PAPR at the IFFT output.

The OFDM technology helps an optical transmission system to create a flexible and elastic transmission paradigm, so as to achieve better spectrum efficiency and flexibility

of the fiber resources [1]. The authors in [5] discussed the limits of spectral efficiency and transmission reach over SSMF by an O-OFDM WDM system with little or no frequency guard band, in which further degrading effects from intra-channel or inter-channel four wave mixing (FWM), cross phase modulation (XPM), and SPM (self phase modulation) exist. The authors in [10] derived closed-form analytical expressions in densely spaced coherent optical OFDM (CO-OFDM) systems using large number of subcarriers (i.e. 4000, corresponding to large PAPR and little or no frequency guard band, in which further degrading effects are due to intra-channel or inter-channel four wave mixing (FWM), cross phase modulation (XPM), and SPM (self phase modulation). The authors in [11] studied on allowing spectrum-flexible coherent OFDM (CO-OFDM) optical network to adaptively allocate its super-channels to test OSNR requirements by interleaving subcarriers under 2 different modulation levels, which is irrelevant to our research topic (all subcarriers only modulated by 1 candidate modulation format in each result). And they only take QPSK and 16-QAM as examples without testing higher modulation levels.

Numerous theories and hypotheses on determination of the PAPR distribution have been reported in the wireless communication systems, and various schemes for PAPR reduction are reviewed by Jiang and Wu in [12]. And Goebel *et al.* proved that those techniques can be adopted in optical OFDM systems in [13]. Tang *et al.* introduces a combination of MZM pre-distortion and clipping for optical OFDM system [14]. The authors in [15] achieved a step further on the topic for migrating the approach proposed in [31] in an optical OFDM system. Their approach is by replacing the nonlinear high power amplifier (HPA) with an MZM which also causes nonlinear distortion, and the performance of the proposed scheme is compared with selective mapping (SLM). Nonetheless, the model in [15] only considers the noise part due to AWGN and nonlinear MZM from the perspective of RF domain, while ignoring the ASE noise from the optical link. This certainly imposes limits on the precision of the model and the cross layer optimization

result.

2.1.2 Energy Efficiency in Optical Communication Systems

Since the capacity and geographical coverage of the global communications network keeps booming, the issue of energy consumption in optical backbone communication systems takes an increased importance due to the growing realization that global internet service consumes a growing proportion of the planets electricity supply [16], [17]. Meanwhile, the considerably increasing power consumption of the whole communication systems and the expensive cooling systems with high energy cost at BS become one major concern in future radio access network design [18].

To reduce power consumption of optical communication systems, adaptive optical transceivers are considered as the candidate for future optical communications in both long-haul and metro applications [19]. Adaptive transceivers is capable of allocating spectral bandwidth flexibly for traffic demand. To improve the spectral efficiency and capacity of the link, adaptive transceivers employ the highest modulation level allowed by given transmission distance and BER threshold. For example, by decreasing its symbol rate or increasing modulation level, a transceiver can assign a portion of its spectrum to other transceivers that using the same fiber. For expenditure, the price of adaptive transceiver that can work in a wide range of transmission distances will be lower due to higher production volumes. As an enabling technique, adaptive modulation and coding has been explored for optical communications in [20]. By adjusting the modulation format, the code rate of the forward error correction (FEC), the symbol rate (per subcarrier), the number of polarizations per wavelength, and the number of OFDM subcarriers, an adaptive transceiver aims to achieve better energy efficiency and spectral efficiency according to the optical signal-to-noise ratio (OSNR) requirement from the link [21]. Meanwhile, by maximizing spectral efficiency, adaptive transceivers allow a network to

support more data at a given total power consumption, such that the energy efficiency is further improved.

In order to manage the growing energy consumption, [22] provides a framework for exploring the fundamental limits of energy consumption in optically amplified transport systems. In [23], by proposing quantitative models on energy performance of optical devices, the author also extend the analysis in [22] to investigate the lower bound on energy consumption in optical switches and networks.

2.2 System Model

By considering nonlinear effects of Mach-Zehnder modulator (MZM), we first developed a novel analytical model for the BER expression while considering the effect of PAPR in both electrical and optical domains.

2.2.1 CO-OFDM System

Comparing to intensity modulation that only modulate the intensity of the optical carrier, CO-OFDM transmitter also modulate the phase or the polarization. And CO-OFDM receiver detects signal using homodyne or heterodyne detection, rather than direct detection via a photodiode [24]. In recent years, coherent communication techniques attract great interest mainly due to following two reasons. By combining with silicon-based digital signal processing (DSP), optical coherent detection has the ability to compensate linear transmission impairments such as CD and PMD [25]. And, channel impairments due to laser and fiber can be removed via coherent algorithms [26]. For reconfigurable optical networks with high transmission speed, the CO-OFDM can realize robust dispersion transmission, improving computation efficiency, and simplifying channel and phase

estimation [1].

Consider an OFDM transmission with L subcarriers at the frequencies $\{f_l,\, l = 1, \cdots, L\}$. Assigned to the subcarriers at $\{f_l, 1 \leq l \leq L\}$ are, respectively, the M-ary data symbols $\{\bar{x}_l,\, l = 1, \cdots, L\}$ or 0, which are independent and identically distributed random variables with zero mean and variance P.

Let T be the modulation interval and LT be the duration of an OFDM symbol (excluding the guard interval). The OFDM-signal's complex envelope can be expressed as:

$$x(t) \;=\; \frac{1}{\sqrt{L}} \sum_{l=1}^{L} \bar{x}_l e^{j2\pi f_l t}, \quad 0 \leq t \leq LT. \tag{2.1}$$

assuming the above is an idealized rectangular time-domain window, and the cyclic-prefix extension of $x(t)$ would not alter the PAPR.

The above continuous-time definition can be approximated in the discrete time domain as

$$x_k \triangleq x\left(\frac{kT}{KL}\right) = \frac{1}{\sqrt{L}} \sum_{l=1}^{L} \bar{x}_l e^{j2\pi lk/KL}, 0 \leq k \leq KL-1 \tag{2.2}$$

where K represents the oversampling factor.

In [15], a simplified analysis for real OFDM signal in CO-OFDM systems is provided. They expressed the applied voltages $V(t)$ and $V^*(t)$ on MZM as

$$V(t) = a \cdot \sum_{c=1}^{\infty} \sum_{k=0}^{KL-1} x_k^c \cdot \prod (t - k \cdot T/K - c \cdot L \cdot T/K) \tag{2.3}$$

$$V^*(t) = b \cdot \sum_{c=1}^{\infty} \sum_{k=0}^{KL-1} x_k^c \cdot \prod (t - k \cdot T/K - c \cdot L \cdot T/K) \tag{2.4}$$

and

$$\prod(t) \quad = \quad \begin{cases} 1, & 0 \leq t \leq T \\ 0, & \text{else} \end{cases}$$

where a and b are multiplicative factor, x_k^c is the cth symbol of kth OFDM transmitter block.

The input of transmitter laser in optical field $E_{in}(t)$ is defined as [1]

$$E_{in}(t) = \sqrt{\frac{P_{in}}{2}} \cdot e^{-j(\omega_{in} \cdot t + \phi_{in})} \tag{2.5}$$

where P_{in} is the output power of the optical laser diode, ω_{in} and ϕ_{in} are the angular frequency and phase of the transmitter laser respectively.

The output of MZM in optical field $E_{out}(t)$ is expressed as

$$E_{out}(t) = T_{MZM}[V(t), V^*(t)] \cdot E_{in}(t) \tag{2.6}$$

where $T_{MZM}[\bullet]$ is the MZM transfer function introduced in the following Eq. 2.11.

After transmitted through the fiber, the optical input signal of coherent receiver $E_{CR}(t)$ is expressed as

$$E_{CR}(t) = T_{fiber}[E_{out}(t)] \tag{2.7}$$

where $T_{fiber}[\bullet]$ is the fiber propagation operator discussed in the following Eq. 2.25.

The local oscillator laser at the receiver $E_{LO}(t)$ is defined as [1]

$$E_{LO}(t) = \sqrt{\frac{P_{LO}}{2}} \cdot e^{-j(\omega_{LO} \cdot t + \phi_{LO})} \tag{2.8}$$

where P_{LO} is the output power of local oscillator, ω_{LO} and ϕ_{LO} are the angular frequency and phase of the receiver oscillator laser, respectively.

Then, in-phase and quadrature current signals as the output of coherent receiver are defined respectively [27] [28]:

$$I_+(t) = \frac{1}{2}R(E_{CR}(t) + E_{LO}(t)) + R\sqrt{E_{CR}(t) \cdot E_{LO}(t)} \cdot \cos(\omega_{FD} + \phi_{PD}) \tag{2.9}$$

$$I_-(t) = \frac{1}{2}R(E_{CR}(t) + E_{LO}(t)) - R\sqrt{E_{CR}(t) \cdot E_{LO}(t)} \cdot \cos(\omega_{FD} + \phi_{PD}) \tag{2.10}$$

where R is the photodiode responsivity, $\omega_{FD} = \omega_{in} - \omega_{LO}$ is the frequency difference, and $\phi_{PD} = \phi_{in} - \phi_{LO} + \pi/2$ is the phase difference. As shown in Fig. 2.1,the OFDM symbols can be extracted after further ADC and post-processing for removing channel impairments [26].

2.2.2 BER Analytical Model with MZM Distortion

As a waveguide-based external modulator, MZM is widely considered in CO-OFDM systems with chirp-free signals for achieving high data rate transmissions. As shown in Fig. 2.1, the CO-OFDM signal is modulated based on the electrical OFDM signal by using the MZM, and the modulation process is subject to nonlinear and peak-limited transfer characteristics [29]. The output optical field is expressed as

$$\frac{E_{out}(t)}{E_{in}(t)} = \frac{1}{2}[e^{j\frac{\pi V(t)}{2V_\pi}} + e^{j\frac{\pi V^*(t)}{2V_\pi}}] \tag{2.11}$$

When using differential input data in a push-pull configuration ($a = (-b) = 1$), the transfer function of a single drive MZM is given by [30]

$$\frac{E_{out}(t)}{E_{in}(t)} = \cos\left(\frac{\pi V(t)}{2V_\pi}\right) \tag{2.12}$$

where $E_{in}(t)$ and $E_{out}(t)$ is the input and output in optical field, respectively, $V(t)$ is the electrical OFDM signal, and V_π is the required voltage difference applied to a single electrode in order to generate a phase shift between two waveguides.

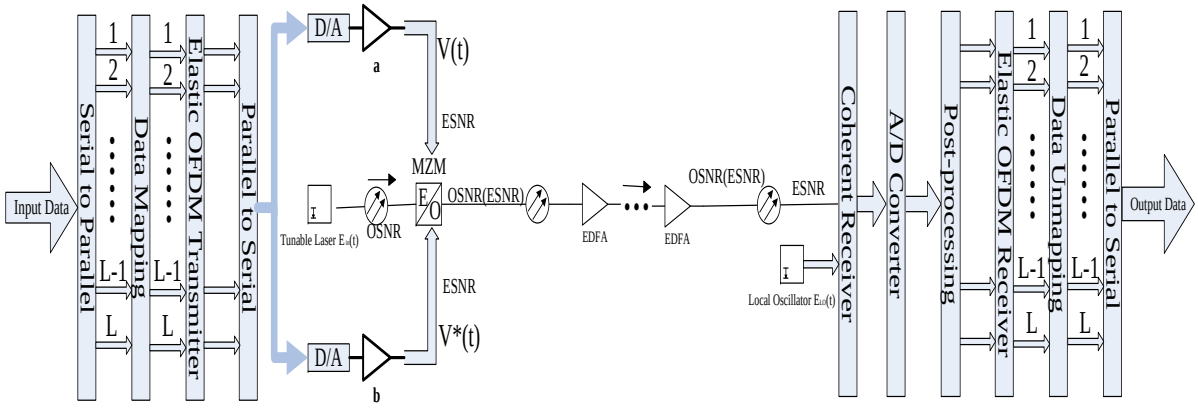

Figure 2.1: Elastic CO-OFDM Transmission System

Expanding the MZM nonlinear transfer function into a Taylor series as:

$$\frac{E_{out}(t)}{E_{in}(t)} = \cos\left(\frac{\pi V(t)}{2V_\pi}\right) \approx 1 - \frac{1}{2!}\left(\frac{\pi V(t)}{2V_\pi}\right)^2 + ... \tag{2.13}$$

The baseband equivalent polynomial model for the output electrical field of the MZM at $\phi_{Bias} = 3\pi/2$, as described in 2.12, is given as [15]

$$\begin{aligned} y_k &= \sum_{q=1}^{Q} \alpha_q \cdot (x_k)^Q, \;\; q - odd \\ &\approx \alpha_1 \cdot x_k + \alpha_3 (x_k)^3 \end{aligned} \tag{2.14}$$

where x_k and y_k is the discrete vectors of the applied voltage and the output voltage at the MZM, respectively, q is the order of nonlinearity, and α_q is the complex nonlinear odd coefficient of the MZM with an operating region $3V_\pi \pm V_\pi$ (i.e., at the null intensity bias point), whose output signal is approximated as a third order polynomial.

By assuming the optical fiber channel subject to AWGN, the signal vector obtained at the receiver side is [31]

$$x_l = \tilde{x}_l \cdot \mu + \eta + n_0(l) \tag{2.15}$$

where $\tilde{x}_l$ is the received symbol of l^{th} subcarrier, $n_0(l)$ is the AWGN noise with variance N_0.

Based on the above, each received OFDM symbol contains a complex phase shift term μ, nonlinear noise component η, and AWGN term N_0. When the number of subcarriers L is large, the variance of x_k can be assumed as P/L based on central limit theorem [32]. Then, we have the electrical SNR (ESNR) for each subcarrier calculated by

$$ESNR = \frac{P \cdot \mu^2}{\sigma^2 + N_0} \tag{2.16}$$

The complex phase shift μ is defined as

$$\mu = \alpha_1 + \frac{\alpha_3}{L} \sum_{k=0}^{KL-1} |x_k|^2 \tag{2.17}$$

The nonlinear noise components η are defined as [31]

$$\eta = \frac{\alpha_3}{L} \sum_{p=0, p\neq l}^{L-1} \tilde{x}_p \left[\sum_{k=0}^{KL-1} |x_k|^2 e^{j2\pi k(-l+p)/KL} \right] \tag{2.18}$$

σ^2 is the variance of the nonlinear noise from the MZM, given by [31]

$$\begin{aligned} \sigma^2 &= E[|\eta|^2] \\ &= \frac{|\alpha_3|^2 P^3}{L^3} \left(\frac{3L^2 - 11L + 12}{L} \right) \end{aligned} \tag{2.19}$$

With a high ESNR and Gray code bit mapping, the BER of M-ary quadrature amplitude modulation (QAM) under an AWGN channel can be approximated as [33]:

$$\begin{aligned} BER \cong & \frac{\sqrt{M} - 1}{\sqrt{M} \cdot \log_2 \sqrt{M}} \\ & * erfc \left(\sqrt{\frac{3 \log_2 M \cdot ESNR}{2(M-1)}} \right) \end{aligned} \tag{2.20}$$

where $erfc(\cdot)$ is the complementary error function.

2.2.3 Deterioration of ESNR due to ASE Noise

In light of the fact that the CD and PMD induced delay spread and the inter symbol interference (ISI) can be completely removed in an ideal coherent detection of CO-OFDM system where the line-widths of the transmit/receive lasers are assumed to be zero (background noise mainly from phase noise of transmit/receive lasers are to be zero). The study takes an approximation on the relation between the SNR in the optical domain (OSNR) and the ESNR for an ideal detection as follows [34]:

$$OSNR \;=\; ESNR\frac{D}{2B_{ref}\cdot m_{sys}} \tag{2.21}$$

where B_{ref} is the optical amplified spontaneous emission (ASE) noise bandwidth used for the OSNR measurement ($\approx$ 12.5 GHz for 0.1-nm bandwidth around 1550 nm). m_{sys} is the system margin $\approx$ 12 dB [35]. $D = 2m \cdot C \cdot L$ is the total system transmission rate, where L is the number of subcarriers, $M = 2^{2m}$ for M-ary QAM, and $C = 0.5$ Gbps is taken as the base capacity of 1 subcarrier using BPSK. And, this relationship is independent of whether one uses polarization multiplexing or not [34].

For multispan transmission line, the OSNR of each span is expressed as [36]:

$$OSNR = \frac{P_{out}}{F_{EDFA}hv\nabla f} \tag{2.22}$$

where P_{out} is the input power of fiber, F_{EDFA} is the EDFA noise figure due to the ASE noise with a typical value of 6dB, h is Planks constant with a value of 6.626×10^{-34}, v is the optical frequency 193 THz, and ∇f the bandwidth with a typical value of 0.1 nm (12.5GHz).

The total OSNR for chained EDFAs along N_{span} spans can be considered by a reciprocal method:

$$\frac{1}{OSNR} = \frac{1}{OSNR_1} + \frac{1}{OSNR_2} + \frac{1}{OSNR_3} + \cdots + \frac{1}{OSNR_{N_{span}}} \tag{2.23}$$

In sum, the total OSNR for chained EDFAs system is calculated as [36]

$$OSNR = \frac{P_{out}}{F_{EDFA}\alpha_{span}hv\nabla f N_{span}} \tag{2.24}$$

where α_{span} is the span loss.

By taking logarithm to the common base, the available OSNR of a 0.1 nm band at around 1550 nm at the output of a series of chained EDFAs along a multispan transmission line can be given by [36]:

$$OSNR[dB] = P_{out} - \alpha_{span} - F_{EDFA} - 10log_{10}N_{span} + 58 \tag{2.25}$$

where $\alpha_{span} \approx$ 25dB is the loss of 80km single mode fiber (SMF) span (including fiber attenuation, splice attenuation, connector attenuation, in-line device losses, nonlinear losses and safety margin)[37].

Based on the system architecture shown in Fig. 2.1 and given ESNR or BER threshold at receiver, we can derive the required power P_{out} (in dBm) of decodable signal at the input of fiber in an optical transmission line.

2.3 Proposed PAPR Reduction Method

In this section, we propose a PAPR reduction scheme to the scenario of optical transmission, namely simplified null shifting (SNS).

2.3.1 Various PAPR-Reduction Strategies

(1) Clipping, Filtering and Peak Window

Power amplifier at transmitter with saturation level below the signal span automatically cause the signal to be clipped [38]. Receiver needs to estimate two parameters of the transmitter's clipping operator: location and size, which are difficult to

get. However, clipping introduces both in-band distortion like self-interference and out-band radiation like nonlinear-distortion into OFDM signals, which degrades system's BER and spectral efficiency.

As improved clipping methods, peak windowing schemes minimize out-band radiation by using narrowband windows such as Gaussian window to attenuate peak signals. Filtering can reduce out of band radiation after clipping [39] [40]. Besides, clipping may cause some peak re-growth so that the signal after clipping will exceed the clipping level at some points. To reduce peak re-growth, a repeated clipping-and-filtering operation can be used to obtain a desirable PAPR at a cost of increasing computational complexity.

(2) Selected Mapping

In the SLM technique [41] [42], the transmitter generates a set of sufficiently different candidate data blocks by multiplying the same number of different phase sequences, all representing the same information as the original data block. And the one with the lowest PAPR is selected for transmission. Information about the selected phase sequence should be transmitted to the receiver as side information.

In the SLM-OFDM transmitter, one of the alternative subcarrier vectors can be the unchanged original one. Differentially encoded modulation may be applied before the IDFT and right after generating the alternative OFDM symbols. At the receiver, differential demodulation has to be implemented right after the DFT.

(3) Partial Transmit Sequence

The transmitter constructs its transmit signal with low PAPR by scrambling appropriate rotation factors to subcarrier subblocks [43] [44].

The difference between SLM and PTS is that the first applies independent scrambling rotations to all subcarriers, while the latter only applies scrambling rotations

to subcarrier subblocks.

(4) Interleaving technique

In interleaving approach [45] [46] [47], a set of interleavers is used to reduce the PAPR of the multicarrier signal. An interleaver is a device that reorders data blocks. To make a set of modified data blocks, different interleavers are used to permute data blocks from the original data block. And the modified data block with the lowest PAPR is then chosen for transmission. To recover the original data block, the receiver need only know which interleaver is used at the transmitter.

(5) Tone Reservation

TR scheme [48] is to choose the frequency-domain reserved-subcarriers as cancellation signal such that it minimizes the PAPR of TR transmitted signal.

At the receiver, symbol is demodulated in the frequency domain on a tone-by-tone basis, so the tone-reserved subcarriers can be discarded at the receiver, thus distortionless.

(6) Tone Injection

The basic idea of tone injection is to increase the constellation size so that the same data point can be mapped into multiple possible points in the expanded constellation [48]. And substituting a point in the basic constellation for a new point in the extended constellation for PAPR reduction is equivalent to injecting a tone with appropriate frequency and phase in the original signal.

At the receiver, TI does not require the extra side information, but only needs to know how to map the redundant constellations on the original one. However, comparing with TR technique, the TI technique injected signal by occupying the same frequency band as the information bearing signal, and also increases the transmitted signal's power.

(7) Active Constellation Extension

In this technique, some of the outer signal constellation points of the data block are dynamically extended toward the outside of the original constellation so that the PAPR of the data block is reduced [49]. The ACE approach can be applied to many kinds of constellation schemes with large constellation size, such as QAM, MPSK and QPSK, in which data points that lie on the outer boundaries of the constellations have room for increased margin without increasing the error probability for other data symbols. Furthermore, there is no need for data rate hit and channel side information. However, these modifications result in a power increase in the transmitted signal.

(8) Coding

Coding methods are used to reduce the PAPR by selecting appropriate codewords for transmission. For example, Block coding [50] is based on Golay sequences [51] (with dual capabilities of error correction and peak reduction), where the data sequence is embedded in a larger sequence and only those larger sequences with low peak powers are used. The data is encoded using a block code. In order to reduce the PAPR, a different sequence is transmitted where some of the data symbols are replaced by others, instead of transmitting the data symbol sequence corresponding to the codeword. The errors that are deliberately introduced could be corrected by the error correcting code. Hence, part of the error correcting capability of the code is sacrificed to PAPR reduction.

2.3.2 PAPR in OFDM

Consider an OFDM transmission with L subcarriers at the frequencies $\{f_l, l = 1, \cdots, L\}$. Assigned to the subcarriers at $\{f_l, 1 \leq l \leq L\}$ are, respectively, the M-ary data sym-

bols $\{\bar{x}_l, l = 1, \cdots, L\}$ or 0, which are independent and identically distributed random variables with zero mean and variance P.

Let T be the modulation interval and LT be the duration of an OFDM symbol (excluding the guard interval). The OFDM-signal's complex envelope can be expressed as:

$$x(t) = \frac{1}{\sqrt{L}} \sum_{l=1}^{L} \bar{x}_l e^{j2\pi f_l t}, \quad 0 \le t \le LT. \tag{2.26}$$

assuming the above is an idealized rectangular time-domain window, and the cyclic-prefix extension of $x(t)$ would not alter the PAPR.

The PAPR of the continuous-time signal $x(t)$ is defined as

$$\zeta(x(t)) \stackrel{\text{def}}{=} \frac{\max_{0 \le t < LT} \{|x(t)|^2\}}{E[|x(t)|^2]} \tag{2.27}$$

where $E[\cdot]$ denotes the expectation value.

The above continuous-time definition can be approximated in the discrete time domain as

$$\begin{gathered} x_k \triangleq x\left(\frac{kT}{K}\right) = \frac{1}{\sqrt{L}} \sum_{l=1}^{KL} \bar{x}_l e^{j2\pi f_l / KL} \\ , 0 \le k \le KL - 1 \end{gathered} \tag{2.28}$$

where K represents the oversampling factor, recommended to be 4 by [52] and 8 by [53].

2.3.3 Null Subcarriers in OFDM

Inherent in many multi-carrier standards are null-subcarriers (a.k.a., virtual / unused /unmodulated subcarriers), where no energy is transmitted. For example, in the IEEE 802.11a/g standard (i) 6 null-subcarriers serve as guard-band at the low-frequency end

and 5 null-subcarriers serve at the high-frequency end as guard-bands. (ii) A mid-band null subcarrier (indexed 0) for accommodating low cost RF-filters that avoids delay of DC energy.

In the IEEE 802.11a/g standard, using some of the "innermost" null subcarriers in the guard-band is sometimes tolerable because the spectral mask has its transition-band over those null subcarriers, thereby passing a good portion of the energy in these "innermost" null subcarriers as shown in Fig. 2.2. So, as long as the null subcarriers for mid-band reference and spectrum mask are kept intact, using the rest of null subcarriers in guard-bands is allowed.

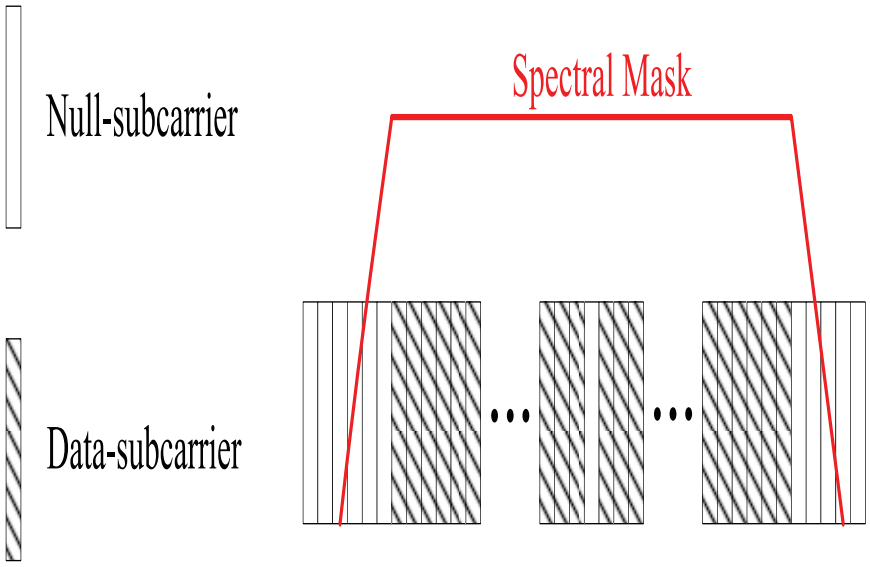

Figure 2.2: Spectral Mask

2.3.4 Proposed Simplified Null-Shifting (SNS) Method

The simplified null-shifting (SNS) scheme can achieve superb PAPR reduction performance and little dependence on the channel side information, which is considered very

suitable in an optical OFDM system. It can be modified and manipulated to take full advantage in the considered adaptive transmission scenario for an elastic OFDM optical communication systems, where the spectrum, transmit power, and modulation level are dynamically determined.

Consider OFDM transmission with $L+N$ subcarriers at the frequencies $\{f_{ln}, ln = 1, \cdots, L+N\}$. Label $\{ln = 1, \cdots, L+N\}$ as $\mathcal{S}$. Of these, N are null-subcarriers as guard-bands, with distinct indices drawn from the ascending set $\mathcal{N} = \{g_n, n = 1, \cdots, N\} \subset \mathcal{S}$. These N null-subcarriers respectively occupy the increasing frequencies $\{f_{g_n}, n = 1, \cdots, N\}$, while the remaining L subcarriers serve as data-subcarriers, with distinct indices from the ascending set $\mathcal{D} = \{l, l = 1, \cdots, L\} \subset \mathcal{S}$. These L data-subcarriers respectively occupy the increasing frequencies $\{f_l, l = 1, \cdots, L\}$. Moreover, $\mathcal{N} \cup \mathcal{D} = \mathcal{S}$, and $f_{g_n} \neq f_l, \forall n, d$. Assigned to the data-subcarriers at $\{f_l, 1 \leq l \leq L\}$ are, respectively, the M-ary data symbols $\{\bar{x}_l, l = 1, \cdots, L\}$, taken from a quadrature-amplitude modulation (QAM) or quadrature phase-shift keying (QPSK) constellation.

The input OFDM symbols $\bar{x}$ are partitioned into $\bar{V}$ disjoint subblocks

$$\bar{x}^{(\bar{v})} \triangleq [\bar{x}_0^{(\bar{v})} ... \bar{x}_{L/\bar{V}-1}^{(\bar{v})}] \tag{2.29}$$

with $\bar{x}_k^{(\bar{v})} = \bar{x}_l$, $0 \leq \bar{v} \leq \bar{V} - 1$, such that

$$\bar{x} = \sum_{\bar{v}=0}^{\bar{V}-1} \bar{x}^{(\bar{v})} \tag{2.30}$$

By taking L and N as constant, the SNS method shifts H elements $\{\tilde{g}_h, h = 1, \cdots, H\}$ of the null-subcarrier set $\mathcal{N} = \{g_n, n = 1, \cdots, N\}$ at the frequency $\{f_{\tilde{ln}_h}, h = 1, \cdots, H\}$ corresponding to H elements $\{\tilde{ln}_h, h = 1, \cdots, H\}$ of the subblock set $\bar{x}^{(\bar{v})}$ with the largest PAPR, such that if $f_{\tilde{ln}_h} < f_{\tilde{ln}_{h+1}}$, then $f_{\tilde{g}_h} < f_{\tilde{g}_{h+1}}$. Meanwhile, the permutation of the data-subcarrier set $\mathcal{D}$ remain unchanged after the shifting as shown in Fig. 2.3.

The goal is that the transmitter identifies the most advantageous frequencies for the H "innermost" null subcarrier(s) to shift to, in order for achieving the largest PAPR reduction. We assume that the spectrum will not be changed after the shifting of null-subcarriers (shifted null-subcarriers are in the transition-band of the transmit spectrum mask). The optimization problem is to identify $\{f_{\tilde{ln}_h}, h = 1, \cdots, H\}$ to minimize the PAPR. There are altogether $\binom{L/\bar{V}+H}{H} = \frac{(L/\bar{V}+H)!}{H!(L/\bar{V})!}$ different "shifting" possibilities. Only the indices of $\{f_{\tilde{ln}_h}, h = 1, \cdots, H\}$ is to be sent to the receiver as channel side information (CSI).

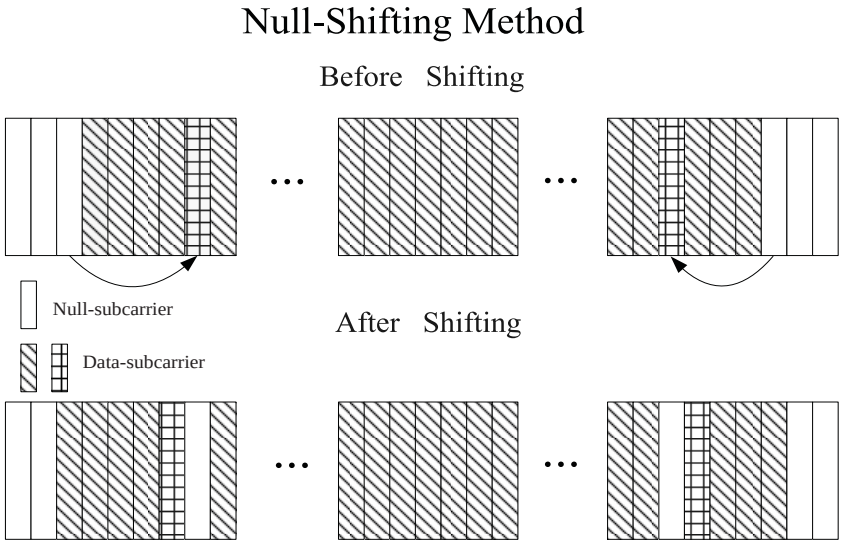

Figure 2.3: An illustration of the SNS method with $H = 2$.

2.3.5 PAPR Reduction Performance Comparison

We compare the PAPR reduction performance by using the proposed SNS scheme with that by using a state-of-the-art scheme, namely partial transmit sequence simulated annealing (PTS-SA) [54].

For the PTS-SA method with PTS-OFDM transmitter shown in Fig. 2.4, the optimization problem of PTS attempts to search the set of phase factors $\mathbf{b} = \{b_v = e^{j\theta_v}, \theta_v \in \{\frac{2\pi v}{W} | v = 0, 1, \cdots, V-1\}$ (W possible phase angles) for all corresponding partial sequences $x^{(v)} \triangleq [x_0^{(v)} ... x_{L/V-1}^{(v)}]$ to obtain the OFDM signals with the minimum PAPR.

A simulated annealing (SA) technique is used to obtain solutions for PTS-SA. Each rotation phase vector $\mathbf{b}$ represents a system state, and the objective function $f(\mathbf{b}) = \|x\|_\infty^2 = \|\sum_{v=0}^{V-1} b_v x^{(v)}\|_\infty^2$ corresponds to the energy of the system at state $\mathbf{b}$. Let $\tilde{\mathbf{b}}$ denote the current solution and $\hat{\mathbf{b}}$ denote the best solution so far. Whether a track orientation from one state to another is accepted or rejected is determined by the following criterion: $\Delta E = f(\tilde{\mathbf{b}}) - f(\hat{\mathbf{b}})$, and if $\Delta E < 0$, then $\tilde{\mathbf{b}}$ is accepted. In the case of $\Delta E > 0$, $\tilde{\mathbf{b}}$ is still accepted if the acceptance probability is greater than a random number between 0 and 1. When the system based on SA is cooled down slowly, it returns a value corresponding to a crystalline structure with lowest energy and steadiest state, in which the obtained optimal solution is the global minimum.

To have a fair comparison, we take the same computational complexity when implementing both schemes. The key parameters taken in the simulated annealing (SA) implementation are as follows: Iteration=28, Initialize annealing temperature=100, temperature decrement factor=0.98 for cooling schedule, acceptance factor=5 for transition acceptance probability, and final simulated annealing temperature=0.00001. The results shown in Fig. 2.5 demonstrate that proposed SNS (A.K.A. reduced-complexity version) method with 28 IFFT operations, only using 12 bits CSI, which is less than the 16 bits CSI of PTS-SA method, still has better PAPR reduction performance than PTS-SA method under same computational complexity.

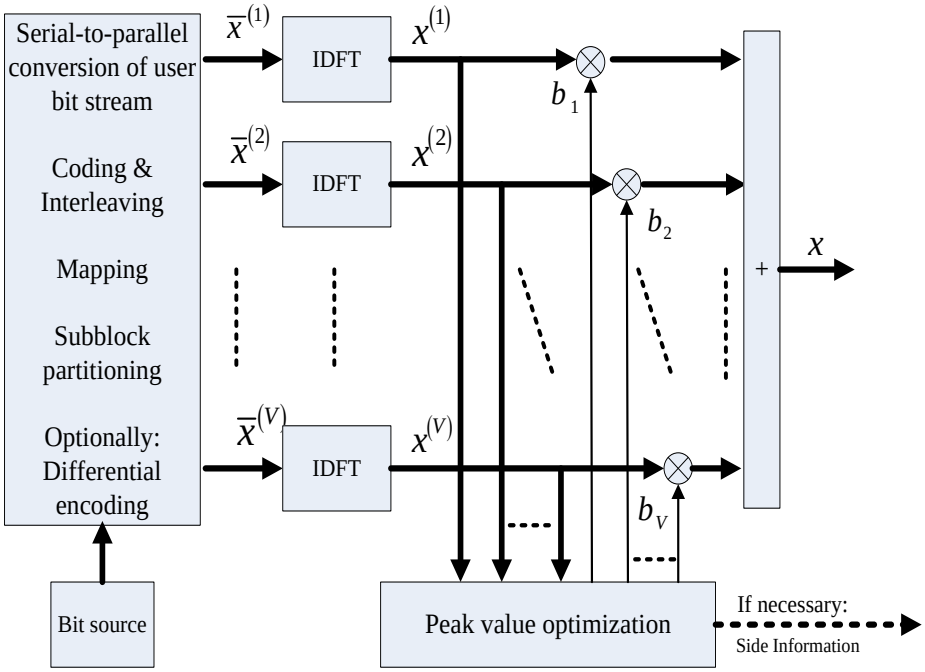

Figure 2.4: A block diagram of the PTS technique [43].

2.4 Optimization Problem

Based on the BER analysis and PAPR reduction method, a novel adaptive transmission strategy is developed to minimize the operational cost in terms of the consumed power and spectrum resources. The former concerns the energy efficiency and environmental friendliness of the system operation, while the latter is related to the system utilization and throughput. The formulated optimization problem is expected to come up with the best strategy of adaptive transmission regarding the BVT power, allocated spectrum, and modulation level for a specific transmission request with a given data rate.

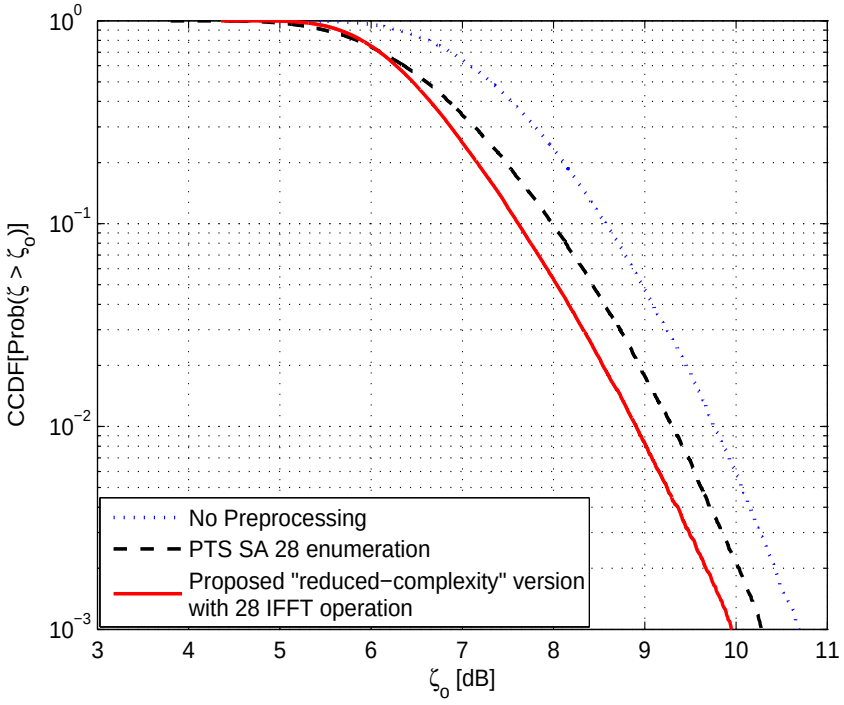

Figure 2.5: The PAPR's CCDF at $H = 2, L = 48, V = 8, W = 4$, QPSK modulation.

2.4.1 Power Consumption Analysis of Optical Transceiver

The fiber input power P_k (in Watt) is calculated by:

$$P_k = 10^{(P_{out}-30)/10} \tag{2.31}$$

for a given L and BER, P_{out} (in dBm) is calculated based on Eq. 2.21, Eq. 2.25 by taking L and $ESNR$ as variables.

The laser continuous wave (CW) power P_{CW} (in Watt) of MZM is calculated by [22]:

$$P_{CW} = P_k \cdot 10^{L_{mod}/10} \tag{2.32}$$

where $L_{mod} \approx 2.5$dB is optical excess loss of MZM [55].

The power consumption of the externally modulated optical transmitter (electrooptic modulator) and optical receiver (optical-to-electrical module) in Fig. 2.1 is respectively defined as follows:

$$P_{OTran} = (E_{MUX} + E_{Driver} + E_{Laser}) \cdot 10^6 \cdot D + P_{CW} \tag{2.33}$$

$$P_{OReceiver} = (E_{DEMUX} + E_{Bias} + E_{Preamp}) \cdot 10^6 \cdot D \tag{2.34}$$

where E_{MUX}, E_{Driver}, and E_{Laser} is the power consumption of the multiplexer, the driver, and the laser of the MZM, respectively, with a nominal value as 2pJ, 3pJ, and 0.5pJ per bit for 2020-era technology (100Gb/s); E_{DEMUX} is the power assumption of the demultiplexer at the receiver with a nominal value of 2pJ per bit for 2020-era technology; $E_{Bias} + E_{Preamp}$ is the power consumed by the EDFA preamplifier and bias circuit at the receiver with a nominal value as 1.6pJ per bit for 2020-era technology [22].

Thus, the total power consumption of the externally modulated optical transceiver can be expressed as:

$$\begin{aligned} P_{OTranceiver} &= P_{OTran} + P_{OReceiver} \\ &= P_{TOEO} \cdot D + P_{CW} \\ &\approx 0.0091 \cdot D + P_{CW} \end{aligned} \tag{2.35}$$

where P_{TOEO} (in Watt) is the power consumption of OEO conversion in optical transceiver (per Gbps).

2.4.2 Mathematical Formulation

Based on the mathematical analysis of the transmission power consumption, the cost function considered in the study is a linear combination of consumed power and spectrum resources, which is given as follows:

Objective:

$$\begin{aligned} \textbf{Min } & P_{SC}^{m} + P_{FT} + P_{AMP} \cdot N_{span} \\ & + P_{TOEO} \cdot D + P_{CW} + B \cdot \beta \end{aligned} \tag{2.36}$$

where D (in Gbps) denotes the required transmission rate; $B = F \cdot L$ (in GHz) is the consumed spectrum bandwidth with the channel width F (default value as 0.5 GHz) and the number of subcarriers L; and $\beta \geq 0$ is a parameter used to weight the spectrum consumption. Clearly, a small (or large) β should be used when the spectrum consumption is not a concern (or a serious concern); e.g., in the circumstance that the network is in low (or high) utilization. Thus it serves an important role in determining the tradeoff between the two performance metrics of interest.

The power consumption by an OFDM transponder includes the power consumption figures of the digital signal processing (DSP) module, digital-to-analog convertor(DAC), analog-to-digital convertor (ADC), electrical-to-optical module (transmitter), and optical-to-electrical module (receiver). For a BVT supporting up to 100 Gbps, the total energy consumption with two DSP modules, one DAC, and one ADC module is denoted as P_{FT}, which is the fixed part of the power consumption independent of the transmission modulation and bandwidth (with a nominal value of 120W [56]). On the other hand, P_{SC}^{m} denotes the variable part of the power consumption expressed as $\delta \cdot L \cdot m$ W, where L and m is the number of subcarriers and modulation level, respectively; and δ is a constant nominally given as 0.18 [56]. The power consumption of an in-line EDFA per 80KM fiber span P_{AMP} is assumed to be 8.750W [56].

The above formulated problem aims to determine the required laser power P_{CW} of the BVT, allocated spectrum width B, and the modulation level (i.e., m) in order to optimize the transmission cost while meeting the minimum rate D for the transmission request. The optimization problem exists due to the following tradeoff: to transmit with a specific transmission rate, using smaller (or larger) transmit power requires larger (or smaller)

spectrum to support a specific modulation level, which determines the total operational cost.

The above target function is subject to the following constraints.

Constraints:

$$BER \cong \frac{\sqrt{M}-1}{\sqrt{M}\cdot \log_2 \sqrt{M}} * erfc\left(\sqrt{\frac{3\log_2 M \cdot ESNR}{2(M-1)}}\right) \leq BER_{th} \tag{2.37}$$

$$D \leq 2m \cdot C \cdot L \tag{2.38}$$

The receiver side BER is defined as in 2.20 and is rewritten as 2.37 by taking ESNR and modulation level m as variables, i.e., $M = 2^{2m}$ for M-ary QAM; ESNR ($= \frac{P\cdot\mu^2}{\sigma^2+N_0}$) is defined in 2.16 by taking L as variable; BER_{th} is the BER threshold without using forward-error-correction (FEC). In 2.38, $C = 0.5$ Gbps is taken as the base capacity of 1 subcarrier using BPSK [57].

2.4.3 Proposed Heuristic Algorithm

In the objective function, laser transmit power P_{CW} involves square and cubic. The BER constraint 2.37 involves square root. So the formulated problem is a nonlinear programming (NLP). An optimization problem is convex if both the objective function and constraint functions are convex. Unfortunately, our NLP problem is not convex since the objective function and data rate constraint 2.38 are not convex.

Since the above optimization formulation is a NLP problem rendering a large search space, here a heuristic mechanism is developed to achieve an approximated solution to the global optimum. We have tried to solve the NLP problem analytically but did not find a

way better than the proposed heuristic. Note that the proposed heuristic mechanism does not blindly search for the whole search space, but it calculates the required lowest number of subcarriers L first, and then searching for the required lowest laser transmit power P_{CW} for each candidate modulation levels m given the derived L value. So, the complexities of proposed algorithm is the number of all possible laser output power smaller than the required lowest laser transmit power.

The procedure to search for a solution is given as follows and described in Fig. 2.6 as flowchart:

1 Initialize data rate D, BER threshold without using FEC BER_{th}, modulation level $\mathbf{m}$, MZM required voltage difference V_π, etc.

2 Generate uniformly distributed laser CW output power, and select the lowest as initial laser power solution $\mathbf{P_{CW}}$.

3 Compute the required lowest number of subcarriers $\mathbf{L}$ for modulation level $\mathbf{m}$, and the corresponding BER. If the $\mathbf{BER} \leq BER_{th}$, then the $(\mathbf{P_{CW}}, \mathbf{L})$ is the optimal solution for modulation level $\mathbf{m}$. If not, increase the $\mathbf{P_{CW}}$ until $\mathbf{BER} \leq BER_{th}$.

4 Calculate the cost of modulation level $\mathbf{m}$ by using $(\mathbf{P_{CW}}, \mathbf{L})$, and consider it as the lowest cost of modulation level $\mathbf{m}$.

5 Increase the modulation level $\mathbf{m}$ to a higher candidate modulation level $\tilde{\mathbf{m}}$, and search the required lowest $(\tilde{\mathbf{P_{CW}}}, \tilde{\mathbf{L}})$ to compute the lowest cost for modulation level $\tilde{\mathbf{m}}$.

6 Compare the lowest cost of all candidate modulation levels, and select the modulation level $\hat{\mathbf{m}}$ with corresponding $(\hat{\mathbf{P_{CW}}}, \hat{\mathbf{L}})$ whose lowest cost has the smallest value.

7 Return optimal solution $(\hat{\mathbf{P}_{\mathbf{CW}}}, \hat{\mathbf{L}}, \hat{\mathbf{m}})$.

2.5 Preliminary Results

In this section, preliminary results are conducted to demonstrate the performance improvement by using the proposed transmission strategy in Section 2.4 for a single transmission line and verify its effectiveness. In current research, we first consider implementing proposed strategy in a single CO-OFDM based optical transmission line with required transmission rate. By dynamically and adaptively manipulate a few system parameters (i.e., the required laser output power P_{CW} of the BVT, allocated number of subcarriers L, and corresponding modulation level M), proposed strategy attempts to minimize the operational cost in terms of consumed power and spectrum resources. We also compare the performance of SNS (in Section 2.3) with that of Partial Transmit Sequence Simulated Annealing (PTS-SA) method in elastic optical systems and demonstrate its efficiency.

Given $D = 100$Gbps which enables the desired bulk data transfers and a range of transmit power $P_{CW} \leq 40mW$ for achieving sufficient ESNR at the receiver, we target to obtain the optimal operational cost and the corresponding number of subcarriers, modulation schemes, and laser transmit power. The required voltage difference V_π applied to a single electrode for a single drive MZM is set to be 9. We define $m = 1$ for QPSK, $m = 2$ for 16-QAM, $m = 3$ for 64-QAM, $m = 4$ for 256-QAM, $m = 5$ for 1024-QAM to be the candidate modulation levels that the transmitter side can adaptively take.

By using proposed heuristic algorithm in Subsection 2.4.3, Fig. 2.7 provides the required lowest number of subcarriers and normalized lowest laser CW output powers under all candidate modulation levels for the proposed SNS scheme and two other counterparts, namely PTS-SA and no PAPR reduction, where the BER threshold without using FEC

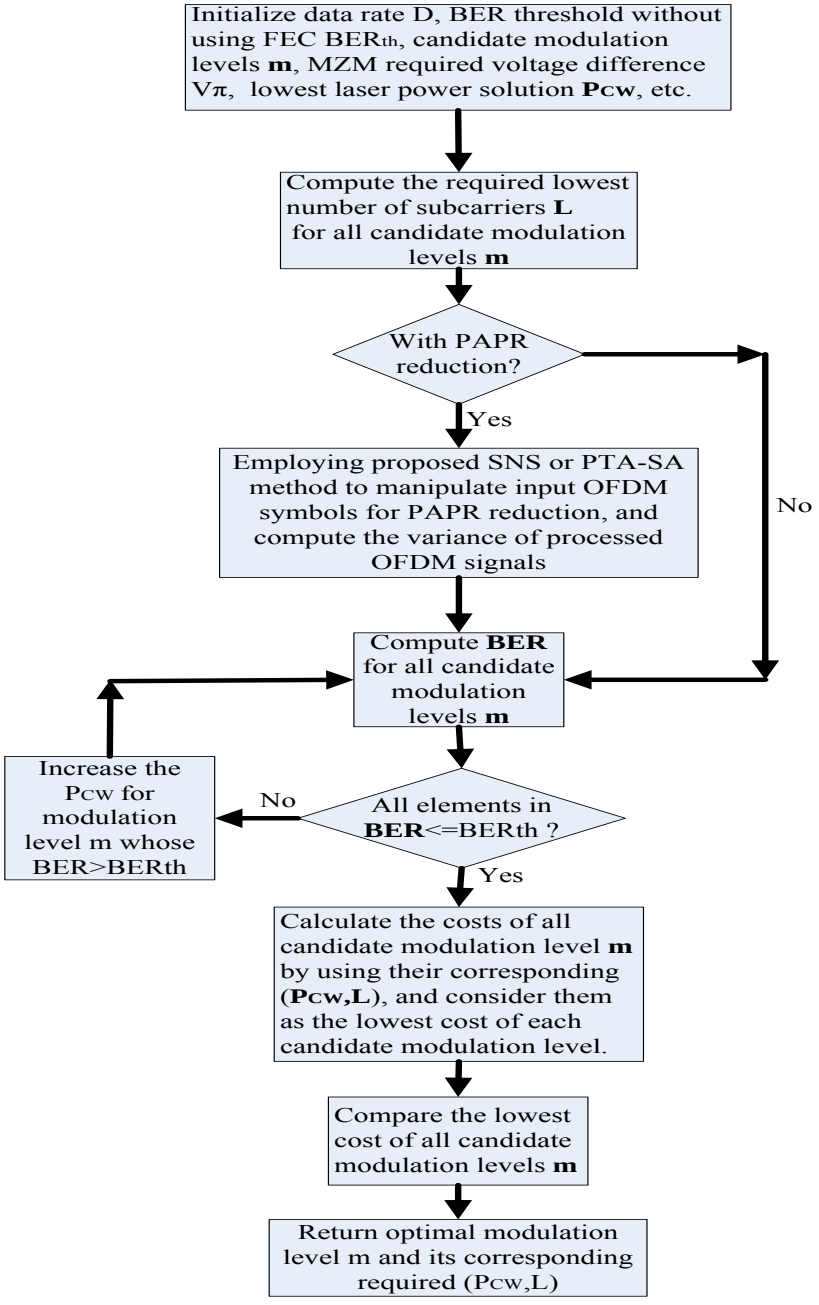

Figure 2.6: Flowchart of proposed heuristic algorithm

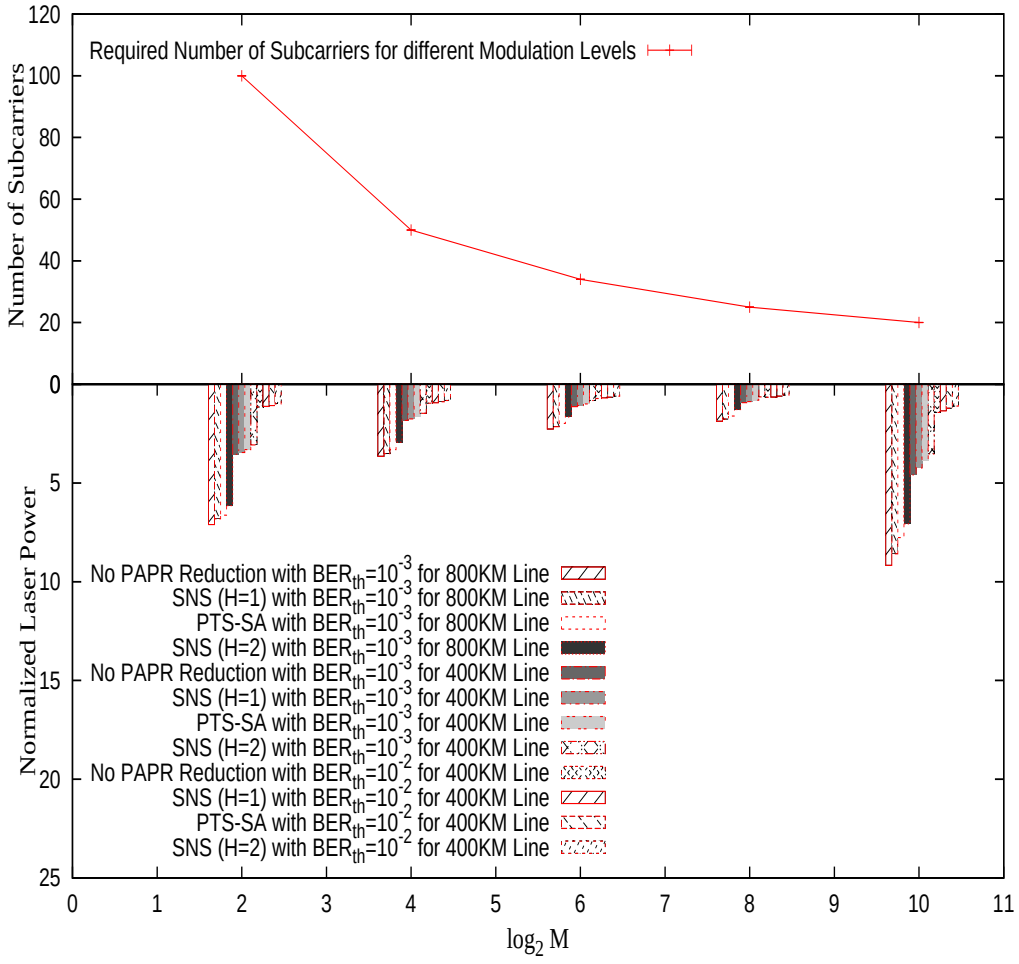

Figure 2.7: Required lowest number of subcarriers and normalized laser power of a single transmission with and without PAPR reduction VS Modulation level

at the receiver BER_{th} is 10^{-3} and 10^{-2}, respectively, and the distance of the long-haul transmission line is 400 km and 800 km, respectively. Fig. 3 clearly shows that the energy consumption is large when the modulation level is rather conservative or aggressive (e.g., $m = 2$ or $m = 5$), and is significantly reduced by choosing a moderate m (e.g., $m = 4$). On the other hand, the bandwidth consumption is monotonously decreasing when

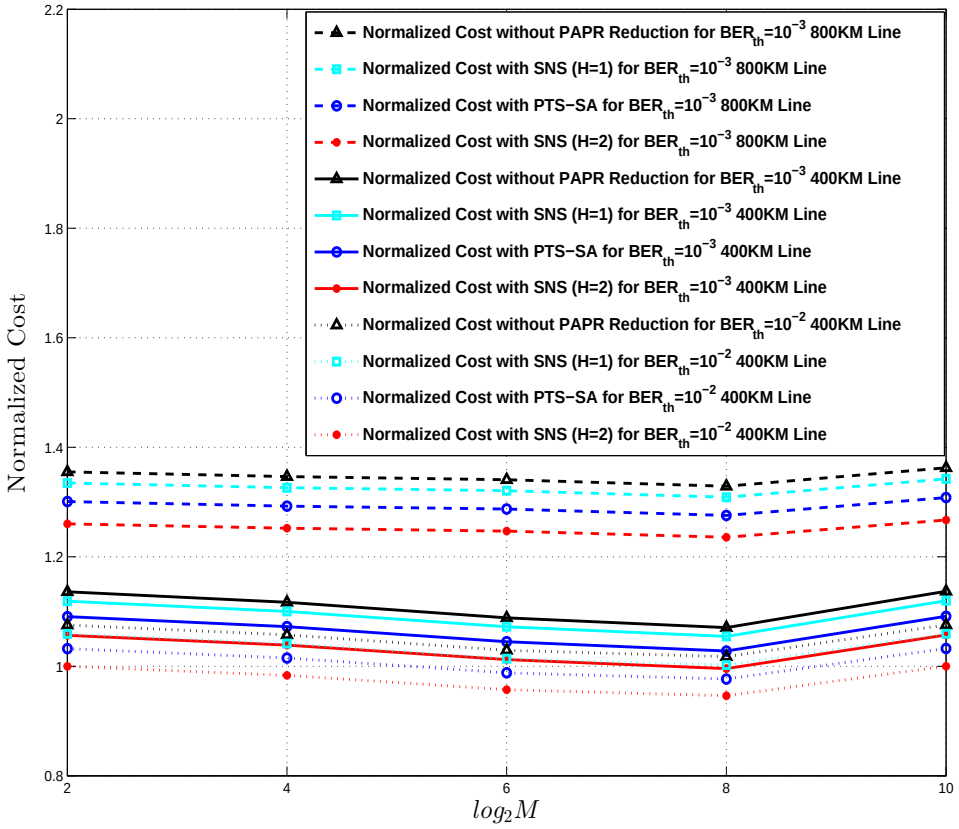

Figure 2.8: Normalized cost of a single transmission with and without PAPR reduction for $\beta = 0$ VS Modulation level

m is increasing. In particular, we have seen that the proposed SNS scheme with $H = 2$ consumes significantly less energy than the other counterparts under all the considered scenarios. Note that the modulation scheme and transmission rate solely determine the required lowest bandwidth and laser output power, thus the data of each scheme is independent of β.

In Fig. 2.8-2.11, the normalized optimal operational costs by adopting different candi-

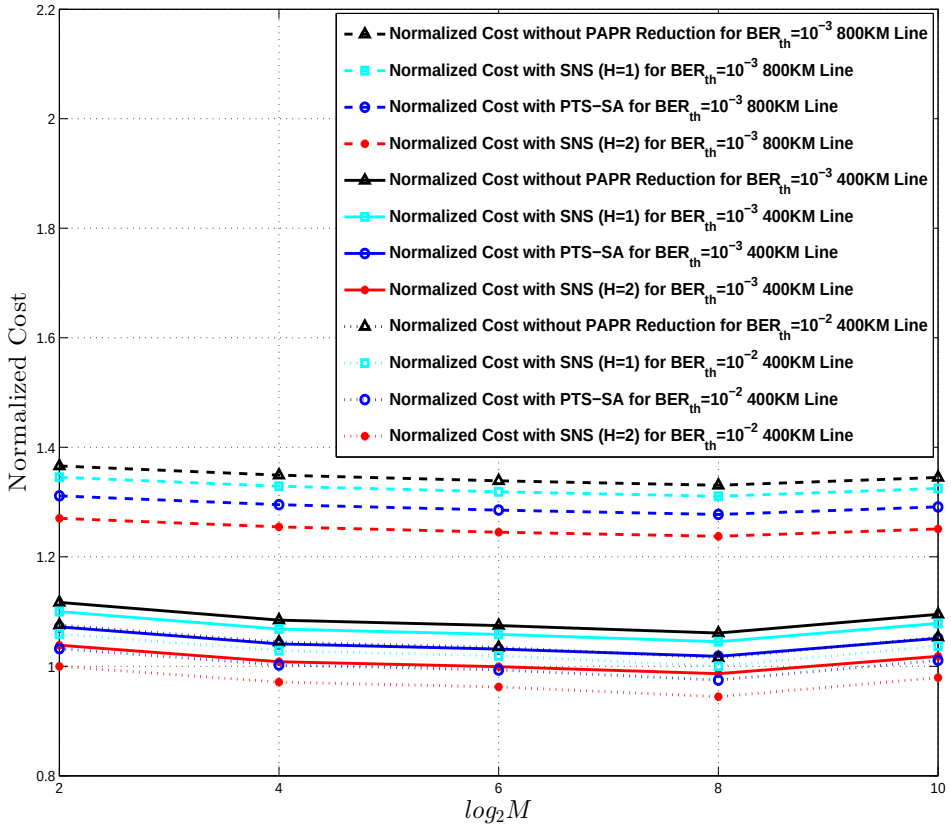

Figure 2.9: Normalized cost of a single transmission with and without PAPR reduction for $\beta = 0.1$ VS Modulation level

date modulation levels with and without adopting the proposed PAPR reduction method are compared under different value of β. The total cost (170 for $\beta = 0$, 177 for $\beta = 0.1$, 207 for $\beta = 1$, 616 for $\beta = 10$) of QPSK by adopting SNS for 400KM line with $BER_{th} = 10^{-2}$ in each figure is set to be 1 unit, respectively. They illustrate how an optimal operation with a minimum cost can be achieved corresponding to each possible laser transmit power, bandwidth, and modulation scheme under different BER thresholds and transmission distances. Here β is shown to be an important parameter on the optimization result that

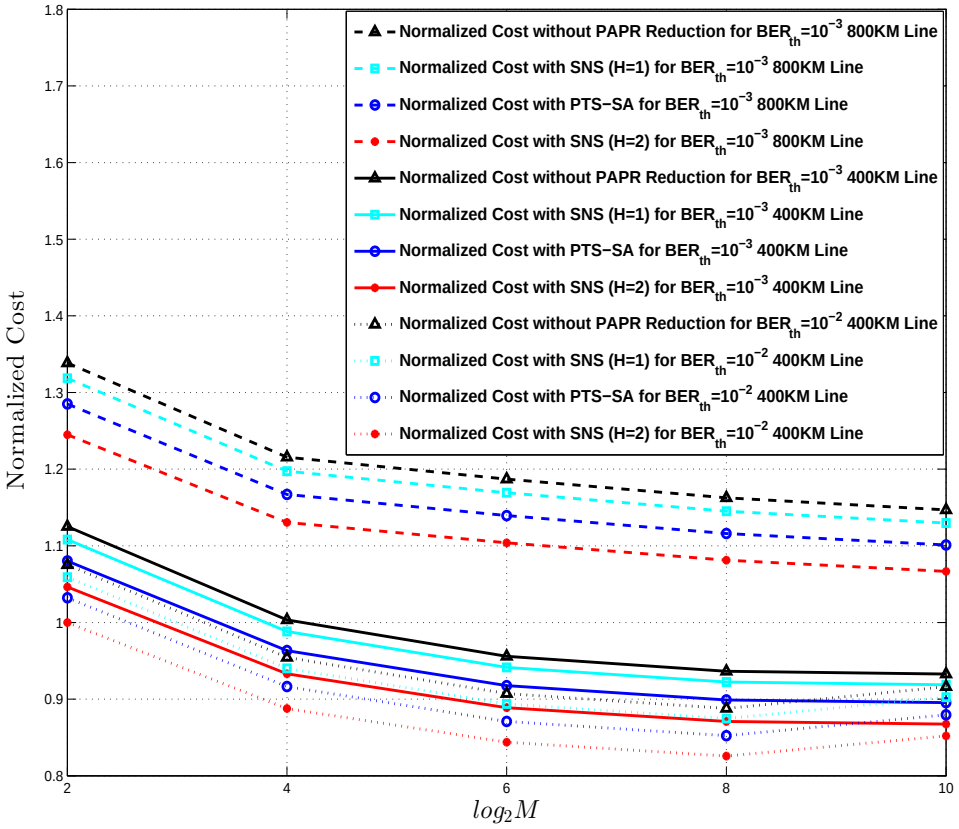

Figure 2.10: Normalized cost of a single transmission with and without PAPR reduction for $\beta = 1$ VS Modulation level

can meet a given operation target under a specific transmission request. For example, when we adopt SNS with $H = 2$ for 800KM line transmission with $BER_{th} = 10^{-3}$, 256-QAM using 1.29 unit laser transmit power and 25 subcarriers is the optimal operation with a minimum cost for $\beta = 0, 0.1$; 1024-QAM using 7.1 unit laser transmit power and 20 subcarriers is the optimal operation with a minimum cost for $\beta = 1, 10$.

Meanwhile, Fig. 2.8-2.11 show that the use of PAPR reduction methods can signif-

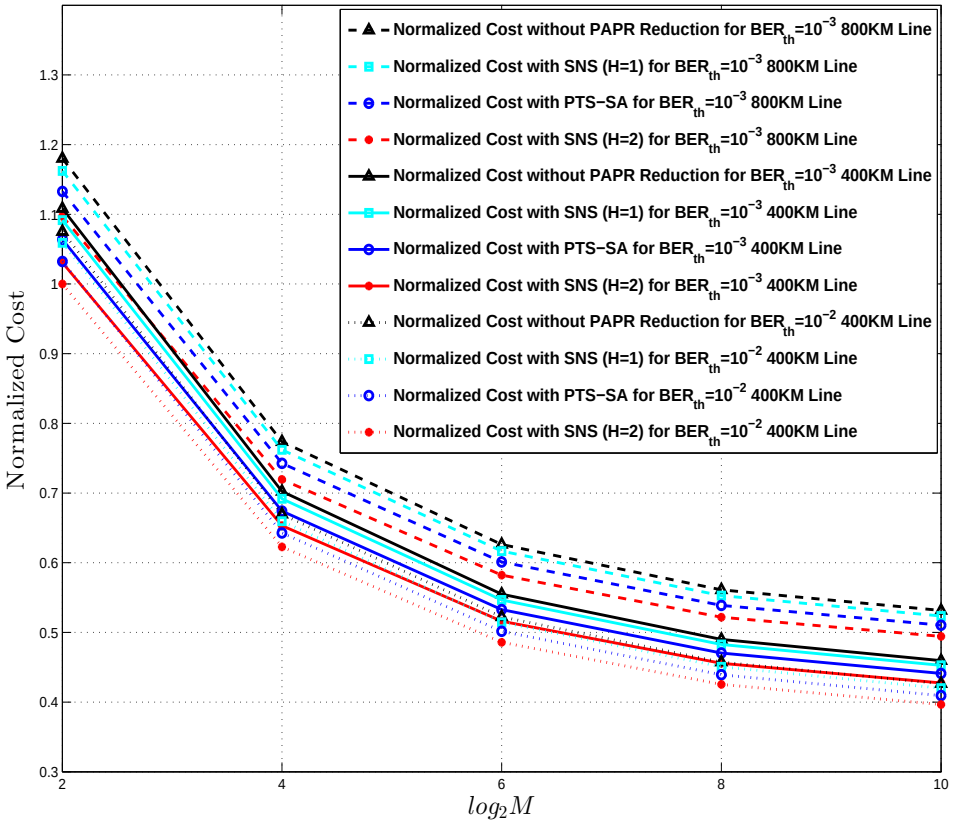

Figure 2.11: Normalized cost of a single transmission with and without PAPR reduction for $\beta = 10$ VS Modulation level

icantly reduce the operational cost when the tested β value is not too large. We also compare the performance by using the proposed PAPR scheme (in Section 2.3) with that by using a state-of-the-art scheme reported for the wireless scenario, namely Partial Transmit Sequence Simulated Annealing (PTS-SA) [54]. To have a fair comparison, we take the same computational complexity when implementing both schemes. The key parameters taken in the simulated annealing (SA) implementation are as follows: Iteration=28, Initialize annealing temperature=100, temperature decrement factor=0.98

for cooling schedule proposed by Kirkpatrick [58], acceptance factor=5 for transition acceptance probability proposed by Tsallis [59], and final simulated annealing temperature=0.00001. The results shown in Fig. 2.8-2.11 demonstrate that the proposed SNS method with $H = 2$ outperforms the PTS-SA scheme under the same condition, while the required CSI of the SNS method is about 30% less. This verifies that the proposed SNS scheme is very suitable to the optical OFDM environment and could be a competitive candidate for achieving an intelligent and efficient elastic optical transmission.

To the best of our survey, using 1024-QAM has not been reported in a practical OFDM system with over 800KM distance due to the channel impairments by the laser and fiber. So we say taking a higher modulation level can always yield better system performance (or lower cost) in practical systems with 800 km or less in distance.

2.6 Summary

In this chapter, we introduced a novel adaptive transmission strategy for elastic CO-OFDM optical systems in which both costs on energy and spectrum resource consumption are considered. We investigated the performance improvement when a PAPR reduction mechanism is equipped. For this purpose, we extended our previously developed PAPR reduction scheme to the scenario of optical transmission, namely Simplified Null Shifting (SNS), which is featured as subject to minimum dependence on CSI in order to fit into the optical transmission scenario. By considering nonlinear effects of Mach-Zehnder modulator (MZM) and optical amplified spontaneous emission (ASE) noise, we first developed an analytical model of the BER expression for the considered elastic CO-OFDM transmission systems where the effect of high PAPR in both RF and optical domains is jointly considered. Based on the model, an optimization problem was formulated for the determination of laser transmit power, spectrum, and modulation level of a single transmission request under a given transmission data rate. Case studies were performed, where the mathematical formulation was numerically solved, in order to gain better understanding of the proposed approach. We demonstrated that by adaptively choosing coupled laser power, spectrum width, and modulation scheme, the proposed mathematical model can accurately capture the BER performance of a transmission in the considered elastic CO-OFDM optical systems, where a superb performance compared with other counterparts can be achieved.

Chapter 3

Energy-Efficient Elastic Optical Networks

In this chapter, we extend proposed transmission strategy in Chapter 2 for 5-node network, 8-node network and NSFNet with given traffic matrix and dynamic scenario. By introducing a novel routing and bandwidth allocation strategy for OFDM-based elastic optical networks, we aim to optimize the network operation cost in terms of energy consumptions. Based on the previously reported analytical BER (bit error rate) model for OFDM-based optical transmission line, an optimization problem is formulated to allocate a set of lightpaths according to realistic network topologies, where the routing path, modulation level, bandwidth, and optical transceiver power of each lightpath are jointly determined for achieving minimum power consumption. To reduce computational complexity, a suboptimal iterative flipping method for solving the above NP-complete optimization problem is proposed, which achieves better performance than simulated annealing (SA) scheme while consuming considerably less searching iteration.

3.1 Literature Review

The use of OFDM-based elastic optical networks aims to achieve high scalability and flexibility in bandwidth granularity, compared with the conventional fixed-grid and rigid-bandwidth WDM technology. By dividing the total frequency spectrum into a number of uniform frequency subcarriers, the CO-OFDM elastic optical networks considered in this chapter provide each optical path to occupy a variable number of adjacent subcarriers for elastic data transmission. The routers equipped with bandwidth variable wavelength cross-connects (BV-WXCs) allocate cross-connections for each optical path. For subcarriers assigned to each path, prefixed and suffixed guard band subcarriers are used to separate adjacent optical paths so as to avoid inter-modulation products as shown in Fig. 3.1.

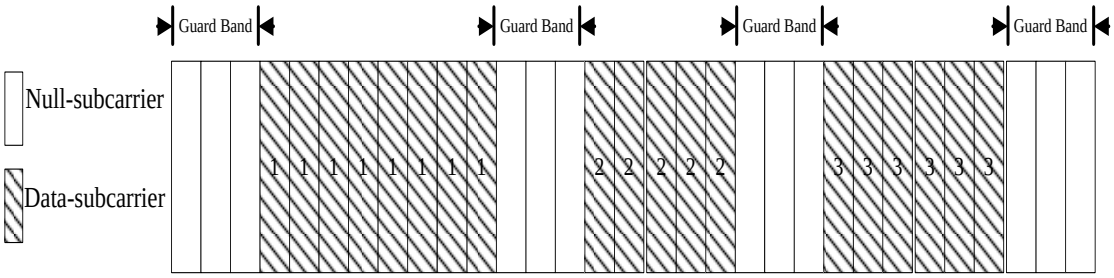

Figure 3.1: Bandwidth allocation as subcarrier slots assigned to each paths with guard band [57].

To launch the OFDM technology in optical networks, the research in [3] studied elastic bandwidth allocation in the spectrum domain of fiber optics where a connection request for a specific transmission rate can be provisioned by elastically and adaptively allocating spectrum bandwidth using a proper number of OFDM subcarriers and a modulation level. Moreover, the research in [57] reported that the selected modulation level and allocated spectrum bandwidth to the connection request is a function of linear and non-linear

physical layer impairments.

As the energy efficiency emerged as a new design dimension for optical transmission systems and networking, elastic bandwidth provisioning in energy-efficient OFDM optical networks has attracted extensive attention in the past few years. Ref. [22] provided a framework for exploring the fundamental limits of energy consumption in optically amplified transport systems. By manipulating the allocated subcarriers on any of its links, [56] introduces an energy-efficient design for OFDM-based optical networks. Without considering any physical layer constraint along a link, such as data rate, BER, laser transmit power, and consumed bandwidth, [56] has focused on the system performance when 16-QAM is taken as the only modulation level with time-consuming exhaustive search (40 minutes to an hour for running each case). In [60], a differentiated quality of protection (Diff QoP) scheme with adaptive modulation is involved for energy efficiency in network protection. But they calculated power consumption of transponder for different modulation formats by using constant parameters. That is, the transmit power is set to be constant for each lightpath and cannot be manipulated under different transmission distances and modulation schemes. Thus, although comprehensive, it left some space for further exploration.

Comparing to [56] and [60], [61] incorporated adaptive modulation under static traffic demands, where the launch power for different modulation levels was calculated by considering link constraint. Nonetheless, the power consumption model of single transmission line in [61] only considered the fiber loss and the optical amplifier noise from the optical link, while ignoring the noise part due to additive white Gaussian noise (AWGN) and nonlinear Mach-Zehnder modulator (MZM) from the perspective of electrical domain with peak-to-average power ratio (PAPR) issue of OFDM-based optical transponder. Further, the research in [61] only considered the shortest-path as the possible routing path, which certainly imposed limits on the precision of the model and the performance

of cross layer optimization results.

By witnessing that all the previously reported research on routing and bandwidth allocation (RBA) in optical OFDM networks have used outdated transmission models, it is expected to gain new insights into the problem with the newly reported transmission model and adaptive transmission strategy. As an effort of improving the state-of-the-art, this chapter investigates energy-efficient RBA problem in elastic optical OFDM networks by using the transmission model provided in Chapter 2.

3.2 Adaptive Transmission for Single OFDM-based Optical Transmission Line

By using the transmission model in Subsection 2.2.2 and Subsection 2.2.3, adaptive transmission is expected to come up with the best strategy regarding the required laser output power of optical transponder, allocated number of subcarriers, and corresponding modulation level for a given set of transmission requests in OFDM-based elastic optical networks. The procedure to search for a solution including laser output power P_{CW}, number of subcarriers L, and modulation level M is described in Algorithm 1.

3.3 Optimization Problem

We assume the energy consumption in the elastic optical networks is the accumulation of the following four parts: optical transponders (Subsection 2.4.1), optical amplifiers, nodal electronic processing, and wavelength conversion (if dedicated devices are used for this purpose). For simplicity, the proposed problem formulation ignores any other energy consumption such as due to optical switching of wavelength channel in the optical

Algorithm 1 Adaptive Modulation for Optical Transmission

Input: Data rate D; Candidate modulation levels $\mathbf{M}$;

BER threshold without using FEC BER_{th};

MZM required voltage difference V_π;

Laser output power upper bound P_{CW}^{up};

Lowest laser output power $\mathbf{P_{CW}}$ as initial solution;

Output: Return optimal solution $(\mathbf{P_{CW}}, \mathbf{L})$ for $\mathbf{M}$;

1: Computing the required lowest number of subcarriers $\mathbf{L}$ for each candidate modulation level in $\mathbf{M}$ through $D = 2m \cdot C \cdot L$, where $M = 2^{2m}$ and $C = 0.5$ Gbps is taken as the base capacity of 1 subcarrier using BPSK;

2: Calculating **BER** for each candidate modulation level in $\mathbf{M}$;

3: If all elements in $\mathbf{BER} \leq BER_{th}$, then the $(\mathbf{P_{CW}}, \mathbf{L})$ is the optimal solution for corresponding modulation levels $\mathbf{M}$;

4: If not, increase corresponding P_{CW} $(\leq P_{CW}^{up})$ for modulation level M whose $BER > BER_{th}$, then go to step 2;

5: **return** $(\mathbf{P_{CW}}, \mathbf{L})$;

cross-connect (OXC) [62], since they are negligibly small. By uniformly dividing the total frequency spectrum into a number of frequency subcarriers, the OFDM-based elastic optical networks have each optical path to occupy a variable number of adjacent subcarriers for a single transmission, which is supported by the optical transponders at the sender of each optical path segment. For a given network topology and traffic scenario, the locations of the optical amplifiers are given, and employed routing and bandwidth allocation strategy determines the amount of traffic that can be simultaneously supported. All-optical wavelength converters can be used for achieving better spectrum efficiency [61].

3.3.1 Mathematical Formulation

Input Parameters:

- P_{OEO}: power consumption of OEO conversion at intermediate nodes due to electronic switching (17.5W per Gbps) [56].
- P_{OT}: power consumption at optical transceiver, and it is approximately 0.0091W per Gbps.
- P_{FT}: power consumption of fixed part in OFDM-based optical transponder, and it equals to 120W [56].
- P_{AMP}: power consumption of an in-line EDFA per 80KM fiber span, and it is assumed to be 8.750W [56].
- P_{SC}: power consumption of variable part in transponder, and it equals to 0.18W per Gbps.
- P_{CW}^{up}: upper bound of laser continuous wave (CW) output power.
- BER_{th}: BER threshold without using forward-error-correction (FEC) for all lightpaths.
- BW: spectrum bandwidth on each fiber (1THz).
- $[D_{s,d}]$: traffic matrix with traffic demands $D_{s,d}$ between a source to destination (s, d) pair.
- P_W: power consumption of wavelength converter, and it equals to 1.65W per wavelength.
- F: channel width of each subcarrier (default value as 0.5 GHz).

- NF_{max}: maximum number of fibers available in each physical link.
- $NP_{s,d}$: number of possible paths for groomed traffic flow between (s, d).
- $H_{s,d,r}$: number of hops in r_{th} routing path of groomed traffic flow between (s, d).
- GB: guard-band for each optical channel (default value as 20 GHz) [61].
- R_{TP}: transmission bit rate of each transponder (default value as 100Gbps).

Variables:

- $N_{WC}^{s,d,k}$: number of wavelength conversions for k_{th} segment of groomed traffic flow between (s, d).
- $NF^{a,b}$: number of fibers lighted up for physical link (a, b).
- m: Modulation level parameter, $2^{2m} = M$ for M-ary QAM.
- R: Rate of each subcarrier based on different modulation level m, and it equals to $0.5 \cdot m$ Gbps when the base capacity of 1 subcarrier using BPSK is 0.5 Gbps.
- $P_{CW}^{s,d,k}$: required laser continuous wave (CW) output power on k_{th} lightpath of groomed traffic flow between (s, d).
- $BER_{s,d,k}^{m}$: BER adopting modulation level m on k_{th} lightpath of groomed traffic flow between (s, d).
- $N_{span}^{a,b}$: the total number of spans on physical lightpath (a, b).
- $K_{s,d}$: total number of traffic segments of groomed traffic flow between (s, d).
- $D'_{s,d}$: total groomed traffic flow between a source to destination (s, d) pair.
- $D'_{s,d,k}$: traffic demand on k_{th} segment of groomed traffic flow between (s, d).

- $T_{s,d,b}$: partition of traffic flow $D_{s,d}$ to be delivered through lightpaths (s,b) and (b,d) with electronic switching at node b.
- $\sigma_{s,d,k}^{a,b,n}$: equal to 1 if the k_{th} lightpath of groomed traffic flow between (s,d) is routed through fiber number n in physical link (a,b), and 0 otherwise.
- $\delta_{s,d}^{k,r}$: equal to 1 if the r_{th} routing path is chosen for k_{th} lightpath of groomed traffic flow between (s,d), and 0 otherwise.
- $t_{1,sdk}$: lower subcarrier index allocated to k_{th} lightpath of groomed traffic flow between (s,d).
- $t_{2,sdk}$: upper subcarrier index allocated to k_{th} lightpath of groomed traffic flow between (s,d).

Objective:

$$\begin{aligned}\textbf{Min} \sum_{s,d} \sum_{1\le k\le K_{s,d}} & D'_{s,d,k}\cdot(P_{SC}+P_{OT})+P_{FT}+P_{CW}^{s,d,k} \\ & + \sum_{a,b} N_{span}^{a,b}\cdot P_{AMP}\cdot NF^{a,b} \\ & + P_W \sum_{s,d} \sum_{1\le k\le K_{s,d}} N_{WC}^{s,d,k} + P_{OEO}\sum_{s,d,b} T_{s,d,b}\end{aligned} \tag{3.1}$$

Constraints:

$$NF^{a,b} = \sum_{n=1}^{NF_{max}} \bigcup_{s,d,k} \sigma_{s,d,k}^{a,b,n} \qquad \forall a,b \tag{3.2}$$

$$N_{WC}^{s,d,k} = \sum_{r=1}^{NP_{s,d}} \delta_{s,d}^{k,r}\cdot H_{s,d,r} \qquad \forall s,d,k \tag{3.3}$$

$$\sum_{r=1}^{NP_{s,d}} \delta_{s,d}^{k,r} = 1, \qquad \forall s, d, k \tag{3.4}$$

$$BER_{s,d,k}^{m} \leq BER_{th} \qquad \forall s, d, k, m \tag{3.5}$$

$$t_{2,sdk} - t_{1,sdk} = \lceil \frac{R_{TP}}{R} \rceil + \lceil \frac{GB}{F} \rceil \qquad \forall s, d, k, m \tag{3.6}$$

$$\begin{aligned} &\text{If } \bigcup_{a,b,n} \sigma_{s,d,k}^{a,b,n} \sigma_{s',d',k'}^{a,b,n} = 1, \text{ then } (t_{1,sdk} > t_{2,s'd'k'}) = 1 \\ &\qquad \text{or } \ (t_{1,sdk} < t_{2,s'd'k'}) \bigcap (t_{2,sdk} < t_{1,s'd'k'}) = 1 \\ &\qquad\qquad \forall (s, d, k), (s', d', k') \neq (s, d, k) \end{aligned} \tag{3.7}$$

$$\sum_{s,d,k} (\lceil \frac{R_{TP}}{R} \rceil + \lceil \frac{GB}{F} \rceil) \sigma_{s,d,k}^{a,b,n} \leq \frac{BW}{F} \quad \forall a, b, n \tag{3.8}$$

$$\begin{aligned} D'_{s,d} =& D_{s,d} + \sum_{(i:s)\in(i:d)} T_{i,d,s} + \sum_{(d:j)\in(s:j)} T_{s,j,d} \\ &- \sum_{b\in(s:d)} T_{s,d,b} \qquad\qquad \forall (s, d) \end{aligned} \tag{3.9}$$

The objective function in Eq. 3.1 is the power consumption of the whole network. The first and second term denote the power consumption of all OFDM-based transponders and the total power consumption of all in-line EDFAs along fibers, respectively. The third and fourth term account for the power consumption of wavelength conversions

and electronic processing (i.e., OEO conversion) due to traffic grooming. Equation 3.2 calculates the number of fibers lighted up for physical link (a, b). Equation 3.3 calculates the number of wavelength conversions for k_{th} segment of groomed traffic flow between (s, d). Equation 3.4 stipulates only one routing path is assigned to the k_{th} lightpath of groomed traffic flow between (s, d). Equation 3.5 defines the threshold on $BER^{m}_{s,d,k}$ when modulation level m for k_{th} lightpath of groomed traffic flow between (s, d) is adopted. Equation 3.6 calculates the total number of subcarriers allocated to k_{th} lightpath of groomed traffic flow between (s, d). Equation 3.7 stipulates that the allocated spectrum of any two traffic segments must be non-overlapping when they share at least one fiber at a physical link. Equation 3.8 states that the total bandwidth allocated to all lightpaths sharing the same fiber must be less or equal to the bandwidth capacity of the fiber. Equation 3.9 calculates the total groomed traffic flow between (s, d), where $(i : s) \in (i : d)$ means the node s is between i and d, $(d : j) \in (s : j)$ means the node d is between s and j, and $b \in (s : d)$ means the node b is between s and d.

3.3.2 Traffic Grooming

Each lightpath segment corresponds to a transponder in one direction. To decrease the power consumption of all transponders, we need to minimize the number of active transponders for our heuristic solutions by grooming low-capacity traffic connections such that the effective data rate of each lightpath segment is closer its upper bound R_{TP}. Equipping any intermediate node with OEO conversion for launching a lightpath, grooming mechanism accommodates the input traffic of multiple input ports with different lightpaths by possibly using a single transponder and a different modulation level. To this end, we adopt a traffic grooming technique in [61] to minimize the number of traffic segments $\sum_{s,d} K_{s,d}$ of traffic flow between (s, d).

To solve the mixed integer programming problem of traffic grooming, we implement

the iterative grooming algorithm [63]. The iterative algorithm sweeps the maximum grooming size Q ($0 < Q \leq R_{TP}$) by searching for traffic segment of $D'_{s,d}$ smaller than R_{TP}. For grooming smaller traffic segments first, the maximum grooming size Q is increased with step size q. During each iteration, traffic segment of $D'_{s,d}$ that smaller than R_{TP} and less than or equal to Q, is searched for further grooming. For any intermediate node b between s and d, the grooming size $G_{s,d}$ for incomplete $D'_{s,d}$ must be less than or equal to the remaining capacity of $D'_{s,b}$ and $D'_{b,d}$ to avoid extra lightpath for s, b and b, d. Then, the traffic size $G_{s,d}$ for incomplete $D'_{s,d}$ is groomed with $D'_{s,b}$ and $D'_{b,d}$. If the remaining incomplete $D'_{s,d}$ still exist, any other intermediate node $a \neq b$ is chosen to perform grooming until $mod(D'_{s,d}, R_{TP}) = 0$. More details are described in Algorithm 2.

3.3.3 Spectrum Allocation with Wavelength Conversion

The spectrum allocation is performed through routing and wavelength assignment according to a first-fit mechanism. By equipping each node with reconfigurable all-optical wavelength converters (supporting data rates more than 100 Gb/s) [64], the utilization of fiber connection on each physical link can be more efficient through spectrum reallocation. Compared to the saved energy due to reduced number of EDFAs along fibers, the energy costs of all-optical wavelength conversion is small [65].

3.4 Proposed Optimization Methods

Due to the fact that one or a number of EDFAs are deployed in each optical link, and each additional lightpath passing through the EDFA consumes some additional power, the number of EDFAs traversed by each lightpath is certainly an important factor in the power consumption and should be minimized. In this study, K shortest paths (KSP) [66]

Algorithm 2 Traffic Grooming

Input: Initial groomed traffic $\{D'_{s,d}\} = \{D_{s,d}\}$;

Step size q; Data rate capacity of transponder R_{TP};

Maximum grooming size Q $(0 < Q \leq R_{TP})$;

Output: Groomed traffic matrix $[D'_{s,d}]$;

1: Sweeping maximum grooming size Q by searching for traffic segment of $D'_{s,d}$ smaller than R_{TP}, that is, satisfying $0 < mod(D'_{s,d}, R_{TP}) \leq Q$;

2: Finding any intermediate node b between s and d, and the grooming size $G_{s,d}$ for incomplete $D'_{s,d}$ must equal to $min\{mod(D'_{s,d}, R_{TP}), R_{TP} - mod(D'_{s,b}, R_{TP}), R_{TP} - mod(D'_{b,d}, R_{TP})\}$;

3: If $mod(D'_{s,b}, R_{TP}) > 0$ and $mod(D'_{b,d}, R_{TP}) > 0$, then update the value by $D'_{s,d} - G_{s,d}$, $D'_{s,b} + G_{s,d}$, $D'_{b,d} + G_{s,d}$;

4: If the remaining incomplete $D'_{s,d}$ still exist, choosing any other intermediate node $a \neq b$ to perform grooming, and stop when $mod(D'_{s,d}, R_{TP}) = 0$;

5: Grooming traffic flows for all node pairs (s, d);

6: Increasing maximum grooming size Q with size q, and repeat steps 1-5;

7: **return** $[D'_{s,d}]$;

are prepared for each node pair as the candidate paths and are used in the constraints in Eq. 3.2-3.9 in a large searching space of a size:

$$M_c^{\sum_{s,d} K_{s,d}} \times K^{\sum_{s,d} K_{s,d}} \tag{3.10}$$

where M_c is the number of candidate modulations, and $K_{s,d} = \lceil \frac{D'_{s,d}}{R_{TP}} \rceil$ denotes the number of traffic lightpaths between (s, d) after traffic grooming.

3.4.1 Simulated Annealing based Approach

Since the above formulation is nonlinear and computationally intractable with a large search space, we solve it using simulated annealing (SA) to achieve a good approximation to the global optimum solution [58]. As described in Algorithm 3, let vector $\mathbf{k}$ with $\sum_{s,d} K_{s,d}$ elements represents the randomly chosen routing path for all node pairs in the network topology. Let vector $\mathbf{m}$ with $\sum_{s,d} K_{s,d}$ elements represents the randomly chosen modulation level for traffic flow between all node pairs. After selecting random matrix $(\mathbf{k}, \mathbf{m})$ as initial solution $(\hat{\mathbf{k}}, \hat{\mathbf{m}})$, traffic grooming for input traffic flows through Algorithm 2 is performed, and power consumption of OEO conversion is calculated. Then, spectrum allocation is performed through routing and wavelength assignment according to a first-fit mechanism, and power consumption of in-line EDFAs and wavelength conversion are calculated. Based on the above choice of routing path, modulation level, groomed traffic flow, and allocated bandwidth, corresponding P_{CW} and L of each lightpath is decided by running Algorithm 1. If no solution meets the BER_{th} in Algorithm 1, generating new trail factor $(\tilde{\mathbf{k}}, \tilde{\mathbf{m}})$ and repeating steps 3-5. If solution from running Algorithm 1 exists, computing the objective function $f(\mathbf{k}, \mathbf{m})$ ($f(\cdot)$ defined in Eq. 3.1) for the energy of the system at initial solution $(\hat{\mathbf{k}}, \hat{\mathbf{m}})$. Then, after generating new trail factor $(\tilde{\mathbf{k}}, \tilde{\mathbf{m}})$, the constraints in Eq. 3.2-3.9 and $\Delta C = f(\tilde{\mathbf{k}}, \tilde{\mathbf{m}}) - f(\hat{\mathbf{k}}, \hat{\mathbf{m}})$ decide whether a newly derived solution should be accepted or not. After decreasing temperature according to the cooling schedule $T(Iter)$, next searching iteration is implemented by repeating steps 3-9. When all the searching iterations $Iter$ have been explored, the final $(\hat{\mathbf{k}}, \hat{\mathbf{m}})$ is returned as the routing and modulation solution.

Key parameters of the formulated SA mechanism are defined as follows:

{a} Cooling schedule. Cooling schedule includes initialization temperature T_i, attenuation function $T(Iter)$ ($Iter$ is the number of the iteration) and termination temper-

ature T_f. T_i temperature should be high enough such that the process can escape from local minima, while low enough to ensure a thorough search in the regions near solutions. $T(Iter)$ should maintain an equilibrium within the system. The most common cooling schedule was proposed by Kirkpatrick [58], which is based on a geometric decrement function:

$$T(Iter) = \alpha \times T(Iter - 1) \tag{3.11}$$

where α is a constant chosen in the range $0.8 < \alpha < 1$.

{b} Transition acceptance probability. The transition acceptance probability is the chance that new combination of $\tilde{\mathbf{k}}$ and $\tilde{\mathbf{m}}$ can be accepted when $\Delta C > 0$. Considering relative changing of the energy and the absolute changing ΔC, Tsallis proposed the following acceptance probability [59]:

$$Prob(Iter) = [1 - \frac{h \times \Delta C}{T(Iter)}]^{\frac{1}{h}} \tag{3.12}$$

where h is a random nonzero real number.

{c} New combination generation. The new combination of $\mathbf{k}$ and $\mathbf{m}$ generator should possess small random changes, and allow all possible combinations based on the network topology to be reached. For integer control variables, the new trial $(\tilde{\mathbf{k}}, \tilde{\mathbf{m}})$ for each node pair with a fixed temperature are generated according to

$$\theta_{i+1} = \theta_i + \Delta\theta \tag{3.13}$$

where $\theta_0 = 0$. When $\theta_i < 2\pi$ or $\theta_i < 0$, $\Delta\theta = (2\pi \div \bar{W})$, otherwise $\Delta\theta = -(2\pi \div \bar{W})$.

Algorithm 3 Simulated Annealing (SA)

Input: Initial annealing temperature T_i; Temperature decrement factor α; Final temperature T_f; Iteration number $Iter$;

Output: Routing and modulation solution $(\hat{\mathbf{k}}, \hat{\mathbf{m}})$;

1: Generating uniformly distributed random matrix $(\mathbf{k}, \mathbf{m})$ based on the network topology, and select it as initial random solution $(\hat{\mathbf{k}}, \hat{\mathbf{m}})$;

2: Performing traffic grooming for input traffic flows $[D_{s,d}]$ through Algorithm 2, and calculate OEO conversion cost P_{OEO} for electronic switching;

3: Performing spectrum allocation through routing and wavelength assignment according to a first-fit mechanism, and calculate fiber link costs P_{AMP} and optical conversion costs P_W;

4: Run adaptive modulation searching procedure in Algorithm 1 for corresponding P_{CW}, L value of each lightpath. If no solution meet the BER_{th}, jump to step 6;

5: Computing initial objective function $f(\mathbf{k}, \mathbf{m})$ for initial solution $(\hat{\mathbf{k}}, \hat{\mathbf{m}})$ and probability of acceptance $Prob(Iter)$;

6: Generating new trail phase factor $(\tilde{\mathbf{k}}, \tilde{\mathbf{m}})$;

7: Repeat steps 3-5;

8: Constraints in Eq. 3.2-3.9 and $\Delta C = f(\tilde{\mathbf{k}}, \tilde{\mathbf{m}}) - f(\hat{\mathbf{k}}, \hat{\mathbf{m}})$ decide whether a newly derived solution should be accepted or not. If the condition is met, the current stored solution is replaced with the new one, and the objective function is set to the new value. If not, it keeps the old solution;

9: Decreasing temperature according to the cooling schedule $T(Iter)$;

10: Increasing iteration count $Iter = Iter + 1$, and repeat steps 3-9;

11: **return** $(\hat{\mathbf{k}}, \hat{\mathbf{m}})$;

3.4.2 Suboptimal Solution based on Iterative Flipping Algorithm

Alternatively, we apply iterative flipping (IF) algorithm as described in Algorithm 4 to achieve a suboptimal solution. Let vector $\mathbf{k}$ $(k = 1, \cdots, K)$ with $\sum_{s,d} K_{s,d}$ elements rep-

resent the chosen routing path for all node pairs. Let vector $\mathbf{m}$ ($m = 1, \cdots, M_c$) with $\sum_{s,d} K_{s,d}$ elements represent the chosen modulation level for traffic flow between all node pairs. After setting ($\mathbf{k} = \{\mathbf{1}\}, \mathbf{m} = \{\mathbf{1}\}$) as initial solution, traffic grooming for input traffic flows through Algorithm 2 is performed, and power consumption of OEO conversion is calculated. Then, spectrum allocation is performed through routing and wavelength assignment according to a first-fit mechanism, and power consumption of in-line EDFAs and wavelength conversion are calculated. Based on the above choice of routing path, modulation level, groomed traffic flow, and allocated bandwidth, corresponding P_{CW} and L of each lightpath is decided by running Algorithm 1. If no solution meets the BER_{th} in Algorithm 1, increasing the first modulation factor $\mathbf{m}_{[v=1]}$ in vector $\mathbf{m}$ and repeating steps 2-4. If solution from running Algorithm 1 exists, computing the objective function $f(\mathbf{k}, \mathbf{m})$ ($f(\cdot)$ defined in Eq. 3.1) at state ($\mathbf{k} = \{\mathbf{1}\}, \mathbf{m} = \{\mathbf{1}\}$) as initial solution. Then, after increasing the first modulation factor $\mathbf{m}_{[v=1]}$ in vector $\mathbf{m}$, the constraints in Eq. 3.2-3.9 along with $\Delta C = f(\tilde{\mathbf{k}}, \tilde{\mathbf{m}}) - f(\mathbf{k}, \mathbf{m})$ decide whether a newly derived solution should be accepted or reverted to previous $\mathbf{m}_{[v=1]}$. The first modulation factor $\mathbf{m}_{[v=1]}$ is kept increasing until all candidate modulation levels are explored. After increasing traffic segment number as $v = 2$, keep repeating steps 3-8 until all traffic lightpaths are explored. Then, increasing the first routing factor $\mathbf{k}_{[v=1]}$ in vector $\mathbf{k}$, and repeating steps 2-9. The first routing factor $\mathbf{k}_{[v=1]}$ is kept increasing until all candidate routing paths are explored. After increasing traffic segment number as $v = 2$, keep repeating steps 2-11 until all traffic lightpaths are explored. When all $M_c \times K \times \sum_{s,d} K_{s,d}$ possibilities for "Flipping" have been explored, it returns a value corresponding to the suboptimal solution. So, the complexities of proposed algorithm is the multiplication of number of candidate modulation levels, number of candidate routing paths, and number of all lightpath after traffic grooming.

3.5 Preliminary Results

Case studies are conducted to verify the formulated system and observe its performance in terms of energy efficiency and computation complexity, and compare it with previously reported design principles and approaches. An 5-node network, 8-node network and 14-node NSFNet are adopted as shown in Fig. 3.2, Fig. 3.3, and Fig. 3.4, respectively; and the launched traffic of each node pair is expressed in the corresponding entry of a traffic matrix scaled by a factor, where the base traffic matrix (with a unity scaling factor) is shown in Table 3.1, Table 3.2 and Table 3.3. We take $BER_{th} = 10^{-4}$ without using FEC [67] and the upper bound of laser output power P_{CW}^{up} as 40mW, by which the optical reach is limited according to Subsection 2.2.2 and Subsection 2.2.3. BW as 1THz per fiber on each physical link. $NF_{max} = 4$ for 5-node network, 8 for 8-node network and 10 for NSFNet as the maximum number of fibers available in each physical link. Here, we preset the parameters of the SA mechanism as $T_i = 100$, $T_f = 0.00001$, $\alpha = 0.9$, $h = 5$. We define $m = 1$ for QPSK, $m = 2$ for 16-QAM, $m = 3$ for 64-QAM, $m = 4$ for 256-QAM, $m = 5$ for 1024-QAM to be the candidate modulation levels that the transmitter side can adaptively take.

By observing the simulation results of Algorithm 3 and Algorithm 4, we find their computational complexity and running time are mainly determined by the number of searching iterations. Thus, the number of searching iterations are taken as the metric in evaluating the proposed IF method and SA based scheme. Since the performance of SA can be seriously affected by initial condition, we select the best result by running the SA scheme for 10 times with randomly selected initiate conditions in the comparison with proposed IF method.

Both dynamic and static traffic scenarios are considered. In the former, a connection request arrives in a node pair according to Poisson distribution of parameter λ, and it

leaves/departs after an exponential amount of holding time with a parameter μ [68]. The arrival and departure procedures are shown in Fig. 3.5. The data rate of each connection is uniformly distributed between 0 and 10 Gbps. Since the system is steady after 5000 connection requests, we launch 50000 connection requests for each simulation.

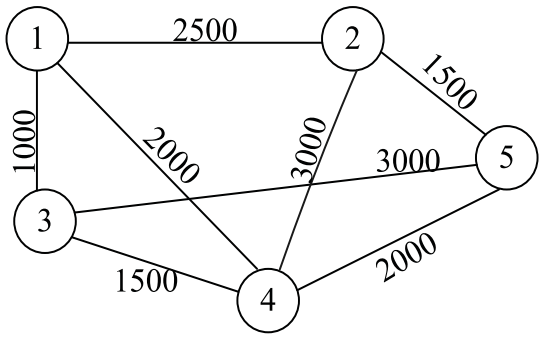

Figure 3.2: 5-Node Topology (Link lengths in unit of km)

Table 3.1: Base Traffic Matrix for 5-Node Network (In unit of Gbps, Total=200Gbps)

Node	1	2	3	4	5
1	0	8	14	10	8
2	8	0	12	6	12
3	14	12	0	10	4
4	10	6	10	0	16
5	8	12	4	16	0

Figures 3.6-3.11 show the comparison among all the considered schemes denoted as follows:

{1} Fixed Modulation level (16-QAM) with shortest path only ($K = 1$).

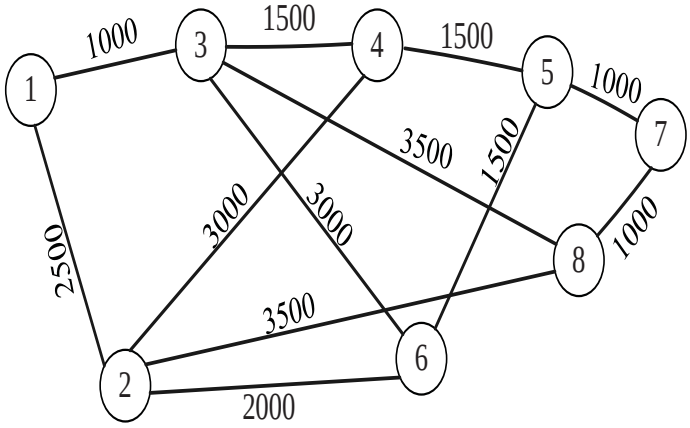

Figure 3.3: 8-Node Topology (Link lengths in unit of km)

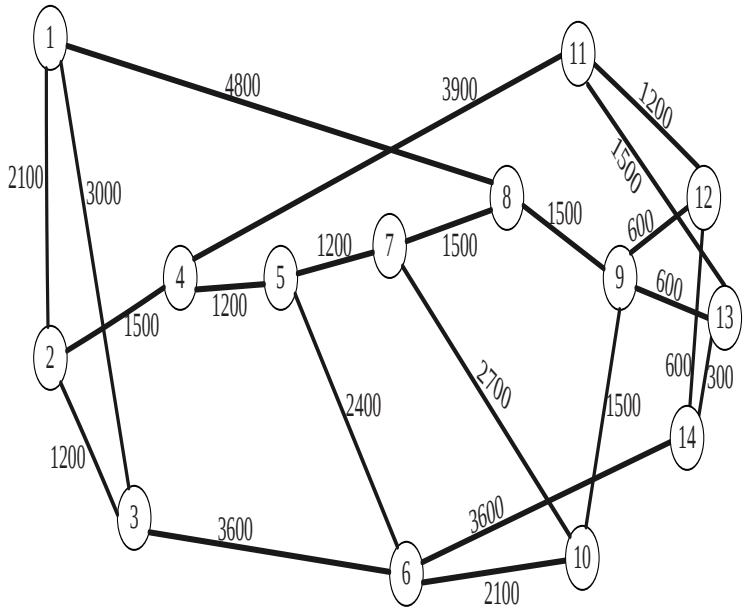

Figure 3.4: NSFNet Topology (Link lengths in unit of km)

Table 3.2: Base Traffic Matrix for 8-Node Network (In unit of Gbps, Total=500Gbps)

Node	1	2	3	4	5	6	7	8
1	0	4	4	2	20	6	8	4
2	4	0	6	6	2	2	2	8
3	4	6	0	10	12	8	6	58
4	2	6	10	0	26	2	2	4
5	20	2	12	26	0	30	6	2
6	6	2	8	2	30	0	2	2
7	8	2	6	2	6	2	0	6
8	4	2	58	4	2	2	6	0

Table 3.3: Base Traffic Matrix for NSFNet (In unit of Gbps, Total=1Tbps)

Node	1	2	3	4	5	6	7	8	9	10	11	12	13	14
1	0	2	2	2	2	4	2	2	4	2	2	2	2	2
2	2	0	2	2	8	4	2	6	4	6	2	6	2	4
3	2	2	0	2	4	4	11	20	6	2	2	2	2	4
4	2	2	2	0	2	2	2	2	2	4	2	2	2	2
5	2	8	4	2	0	4	4	7	4	4	2	6	2	6
6	4	4	4	2	4	0	2	2	4	2	2	2	2	4
7	2	2	11	2	4	2	0	9	4	20	2	8	2	4
8	2	6	20	2	7	2	9	0	27	7	4	4	4	4
9	4	4	6	2	4	4	4	27	0	50	2	9	4	2
10	2	6	2	4	4	2	20	7	50	0	2	2	4	2
11	2	2	2	2	2	2	2	4	2	2	0	2	2	51
12	2	6	2	2	6	2	8	4	9	2	2	0	2	47
13	2	2	2	2	2	2	2	4	4	4	2	2	0	2
14	2	4	4	2	6	4	4	4	2	2	51	47	2	0

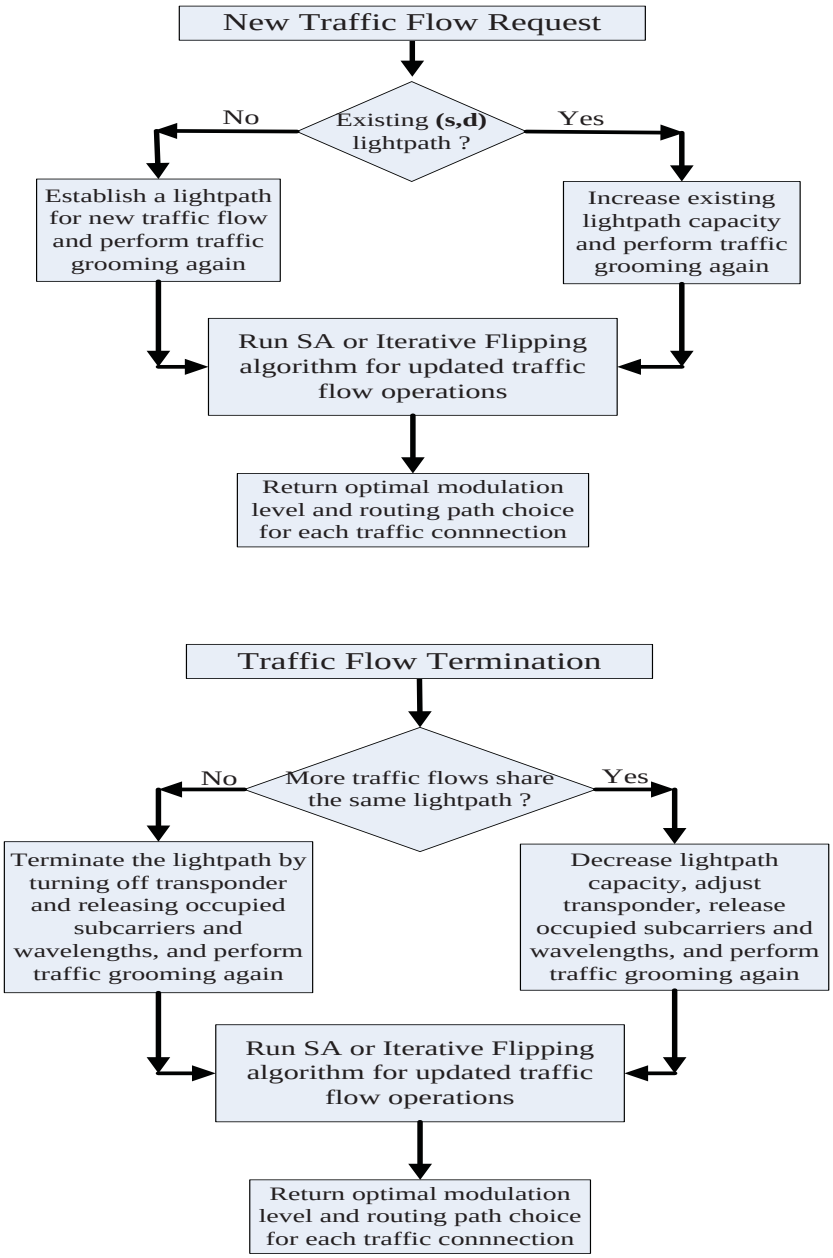

Figure 3.5: Flowchart for evaluating dynamic scenario

{2} Fixed Modulation level (16-QAM) with K-shortest paths ($K > 1$), and searching process based on SA.

{3} Adaptive Modulation levels with shortest path only ($K = 1$), and searching process based on SA.

{4} Adaptive Modulation levels with K-shortest paths ($K > 1$), and searching process based on SA.

{5} Adaptive Modulation levels with shortest path only ($K = 1$), and searching process based on IF.

{6} Adaptive Modulation levels with K-shortest paths ($K > 1$), and searching process based on IF.

Table 3.4: Spectrum Utilization for 5-Node Network with Static Traffic

Load	Algorithm	Average Spectrum Utilization (%)				
0.4 Tbps		$Iter = 35$	$Iter = 70$	$Iter = 100000$	$Iter = 78125$	$Iter = 10^7$
	Fixed via SA, $K = 1$	7.4	7.4	7.4	N/A	N/A
	Fixed via SA, $K = 2$	8.2	7.8	7.4	N/A	N/A
	Adaptive via SA, $K = 1$	6.9	6.9	6.9	N/A	N/A
	Adaptive via SA, $K = 2$	7.5	7.3	6.5	N/A	N/A
	Adaptive via IF, $K = 1, 2$	8.5	6.7	N/A	N/A	N/A
	Adaptive via ES, $K = 1, 2$	N/A	N/A	N/A	6.9	6.3
2 Tbps		$Iter = 60$	$Iter = 120$	$Iter = 100000$	$Iter = 2.4*10^8$	$Iter = 10^{12}$
	Fixed via SA, $K = 1$	10.3	10.3	10.3	N/A	N/A
	Fixed via SA, $K = 2$	11.5	10.9	10.2	N/A	N/A
	Adaptive via SA, $K = 1$	10.1	10.1	10.1	N/A	N/A
	Adaptive via SA, $K = 2$	10.7	10.5	9.8	N/A	N/A
	Adaptive via IF, $K = 1, 2$	11.7	9.5	N/A	N/A	N/A
	Adaptive via ES, $K = 1, 2$	N/A	N/A	N/A	9.8	9.4

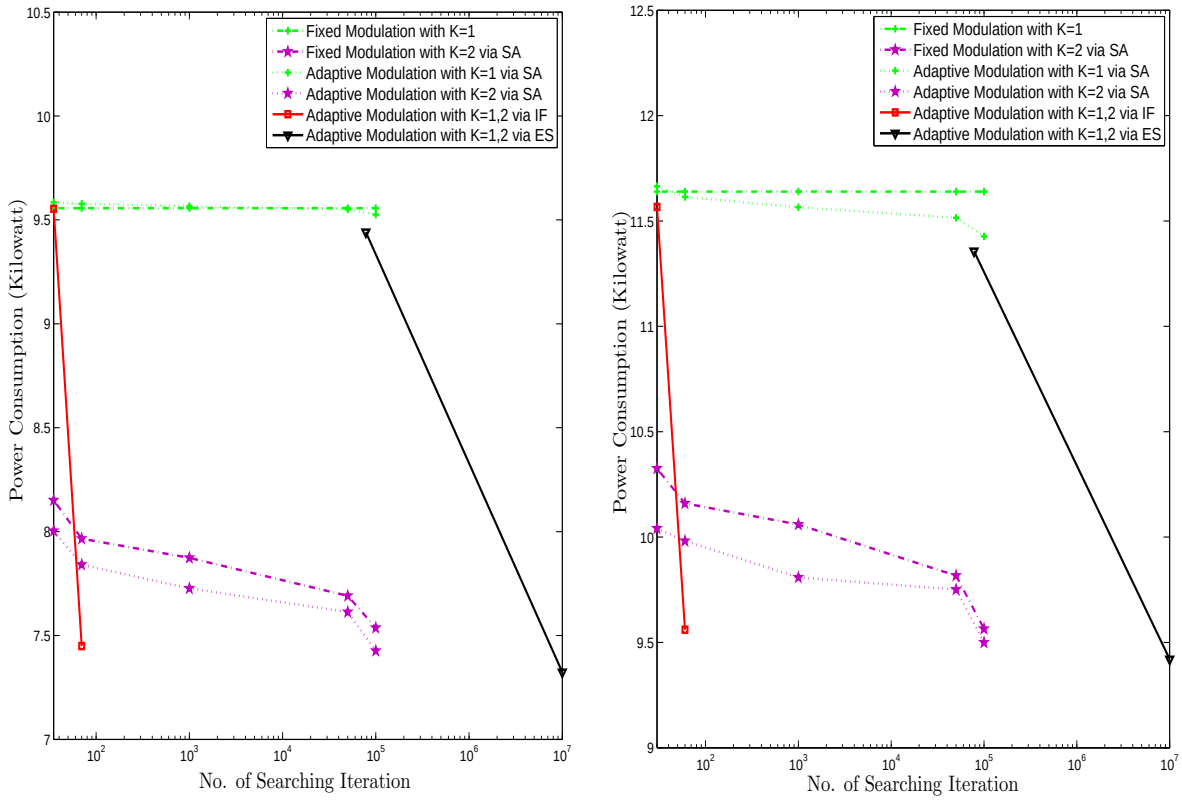

(a) Static Traffic Load 0.4 Tbps

(b) Dynamic Traffic Load 0.66 Tbps

Figure 3.6: Power Consumption of 5-Node Network VS Searching Iteration

Since the optimization problem with a large search space is NP-Complete, to validate the effectiveness of SA and proposed IF method, we solve the problem of 5-node network with low traffic loads and small number of candidate routing paths through exhaustive search (ES). As shown in Fig. 3.6 and Fig. 3.7, heuristic solutions from both SA and IF can achieve a good approximation to the optimal solutions from ES. Comparing to ES or SA method, the proposed IF method can approach the optimal solutions through considerably low computational complexity in terms of the number of iterations.

For practical scenarios, in the 8-node network, when the traffic load is light, {3} or

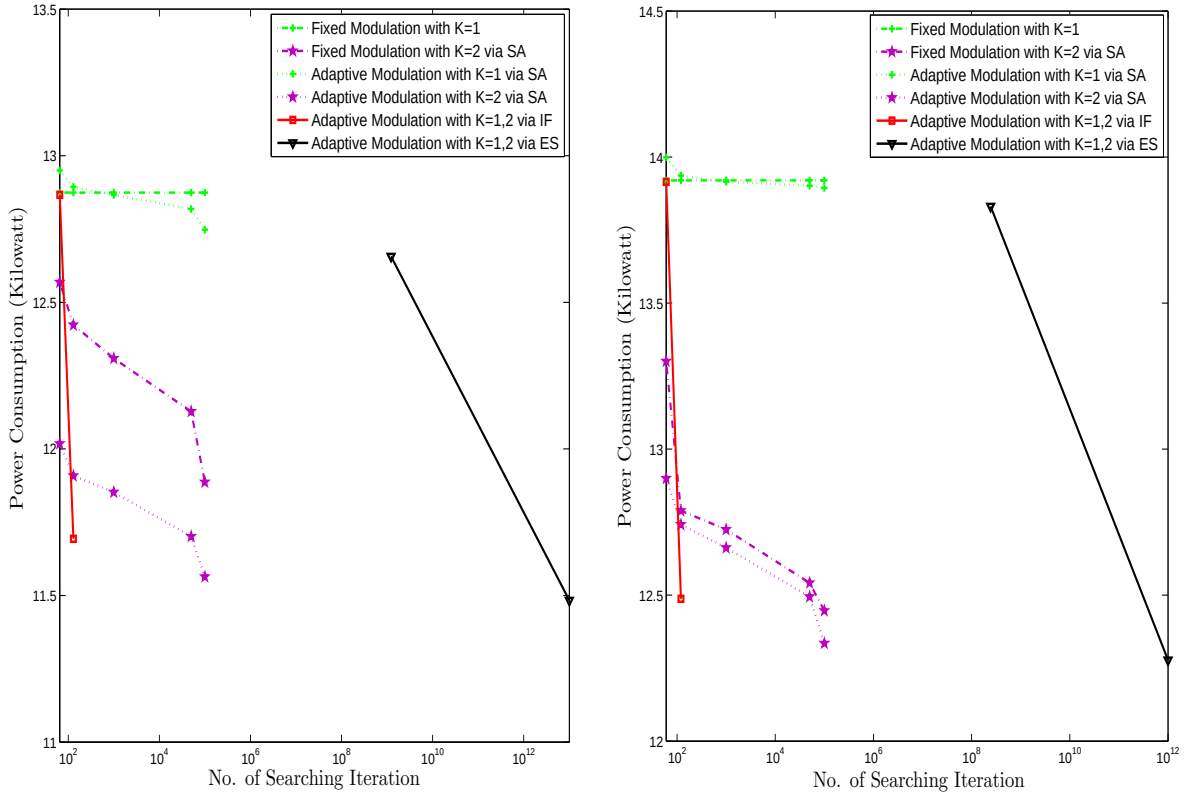

(a) Static Traffic Load 2 Tbps

(b) Dynamic Traffic Load 2.84 Tbps

Figure 3.7: Power Consumption of 5-Node Network VS Searching Iteration

{5} yields very similar energy efficiency to that with fixed modulation {1}, as in Fig. 3.8. This is due to the light traffic loads in which only a small number of fibers along each network link are used under all the candidate modulation levels. Note that the number of lightpaths, or equivalently, the number of active transponders, serves as a dominating factor on the energy consumption, whereby the choice of modulation becomes not that significant. On the other hand, when the traffic load is heavy as in Fig. 3.9, {3} consumes $3\% - 6\%$ less total power than that by {1}, and {5} consumes $5\% - 7\%$ less total power than that by {1}, due to the tradeoff between the power saved by reduced number of fibers

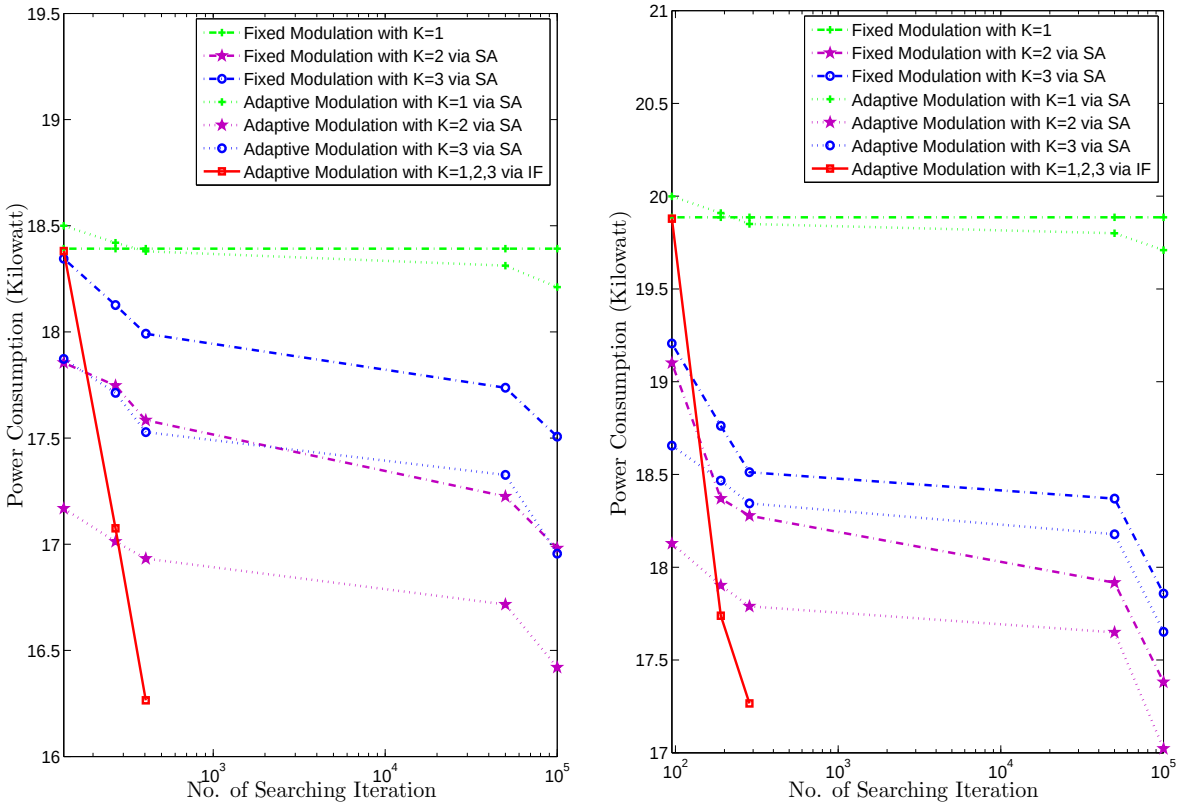

(a) Static Traffic Load 2 Tbps

(b) Dynamic Traffic Load 3.35 Tbps

Figure 3.8: Power Consumption of 8-Node Network VS Searching Iteration

under higher modulation levels and that consumed by the corresponding transponders.

By extending the candidate routing paths as $K = 2$ shortest path for all traffic conditions, {4} consumes $2\% - 7\%$ less total power than that by {2}; {6} consumes $4\% - 12\%$ less total power than that by {2}. Meanwhile, when the traffic load is light, {2} or {4} yields $3\% - 25\%$ more power saving comparing to {1} or {3}, respectively; {6} yields $2.5\% - 23\%$ more power saving comparing to {5}. This is due to the fact that the number of active transponders can be reduced not only by adaptively using higher modulation levels, but also via more routing options such that better traffic grooming

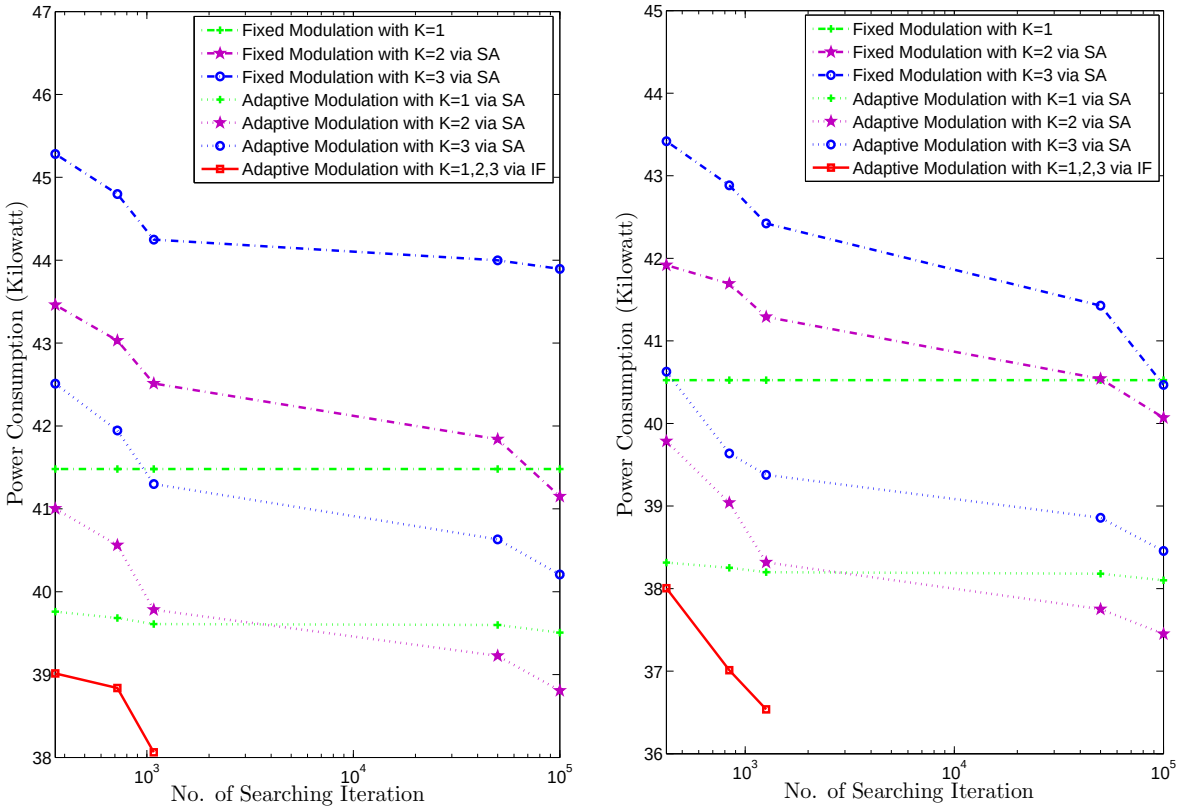

(a) Static Traffic Load 15 Tbps

(b) Dynamic Traffic Load 12.53 Tbps

Figure 3.9: Power Consumption of 8-Node Network VS Searching Iteration

result using less EDFAs/transponders can be obtained. When the traffic load is heavy, on the other hand, {2} or {4} with $K = 2$ takes more searching iterations to achieve better performance than that by {1} or {3}, respectively. Nevertheless, by further increasing candidate routing paths as $K = 3$, the performance of {2} and {4} are getting worse. Specifically, when traffic load is low, {2} or {4} with $K = 3$ even yields worse performance than that of $K = 2$, but still better than that of $K = 1$. When traffic load is high, {2} or {4} with $K = 3$ is worst among all the cases. This is due to the greediness of the algorithm, where a connection request consuming the least amount of power by

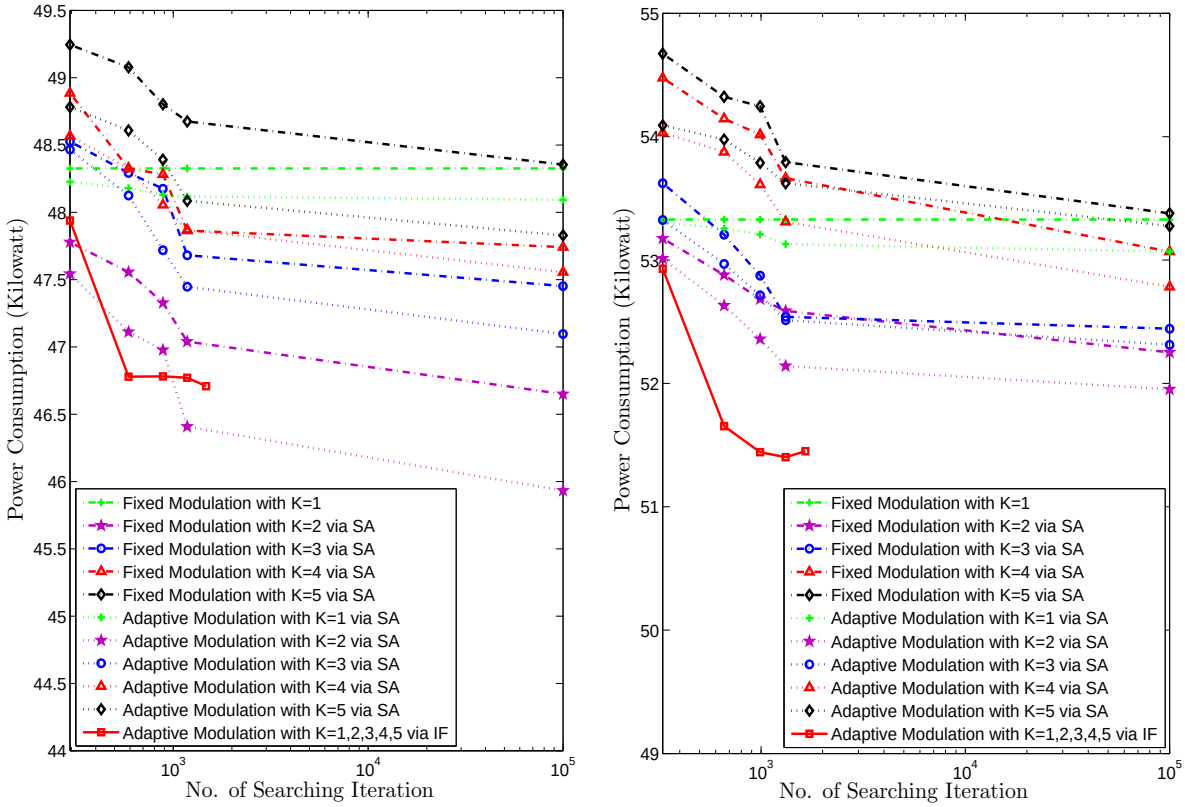

(a) Static Traffic Load 4 Tbps

(b) Dynamic Traffic Load 4.98 Tbps

Figure 3.10: Power Consumption (Kilowatt) of NSFNet VS Searching Iteration

taking a longer path, may occupies more network resources such that the subsequent allocated connections consume even more power than saved. With smaller K yields another important merit in terms of smaller search space, where the SA can better explore the whole search space and thus achieve better results. By considering the tradeoff between search space and consumed transponders and EDFAs, SA with $K = 2$ mechanism outperforms all the other counterparts.

As expected, Figs. 3.8-3.9 show that the proposed iterative flipping (IF) based suboptimal mechanism is found able to achieve a good compromise between the performance

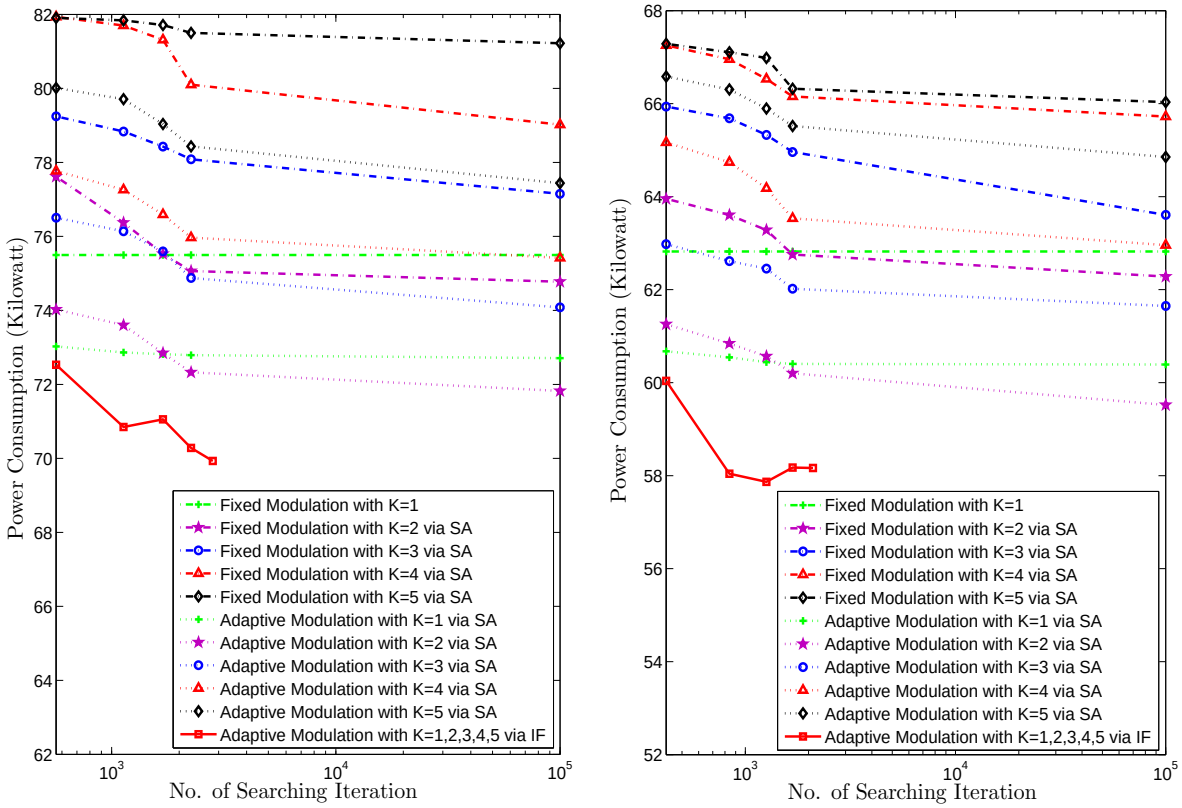

(a) Static Traffic Load 15 Tbps

(b) Dynamic Traffic Load 12.12 Tbps

Figure 3.11: Power Consumption (Kilowatt) of NSFNet VS Searching Iteration

and computation complexity. It yields noticeably improvements with the additional design dimension on modulation levels and routing paths compared with {2}, {3}, {4}, with relatively the least search iteration. Specifically, the proposed IF method yields better performance $(1\% - 11\%)$ than that of the SA based schemes provided with the same computational complexity in terms of the number of iterations in the solution search. With the increase of K, the performance of IF method is getting better with only a slight increase on the number of iterations. Particularly, when the traffic load is heavy, the IF method with less than 1,300 searching iterations can achieve better performance

Table 3.5: Spectrum Utilization for 5-Node Network with Dynamic Traffic

Load	Algorithm	Average Spectrum Utilization (%)				
0.66 Tbps		$Iter = 35$	$Iter = 70$	$Iter = 100000$	$Iter = 78125$	$Iter = 10^7$
	Fixed via SA, $K = 1$	8.2	8.2	8.2	N/A	N/A
	Fixed via SA, $K = 2$	9.0	8.6	8.0	N/A	N/A
	Adaptive via SA, $K = 1$	7.6	7.6	7.6	N/A	N/A
	Adaptive via SA, $K = 2$	8.3	8.0	7.2	N/A	N/A
	Adaptive via IF, $K = 1, 2$	9.4	7.4	N/A	N/A	N/A
	Adaptive via ES, $K = 1, 2$	N/A	N/A	N/A	7.6	6.9
2.84 Tbps		$Iter = 65$	$Iter = 130$	$Iter = 100000$	$Iter = 1.2*10^9$	$Iter = 10^{13}$
	Fixed via SA, $K = 1$	11.3	11.3	11.3	N/A	N/A
	Fixed via SA, $K = 2$	12.7	12.0	11.2	N/A	N/A
	Adaptive via SA, $K = 1$	11.0	11.0	11.0	N/A	N/A
	Adaptive via SA, $K = 2$	11.8	11.6	10.8	N/A	N/A
	Adaptive via IF, $K = 1, 2$	12.9	10.5	N/A	N/A	N/A
	Adaptive via ES, $K = 1, 2$	N/A	N/A	N/A	10.8	10.4

$(1\% - 4\%)$ than SA scheme with 100,000 iteration.

Similar results were observed in the 14-node NSFNET. When the traffic load is light as in Fig. 3.10, {3} and {5} yield very similar energy efficiency to that with fixed modulation {1}, and achieve noticeable improvement $(3\% - 5\%)$ when the traffic load is heavy as shown in Fig. 3.11. We have seen SA with $K = 2$ mechanism outperforms all the other counterparts. Fig. 3.10 and Fig. 3.11 also show that the proposed iterative flipping method yields better performance $(1\% - 6\%)$ than that of the SA based schemes provided with the same computational complexity (i.e., the number of iterations in the solution search). Particularly, the IF method with iteration number less than 3,000 still can achieve lower power consumption $(1\% - 4\%)$ than SA with 100,000 iteration when traffic

Table 3.6: Spectrum Utilization for 8-Node Network with Static Traffic

Load	Algorithm	Average Spectrum Utilization (%)			
2 Tbps		$Iter = 95$	$Iter = 190$	$Iter = 285$	$Iter = 100000$
	Fixed via SA, $K = 1$	13.5	13.5	13.5	13.5
	Fixed via SA, $K = 2$	14.5	13.9	13.4	12.5
	Fixed via SA, $K = 3$	15.3	15.0	13.9	12.9
	Adaptive via SA, $K = 1$	12.8	12.8	12.8	12.8
	Adaptive via SA, $K = 2$	13.9	13.5	12.5	12.0
	Adaptive via SA, $K = 3$	15.3	14.2	13.9	12.7
	Adaptive via IF, $K = 1, 2, 3$	16.7	12.5	11.1	N/A
15 Tbps		$Iter = 420$	$Iter = 840$	$Iter = 1260$	$Iter = 100000$
	Fixed via SA, $K = 1$	41.4	41.4	41.4	41.4
	Fixed via SA, $K = 2$	44.4	43.1	41.2	37.5
	Fixed via SA, $K = 3$	48.6	47.2	45.8	40.3
	Adaptive via SA, $K = 1$	30.9	30.9	30.9	30.9
	Adaptive via SA, $K = 2$	33.3	31.9	30.6	29.2
	Adaptive via SA, $K = 3$	41.7	37.5	36.1	32.9
	Adaptive via IF, $K = 1, 2, 3$	34.7	30.6	27.8	N/A

load is more than 4 Tbps.

Given maximum number of fibers (1THz per fiber) available on each physical link, we present the average spectrum utilization of all physical links with respect to lowest power consumption for 5-node, 8-node, and NSFNet networks under different traffic scenarios. Under the same simulation parameters, average spectrum utilization are calculated corresponding to each case in Figs. 3.6-3.11. For 5-Node network in Table 3.4-3.5, ES outperforms IF, and has similar performance as SA when the traffic loads are small and $K = 1$. By increasing number of routing path as $K = 2$, ES with extremely high

Table 3.7: Spectrum Utilization for 8-Node Network with Dynamic Traffic

Load	Algorithm	Average Spectrum Utilization (%)			
3.35 Tbps		$Iter = 135$	$Iter = 270$	$Iter = 405$	$Iter = 100000$
	Fixed via SA, $K = 1$	18.3	18.3	18.3	18.3
	Fixed via SA, $K = 2$	19.4	18.5	18.0	16.7
	Fixed via SA, $K = 3$	20.8	19.4	18.3	17.1
	Adaptive via SA, $K = 1$	16.8	16.8	16.8	16.8
	Adaptive via SA, $K = 2$	18.1	16.7	16.3	15.7
	Adaptive via SA, $K = 3$	18.8	17.7	16.9	15.9
	Adaptive via IF, $K = 1, 2, 3$	19.4	16.7	15.3	N/A
12.53 Tbps		$Iter = 360$	$Iter = 720$	$Iter = 1080$	$Iter = 100000$
	Fixed via SA, $K = 1$	44.4	44.4	44.4	44.4
	Fixed via SA, $K = 2$	48.6	46.8	44.4	40.3
	Fixed via SA, $K = 3$	52.8	50.0	48.6	45.8
	Adaptive via SA, $K = 1$	34.7	34.7	34.7	34.7
	Adaptive via SA, $K = 2$	37.5	36.1	34.9	33.5
	Adaptive via SA, $K = 3$	40.3	38.9	37.5	36
	Adaptive via IF, $K = 1, 2, 3$	33.7	31.3	27.1	N/A

computational complexity only slightly outperforms SA or IF with low computational complexity. By increasing traffic loads to around 2 Tbps, ES with extremely high computational complexity slightly outperforms SA or IF under different number of routing path K. For 8-Node network in Table 3.6-3.7, adaptive modulation scheme slightly outperforms fix modulation scheme when the traffic loads is light. When the traffic load is heavy, adaptive modulation scheme considerably occupies less spectrum than fix modulation scheme. On the other hand, the lower average spectrum utilization is achieved when $K = 2$ for both adaptive modulation via SA and fix modulation via SA. However,

Table 3.8: Spectrum Utilization for NSFNet Network with Static Traffic

Load	Algorithm	Average Spectrum Utilization (%)					
		$Iter = 295$	$Iter = 590$	$Iter = 885$	$Iter = 1180$	$Iter = 1475$	$Iter = 100000$
4 Tbps	Fixed via SA, $K = 1$	13.5	13.5	13.5	13.5	13.5	13.5
	Fixed via SA, $K = 2$	14.8	14.2	13.6	13.4	13.4	12.5
	Fixed via SA, $K = 3$	14.9	14.4	13.9	13.6	13.5	13.1
	Fixed via SA, $K = 4$	16.5	15.9	15.3	15.0	14.8	13.6
	Fixed via SA, $K = 5$	16.8	15.9	15.5	15.3	14.8	14.2
	Adaptive via SA, $K = 1$	13.0	13.0	13.0	13.0	13.0	13.0
	Adaptive via SA, $K = 2$	13.6	13.4	13.3	13.1	13.1	11.9
	Adaptive via SA, $K = 3$	13.5	13.4	13.1	12.8	12.6	12.4
	Adaptive via SA, $K = 4$	14.8	14.2	13.9	13.6	13.3	12.9
	Adaptive via SA, $K = 5$	14.6	14.3	13.9	13.7	13.6	13.0
	Adaptive via IF, $K = 1, 2, 3, 4, 5$	14.2	12.5	12.4	12.4	12.5	N/A
15 Tbps		$Iter = 565$	$Iter = 1130$	$Iter = 1695$	$Iter = 2260$	$Iter = 2825$	$Iter = 100000$
	Fixed via SA, $K = 1$	32.2	32.2	32.2	32.2	32.2	32.2
	Fixed via SA, $K = 2$	36.4	35.2	33.9	32.4	31.8	31.3
	Fixed via SA, $K = 3$	38.6	37.5	35.8	34.1	33.5	31.9
	Fixed via SA, $K = 4$	39.8	38.6	38.0	36.9	35.8	34.7
	Fixed via SA, $K = 5$	40.2	39.1	38.6	37.9	37.2	35.8
	Adaptive via SA, $K = 1$	25.9	25.9	25.9	25.9	25.9	25.9
	Adaptive via SA, $K = 2$	27.5	27.3	26.7	26.0	25.6	24.4
	Adaptive via SA, $K = 3$	30.7	30.1	28.4	27.8	27.5	26.1
	Adaptive via SA, $K = 4$	31.8	31.3	31.0	30.7	30.4	29.0
	Adaptive via SA, $K = 5$	33.5	33.0	32.4	31.8	31.3	30.0
	Adaptive via IF, $K = 1, 2, 3, 4, 5$	27.8	23.9	25.6	23.3	23.3	N/A

lower spectrum utilization is achieved by increasing K of IF method. In most cases, proposed IF method occupies less spectrum than all the other counterparts based on SA scheme. Similar results were observed in Table 3.8-3.9 for 14-node NSFNet. Specially, when $K \geq 2$, the average spectrum utilization of IF method is not decreased too much by increasing the valve of K.

Table 3.9: Spectrum Utilization for NSFNet Network with Dynamic Traffic

Load	Algorithm	Average Spectrum Utilization (%)					
4.98 Tbps		$Iter = 330$	$Iter = 660$	$Iter = 990$	$Iter = 1320$	$Iter = 1650$	$Iter = 100000$
	Fixed via SA, $K = 1$	15.0	15.0	15.0	15.0	15.0	15.0
	Fixed via SA, $K = 2$	16.5	15.9	15.7	15.3	14.8	14.2
	Fixed via SA, $K = 3$	18.8	18.2	17.6	17.1	16.5	15.3
	Fixed via SA, $K = 4$	18.9	18.6	18.2	18.0	17.8	17.1
	Fixed via SA, $K = 5$	19.3	19.0	18.7	18.5	18.2	17.6
	Adaptive via SA, $K = 1$	14.2	14.2	14.2	14.2	14.2	14.2
	Adaptive via SA, $K = 2$	14.8	14.6	14.4	14.3	13.9	13.2
	Adaptive via SA, $K = 3$	15.8	15.6	15.4	14.9	14.8	14.2
	Adaptive via SA, $K = 4$	16.5	16.2	15.8	15.5	15.2	14.5
	Adaptive via SA, $K = 5$	16.9	16.7	16.3	15.9	15.5	15.0
	Adaptive via IF, $K = 1, 2, 3, 4, 5$	16.5	14.2	13.6	13.6	13.6	N/A
12.12 Tbps		$Iter = 420$	$Iter = 840$	$Iter = 1260$	$Iter = 1680$	$Iter = 2100$	$Iter = 100000$
	Fixed via SA, $K = 1$	26.7	26.7	26.7	26.7	26.7	26.7
	Fixed via SA, $K = 2$	29.0	28.4	27.9	27.3	26.9	25.6
	Fixed via SA, $K = 3$	31.8	31.3	30.7	30.3	29.9	29.0
	Fixed via SA, $K = 4$	32.8	32.4	32.1	31.8	31.2	30.7
	Fixed via SA, $K = 5$	33.2	32.9	32.6	32.4	31.9	31.2
	Adaptive via SA, $K = 1$	23.3	23.3	23.3	23.3	23.3	23.3
	Adaptive via SA, $K = 2$	23.9	23.3	22.9	22.6	22.2	20.8
	Adaptive via SA, $K = 3$	25.6	25.2	24.8	24.3	23.9	23.0
	Adaptive via SA, $K = 4$	28.4	27.9	27.3	26.6	25.8	24.4
	Adaptive via SA, $K = 5$	30.0	29.1	28.5	27.9	27.3	26.2
	Adaptive via IF, $K = 1, 2, 3, 4, 5$	23.3	20.5	19.8	20.5	19.9	N/A

Algorithm 4 Iterative Flipping (IF)

Input: Initial system state ($\mathbf{k} = \{\mathbf{1}\}, \mathbf{m} = \{\mathbf{1}\}$);

Output: Routing and modulation solution ($\hat{\mathbf{k}}, \hat{\mathbf{m}}$);

1: Performing traffic grooming for input traffic flows $[D_{s,d}]$ through Algorithm 2, and calculate OEO conversion cost P_{OEO} for electronic switching;

2: Performing spectrum allocation through routing and wavelength assignment according to a first-fit mechanism, and calculate fiber link costs P_{AMP} and optical conversion costs P_W;

3: Run adaptive modulation searching procedure in Algorithm 1 for corresponding P_{CW}, L value of each lightpath. If no solution meet the BER_{th}, jump to step 5;

4: Computing the objective function $f(\mathbf{k}, \mathbf{m})$, where $f(\cdot)$ refers to the cost function defined in Eq. 3.1 corresponding to the power consumption at state ($\mathbf{k} = \{\mathbf{1}\}, \mathbf{m} = \{\mathbf{1}\}$);

5: Increasing the first modulation factor $\mathbf{m}_{[v=1]}$;

6: Recomputing the resulting power consumption by repeating steps 2-4;

7: Whether the new power consumption value with corresponding $(\mathbf{k}, \mathbf{m})$ is accepted or not is based on the constraints in Eq. 3.2-3.9, along with the following criterion: $\Delta C = f(\tilde{\mathbf{k}}, \tilde{\mathbf{m}}) - f(\mathbf{k}, \mathbf{m})$, where $(\mathbf{k}, \mathbf{m})$ is current solution. When $\Delta C < 0$, $(\tilde{\mathbf{k}}, \tilde{\mathbf{m}})$ is accepted, otherwise, $\mathbf{m}_{[v=1]}$ reverts to its previous value;

8: Keep increasing candidate modulation level until all possible modulation level for $\mathbf{m}_{[v=1]}$ are explored;

9: Increasing traffic segment $v = 2$ and repeat steps 3-8, until all possible modulation level $\mathbf{m}$ for all traffic lightpaths $\sum_{s,d} K_{s,d}$ are explored;

10: Increasing the first routing factor $\mathbf{k}_{[v=1]}$, and repeating steps 2-9;

11: Keep increasing first routing factor until all possible candidate paths for $\mathbf{k}_{[v=1]}$ are explored;

12: Increasing traffic segment $v = 2$ and repeat steps 2-11, until all traffic lightpaths $\sum_{s,d} K_{s,d}$ are explored;

13: **return** $(\hat{\mathbf{k}}, \hat{\mathbf{m}})$;

3.6 Summary

In this chapter, we studied the energy-efficient routing and bandwidth allocation (RBA) problem in OFDM-based elastic optical networks. The proposed RBA problem optimizes the consumed power due to electronic processing, wavelength conversion, in-line EDFAs and OFDM-based transponders at each node, where the logical topology corresponding to the static and dynamic traffic demand of each node pair, as well as the laser transmit power, modulation level, number of subcarriers, and routing path of each node pair, are jointly determined. Since the optimization problem with a large search space is NP-Complete, we first solved the formulated problem via a heuristic method based on simulated annealing (SA) and K shortest paths. It is demonstrated that the proposed strategy can achieve better performance than that using a single modulation level with shortest path routing only. By exploring the unique feature of the problem, we proposed to using an iterative flipping method to solve the problem, which flips the candidate modulation levels and routing paths for each lightpath one by one to reach a suboptimal solution. The proposed method maintains better power saving performance than SA scheme while keeping very low computational complexity.

Chapter 4

Radio-over-Fiber for Next-Generation C-RAN

Based on the transmission strategy in Chapter 2, we further propose a novel radio-over-fiber (RoF) transmission scheme for supporting LTE-Advanced wireless systems, and perform the power consumption analysis for both current and future RoF transmission systems. Based on the RoF system model for current and future cloud radio access network (C-RAN), we evaluate the impact of using different modulation formats on the power consumption by the optical transmitter, link EDFA, and optical receiver. We also compare the total power consumption required by both downlink and uplink for supporting a single BS.

4.1 Introduction

Inspired by infrastructure centralization, a cloud radio access network (C-RAN) has been proposed to meet the rapidly increasing capacity demands of future wireless access net-

works. To provide traffic load balance between high and low demands, C-RAN allocates resource dynamically as traffic load varying around the whole network [69]. This is realized by equipping the central unit (CU) with multi-site and multi-standard baseband units, such that C-RAN can support multiple wireless standards for geographically dispersed base stations with different levels of sector and coverage [70]. Besides, advanced technologies such as enhanced MIMO, co-operative multi-point (CoMP), carrier aggregation, and heterogeneous networks all require change from a distributed RAN to a highly centralized RAN.

In wireless part of RAN, multiple-input multiple-output (MIMO) antenna technology is widely used today, including WiFi (802.11n), the 3G cellular technology, and long term evolution (LTE). By using spatial multiplexing scheme, MIMO can significantly improve the data capacity, such that the traditional Shannon's limit can be surpassed. Since MIMO is implemented in multi-path environment for providing high capacity gain, the robustness to multi-path effects and high spectral efficiency of orthogonal frequency division multiplexing (OFDM) make it suitable to be combined with MIMO to provide high data rate for wireless links.

In optical part of RAN, thanks to the partially overlapped subcarriers and the high-tolerance to chromatic dispersion (CD) and polarization mode dispersion (PMD), an OFDM-based coherent optical (CO) transmission system demonstrates superb spectrum efficiency and bandwidth slicing flexibility, and is expected to play an important role in the emerging applications such as radio access networks and cloud computing. Due to its high resistance to cross phase modulation (XPM) and inter-channel four wave mixing (FWM), CO-OFDM with sufficient guard bands supports longer transmission reach and can afford higher modulation levels [5]. Meanwhile, OFDM is robust to the non-flat frequency response along the radio-over-fiber (RoF) link [71].

For LTE-Advance and those under the banner of 5G, channel bandwidth up to 100

MHz, downlink peak rate around 1 Gb/s, modulation level up to 256-QAM, and orthogonal frequency-division multiple access (OFDMA) with up to 2048 subcarriers are expected to be supported. Supposing at least four radio channels per direction for a single BS and 100 MHz bandwidth for each channel, a serial bit rate of more than 24 Gb/s is to be required [72]. Furthermore, [73] suggests that if all the features of LTE-Advanced wireless system are enabled, the back-haul traffic would boom to 100 Gb/s per site. However, the common public radio interface (CPRI) in current digital transmission supporting up to 6.144 Gb/s [74], is merely adequate for supporting a few 20 MHz channels. That is, CPRI can only support a single 100 MHz radio channel [75]. Comparing to current digital transmission approaches [7], RoF schemes featured by link transparency and lower bandwidth requirement are expected to be a solution for centralized wireless equipments of C-RAN in next generation wireless communications [8]. For these requirements, long-reach passive optical network (LR-PON) was proposed for next generation radio access network. In the long reach extension part, a feeder fiber up to 84.6 km and an EDFA are equipped at the local exchange with a distribution range of 20 km [76].

4.2 Enabling Technology

This chapter is related to a number of additional topics, including MIMO-OFDM technology, optical MIMO-OFDM, cloud radio access network (C-RAN), radio-over-fiber (RoF) technique, PAPR problem in OFDM-based RoF systems, and OFDM-based long-reach PON (LR-PON). These topics are reviewed in the following subsections.

4.2.1 MIMO-OFDM

By increasing the numbers of antennas at the transmitter and receiver, the MIMO technology not only increases the data rate, but also improves the system reliability through spatial diversity [77]. OFDM technique possessing higher spectral efficiency and robustness to multi-path effects is normally implemented in combination with MIMO, such that the capacity gain through multi-path environment can be achieved. Specifically, MIMO-OFDM systems can provide bandwidth efficiency on the order of 10 b/s/Hz for most wireless communications [78].

In OFDM modulation format, by using a discrete Fourier transform, the available bandwidth is spited into many subcarriers, which are carefully designed to keep subcarriers orthogonal to each other for achieving better bandwidth efficiency. Besides, the signal data stream is transmitted simultaneously by employing a number of low rate subcarriers, such that high data rate is achieved. Since the symbol duration increases for the low data rate subcarrier, the relative amount of channel impairment is reduced.

By using the spatially separated antennas at transmitter and receiver in multi-path scattering environment, MIMO system can obtain a capacity gain with less signal fading. Although full spatial diversity is usually not achievable, V-BLAST as a layered approach is generally implemented to increase the capacity gain [79]. Channel capacity can be further approached by decomposing the channel coefficient matrix using singular value decomposition (SVD) for filters at transmitter and receiver [78]. To maximize spatial diversity, techniques including delay diversity, space-time trellis codes (STTC) and space-time block codes (STBC) [80] are implemented, such that the power efficiency is also improved.

4.2.2 Optical MIMO-OFDM

OFDM can provide high capacity, long-reach and cost-effective operation for typical PON architectures [81], due to the fact that OFDM signals are more robust to Rayleigh backscattered light than non-return-to-zero (NRZ) signals [82]. In optical communication, BER deterioration caused by fiber nonlinearity in the high power region limits the modulation level and transmission distance. Since the symbol duration of OFDM signal increases for the low data rate subcarrier, the relative amount of impairment like chromatic dispersion, E/O band response limitation, and distortion is declined. Therefore, aggregated data of several Gbps can travel much longer distance without the need of dispersion compensating modules.

In recent years, coherent communication techniques attract great interest mainly due to the following two reasons. By combining with silicon-based digital signal processing (DSP), optical coherent detection has the ability to compensate linear transmission impairments such as CD and PMD [25]. And, channel impairment due to laser and fiber can be removed via coherent algorithms [26]. Comparing to intensity modulation that only modulates the intensity of optical carrier, coherent optical OFDM (CO-OFDM) transmitter also modulates the phase or the polarization. And, CO-OFDM receiver detects signal using homodyne or heterodyne detection, rather than direct detection via a photodiode [24]. For high transmission rate, the CO-OFDM can realize robust dispersion transmission, improved computation efficiency, and simplified channel and phase estimation [1].

For a single optical channel, all degrees of technique including CO-OFDM, polarization-division multiplexing (PDM), and high order modulation, have already been conducted to increase the spectral efficiency in current optical communication systems. Capacities and outage probabilities of optical MIMO in spatially multiplexed optical transmission

systems are studied in [83]. However, due to the limit on the channel capacity of standard single mode fiber (SSMF) [84], single optical channel will ultimately unable to support exponential growth of data traffic. Space-division multiplexing (SDM) can further improve the capacity limit by using MIMO technique to cancel crosstalk between integrated parallel optical paths. Experimental results show that MIMO-RoF system using single sideband carrier in combination with OFDM modulation can achieve 2 times data rate of MIMO-RoF system employing double sideband single carrier [85]. By using coherent polarization division multiplexing-orthogonal frequency division multiplexing (CO-PDM-OFDM) modulation format with 2×2 MIMO processing, 65.1 Gb/s 32-QAM signals with 7.0 b/s/Hz spectral efficiency are successfully transmitted over 240 km of SSMF within 26.8 GHz optical bandwidth [86]. And, 121.9 Gb/s CO-PDM-OFDM signals 2.0 b/s/Hz spectral efficiency can be continuously detected over 1,000 km of SSMF by using 8-QAM modulation within 22.8 GHz optical bandwidth [87]. In [88], 6×6 MIMO processing unit was used to achieve the simultaneous transmission of six spatial and polarization modes with total 6×40 Gb/s QPSK signals over 96 km of a few-mode fiber.

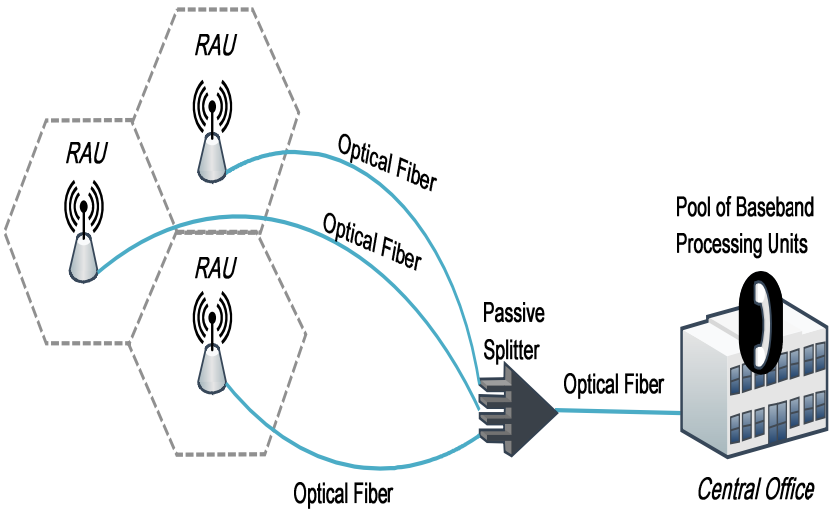

Figure 4.1: Conceptual Description of C-RAN.

4.2.3 Cloud radio access network (C-RAN)

In current distributed antenna systems (DAS), each cell site is equipped with a base station to provide most of processing functions, and the base station is connected to remote radio heads (RRHs) through optical fiber. However, such DAS is designed for the peak load requirement of each radio sector and a fixed set of wireless standards, coverage and frequency bands [89]. In each base station, not only processing equipments need considerable power supply, but also other services such as air conditioning may cost half of the total power consumption [90].

By involving C-RAN concept, the equipments installed at each antenna site are significantly simplified by moving most of processing units to a centralized point in the network, such that processing functions and support services are shared by multiple cell sites to save both power and maintenance costs. For resource centralization, C-RAN creates a pool including all baseband processing units at central office as shown in Fig. 4.1 and Fig. 4.2, such that the capacity of each cell site within controlled area can be elastically allocated. And, the range of distribution to remote antenna units (RAUs) can be increased by using optical technologies such as LR-PON. Consequently, by integrating wireless back-haul and optical networks, C-RAN with central controller can fully support advanced co-processing and synchronization techniques, such as heterogeneous networks [91] and co-operative multi-point (CoMP) [92].

4.2.4 Radio-over-fiber (RoF)

Since fiber has been deployed in current wireless back-haul and the next-generation wireless standards demanding smaller and higher bandwidth cells, RoF technique provides an attractive solution in future C-RAN by enabling dynamic capacity and mobility management [6]. Because RoF only performs marginal impact on the radio range while offers

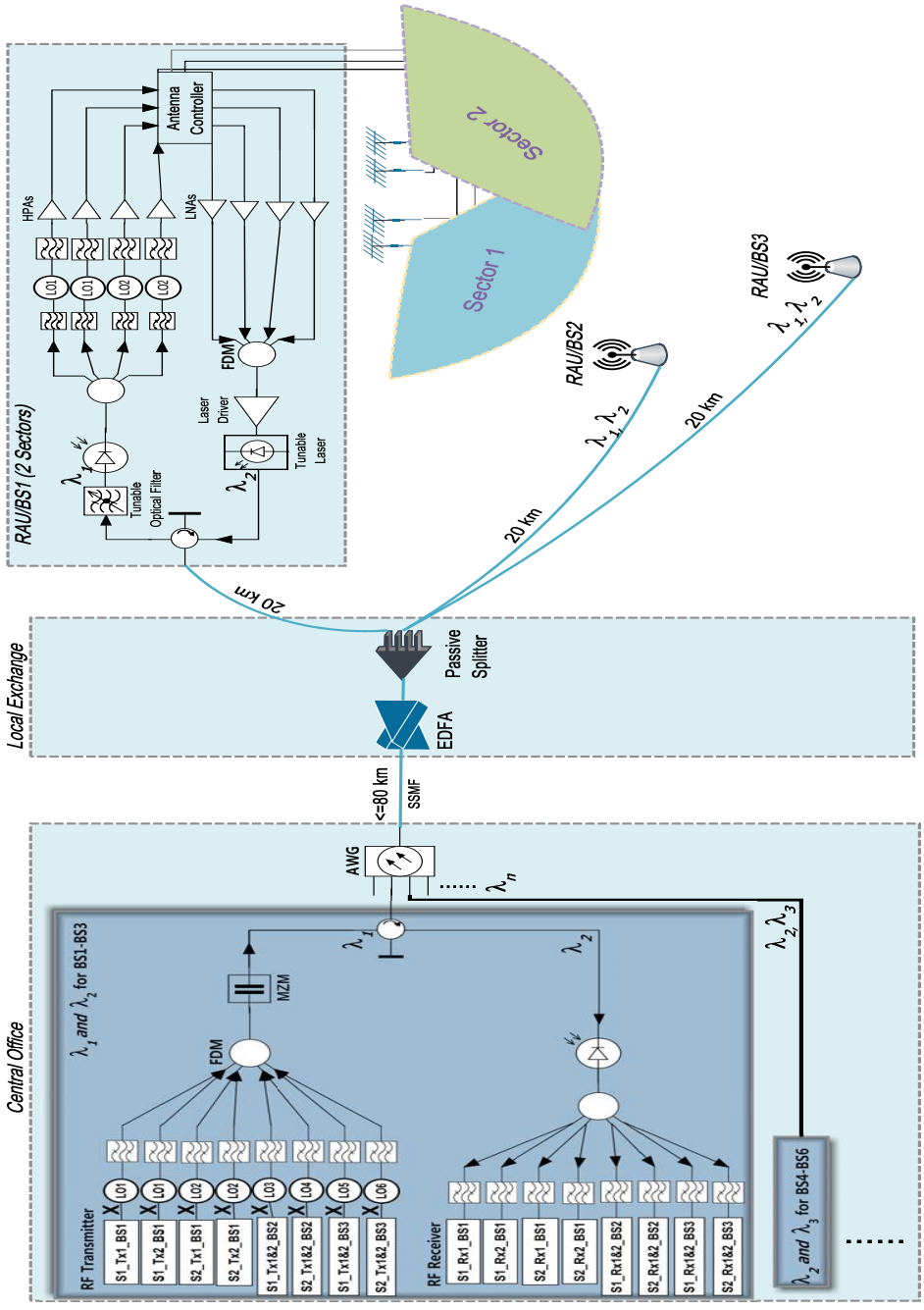

Figure 4.2: Basic Structure of C-RAN

very low implementation cost, it is more suitable for supporting multiple wide band radio channels than digital optical transmission using CPRI [75].

By enabling the use of RAU with frequency division multiplexing (FDM) for individual cell site, RoF can significantly reduce the network installation and maintenance cost. Specifically, RoF transmission links are used to connect a CU that containing most processing units and supporting services to a number of RAUs with dedicated coverage and capacity. In current short range DAS with fiber span up to 10 KM and rate 26.25 MS/s trough 64-QAM, impairment due to noise and distortion that caused by RoF using analog transmission does not have a significant impact on wireless range [75]. However, in next generation wireless systems employing wider channel bandwidth (100 MHz) and higher level modulation schemes (256-QAM), more noise and distortion requirements for the RoF links will be adopted.

To support next generation RAN, OFDM will be employed due to its robustness in wireless channel and providing the basis for a multiple access scheme (OFDMA). The multiple radio channels provided by MIMO antennas also must be transported through the RoF links, which are more challenging than digital CPRI transmission. Since the MIMO-RoF systems generate multiple signals at the same frequency, both wavelength division multiplexing (WDM) by multiplexing them on different wavelengths and subcarrier multiplexing (SCM) through frequency translation are considered as solution.

4.2.5 PAPR in OFDM-based RoF systems

The nonlinear distortion due to high PAPR of OFDM signals happens at both electrical power amplifier and optical MZM. For electrical power amplifier, when the peak amplitude of OFDM signal with high PAPR reaches or exceeds the saturation region of high power amplifier (HPA) at the transmitter, the OFDM signal will suffer from nonlinear dis-

tortion, spectrum spreading, in-band distortion and inter-modulation interference across the OFDM subcarriers. Similarly, when the peak amplitudes of the electrical OFDM signals with high PAPR reach or exceed the linear transformation region of Mach-Zehnder modulator (MZM), the optical OFDM signals will suffer from nonlinear distortion. All these cause bit-error-rate (BER) degradation at the receiver. Simple solutions are using expensive power-amplifiers/MZM with large saturation region or adding a power control unit. However, as high peak amplitudes occur irregularly, these solutions would be inefficient.

4.2.6 OFDM-based Long-reach PON

Similar to digital CPRI transmission, RoF links typically have limitations due to optical component nonlinearity, fiber chromatic dispersion, and difficulties in implementing remote control with large number of BSs. Although these limitations can be overcome by providing dedicated wavelengths to each BS over the PON architecture [93], this solution is very expensive and has scalability problem with the increasing number of wireless cells. Instead of using the currently deployed PONs, long-reach PON (LR-PON) provides a solution of centrally connecting RAUs beyond urban areas, such that the number of expensive back-haul links is significantly reduced. Long-reach bidirectional RoF transmission system was demonstrated in [76], where the 65 km feeder extension of the standard single mode fiber (SSMF) type is added to the PON with passive splitter for multi-wavelength overlay.

By implementing long-reach architecture in combination with OFDM technology, OFDM-LR-PON can flexibly assign sub-carriers to different users and possibly allocate bits or power to each subcarrier. To jointly optimize physical (PHY) and media access control (MAC) layers of the transmission system, the CU dynamically chooses the modulation level and distributes the power budget for each BS, while taking into account their

individual link quality and required data rate [94]. When allocating specific wavelengths and sub-carriers to each BS, the CU and other BSs set those sub-carriers into zero during the OFDM modulation. Then, the RoF system transparently transmits radio channels with data to BSs through pre-assigned optical wavelengths and sub-carriers, and extracts them at the receiver through electrical filters.

One optical fiber as feeder extension carrying all upstream and downstream signals is employed to communicate between the CU and power splitter which broadcasts signals to all BSs. Alternatively, some of feeder fibers may directly connect CU to RAUs without splitter for special cell sites. By allocating sub-carriers for different RAUs, tens or hundreds of sub-carriers are assigned to one channel, and those grouped channels adopt frequency division multiplexing (FDM) to address different access. Specifically, the CU groups sub-carriers for each FDM channel in the electrical domain using OFDM-QAM modulation. Then, electrical signals are transferred into the optical signal to form the downstream signals. At the receiver, the entire optical spectrum is converted into electrical domain, and different FDM channels are extracted by applying RF filters and analog-to-digital converters (ADC) for further processing.

In the downstream, to broadcast signals to all users by power splitting, a single laser module (i.e. MZM) with very high bandwidth (up to 40 GHz) is equipped at the CU. At the RAUs, the bandwidth of avalanche photodiode (APD) or PIN receivers is corresponding to the required bandwidth of pre-assigned wavelength at CU. In the upstream, at each RAU with lower data rate, equipped lasers operate with bandwidth in the range of few GHz. At the CU, after wavelength de-multiplexing, receivers with same bandwidth range are used for signals from each RAU.

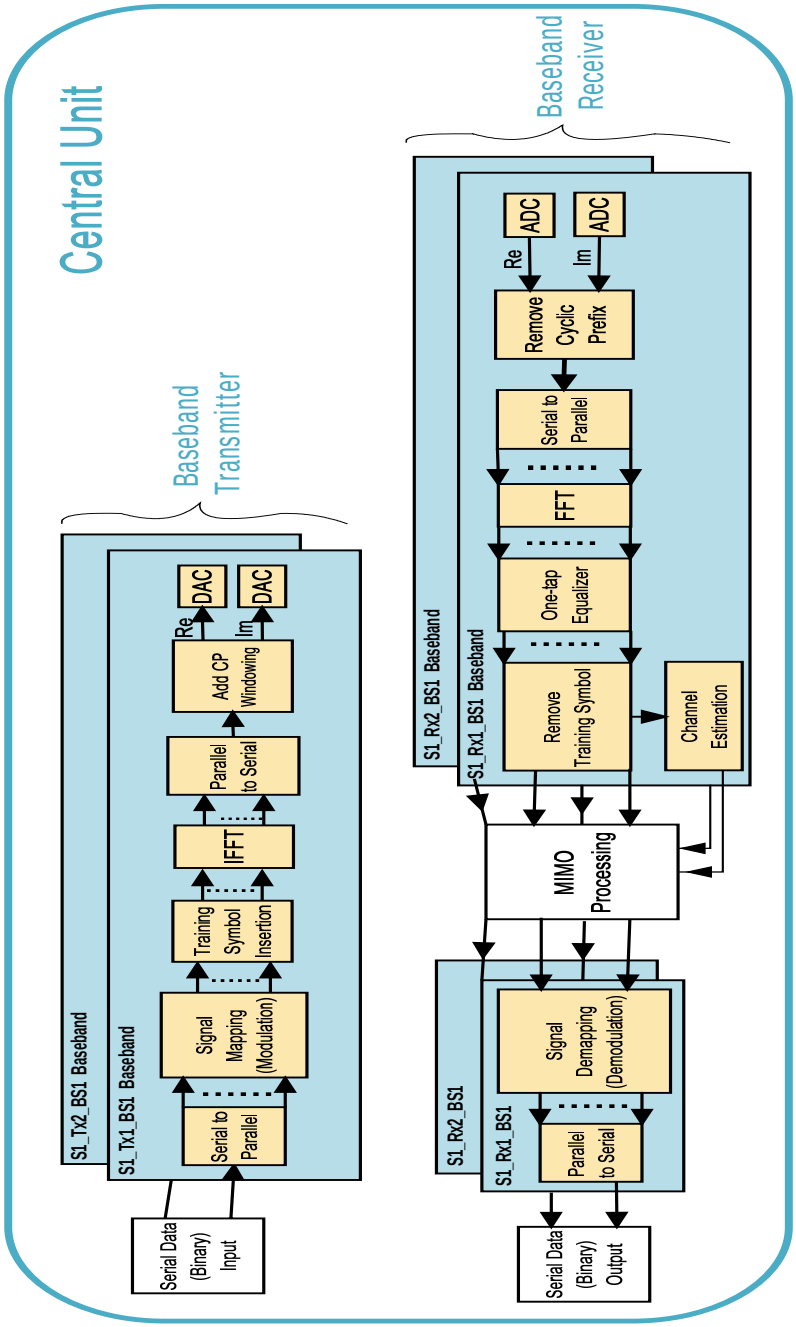

Figure 4.3: 2×2 MIMO-OFDM Baseband Model for RoF Transmission System

4.3 Baseband Model for RoF Transmission System

As shown in Fig. 4.3, a 2×2 MIMO-OFDM baseband model for simulating the required ESNR of end-to-end RoF transmission system is developed by jointly considering non-linear distortion from both Mach-Zehnder modulator (MZM) and high power amplifier (HPA) due to high PAPR.

At the transmitter side of CU, binary data stream is converted from serial to parallel, where a fixed number of bits are modulated into a symbol in the radio frequency (RF) domain and mapped onto individual subcarrier. The binary data is mapped into complex signal based on chosen modulation format. Then, the training symbols (TSs) for channel estimation are periodically inserted among OFDM symbols. The complex signal is then modulated onto corresponding subcarrier through inverse fast Fourier transformation (IFFT) and combined by parallel-to-serial converter. A cyclic prefix (CP) is attached to improve the immunity to multipath delay spread of wireless channel (inter-symbol interference and inter-carrier interference), optical CD, and optical PMD. Meanwhile, the resulting electrical baseband OFDM signal is windowed to suppress the out-of-band power. To convert digital signals into analogue signals, the baseband OFDM signals of each transmitter are split into real and imaginary parts as the input of digital-to-analogue converters (DAC). Then, the real and imaginary parts of baseband OFDM signal in analogue domain are combined and up-converted to the predetermined RF spectrum by RF up-converter.

At the receiver side of CU, after analogue-to-digital converters (ADC), the digitized real and imaginary parts are combined to generate digitized OFDM signal for further removing the CP. After serial-to-parallel conversion, the baseband OFDM signal is transformed back to frequency domain expression by the FFT module. Since each sub-channel is almost flat fading, a simple one-tap equalizer is used to compensate for wireless channel

effect. The embedded TSs are extracted for channel estimation. Based on baseband symbols in frequency domain and channel side information, MIMO processing unit outputs the estimated symbols for each receiver. After parallel-to-serial conversion and demodulation, the estimated symbols for each receiver are converted and combined to form the estimation of transmitted binary data stream.

4.3.1 Electrical Power Amplifier Model

A memory-less nonlinear high power amplifier (HPA) is used. It has a "soft limiter" input-output relationship: for a complex-value input y, the output equals $\Lambda(|y|)e^{j\angle y}$ [95], where

$$\Lambda(a) \quad = \quad \begin{cases} a, & \text{if } a \leq A, \\ A, & \text{if } a > A. \end{cases}$$

The "clipping ratio" is defined as $\gamma = \frac{A}{\sqrt{P_{in}}}$ [95], where P_{in} denotes the average power of the input signal,$\gamma = 3$ dB.

4.3.2 Optical MZM Model

As a waveguide-based external modulator, MZM is widely considered in optical OFDM systems with chirp-free signals for achieving high data rate transmission. As shown in Fig. 4.2, the optical OFDM signal is modulated based on the electrical OFDM signal by using the MZM, and the modulation process is subject to nonlinear and peak-limited transfer characteristics [29].

When using differential input data in a push-pull configuration, the transfer function of a single drive MZM is given by [30, 96]

$$\frac{E_{out}(t)}{E_{in}(t)} \quad = \quad \cos\left(\frac{\pi V(t)}{2V_{\pi}}\right) \tag{4.1}$$

where $E_{in}(t)$ and $E_{out}(t)$ are the input and output in optical field, respectively, $V(t)$ is the electrical OFDM signal, and V_π is the required voltage difference applied to a single electrode in order to generate a phase shift between two waveguides.

Expanding the MZM nonlinear transfer function into a Taylor series as:

$$\frac{E_{out}(t)}{E_{in}(t)} = \cos\left(\frac{\pi V(t)}{2V_\pi}\right) \approx 1 - \frac{1}{2!}\left(\frac{\pi V(t)}{2V_\pi}\right)^2 + ... \tag{4.2}$$

The baseband equivalent polynomial model for the output electrical field of the MZM is given as

$$\begin{aligned} y_k &= \sum_{q=1}^{Q} \alpha_q \cdot (x_k)^Q, \;\; q - odd \\ &\approx \alpha_1 \cdot x_k + \alpha_3 \cdot (x_k)^3 \end{aligned} \tag{4.3}$$

where x_k and y_k are the discrete vectors of the applied voltage and the output voltage at the MZM, respectively, q is the order of nonlinearity, and α_q is the odd coefficient of the MZM nonlinear transfer function with an operating region $3V_\pi \pm V_\pi$ (i.e., at the null intensity bias point), whose output signal is approximated as a third order polynomial [15].

4.4 Proposed RoF System for Next-generation C-RAN

The basic architecture of optical and wireless integrated C-RAN based on RoF and LR-PON is described in Fig. 4.2. Central unit (CU) centralizes all base-band processing units of the metro network, such that the RAU at remote base station (BS) is considerably simplified by only down-converting and filtering the received downstream channels. To provide communication to mobile terminals at customer side, RAUs/BSs are located

at the user premises. Each transmitter pair at CU serves a single radio sector with 2 antennas at a BS. By reusing same frequency windows on multiple wavelengths and overlaying wavelength band, a high order of frequency division multiplexing (FDM) is realized to reduce deployment cost of BSs by the centralization in the CU.

4.4.1 Wireless Back-haul Structure for RAN

For downstream transmission, the OFDM symbols generated by different radio frequency (RF) transmitter are up-converted to different RF channel by a predetermined LO and band pass filter (BPF), which are dedicated to each antenna at RAU. After up-converting to the predetermined RF spectrum, they are combined and modulated onto an optical carrier for fiber downstream transmission. To reduce the deployment cost by exempting pre-amplification at receiver, single-drive MZM with narrow optical BPF is used for optical single sideband (OSSB) modulation to avoid chromatic dispersion for long-reach PONs. Since the single-drive MZM is deployed at CU shared by large number of users, the higher cost is not a concern comparing to its electrical bandwidth up to 40 GHz. The output of MZM modulated on $\lambda_{1,3,...}$ is then launched into a 3-port optical circulator for bidirectional transmission after an optical BPF. By realizing wavelength band overlay and routing optical signals to destination receivers, the centralized array waveguide grating (AWG) allows multiple PONs to be served by a single CU [97]. For longer distribution range, optical signal from output port of AWG is then fed into a varied feeder fiber with length less than 80 km, followed by an EDFA at the local exchange (LE) [76]. For broadcasting the downstream signals from CU and combining the upstream signals from multiple RAUs, the LE is equipped with a passive splitter followed by distribution span with length from 20 to 40 km [98]. At RAUs/BSs, optical circulator and tunable optical filter are used to select the optical signal carried by pre-assigned wavelength. The extracted optical signal is then transformed back to electrical signal by photo detection

technique. A LO is required by operating on the same frequency for the specific sector to downshift the RF channels, and multiple electrical BPFs before high power amplifier (HPA) are needed to select desired channel for the transmission through each antenna.

For upstream transmission, the output of optical circulator is directly applied to a photodiode followed by the electrical BPF to screen out the predetermined RF channel for each OFDM receiver. Since the chromatic dispersion for 20 km SSMF is tolerable [76] and upstream date rate is much lower than downstream, RF channels received from antennas for upstream transmission are directly modulated into optical double sideband (ODSB) signal through a tunable laser, which is equipped with laser driver to bias the laser for required power.

4.4.2 RoF Transmission System for Current C-RAN

The transmission system for short/long-reach RAN is depicted in Fig. 4.4. Block diagram of base-band OFDM transmitter and receiver at the CU with perfect synchronization is illustrated. Supposing each sector is equipped with 2 antennas, 2 RF transceivers at CU are assigned for a single sector in a RAU. Each subcarrier of modulated signal is then converted to the electrical baseband OFDM signal through inverse fast Fourier transformation (IFFT) and digital-to-analog conversion (DAC). Multiple RF channels for transmitters are multiplexed in a given spectrum by using FDM technique. Then, the baseband OFDM signal in the RF domain is up-converted to the optical domain by using a wavelength-tunable laser and Mach-Zehnder modulator (MZM). To control the RF power from different modulation level, power control circuit is employed at the input of the MZM. Single-drive MZM is used to modulate electrical OFDM signals onto OSSB by using optical BPFs in both transmitter and receiver. After transmitting along feeder fiber with link loss, the launch power of optical signal is compensated by a variable-gain EDFA with noise figure of 6 dB and span length of SSMF up to 100 km. At

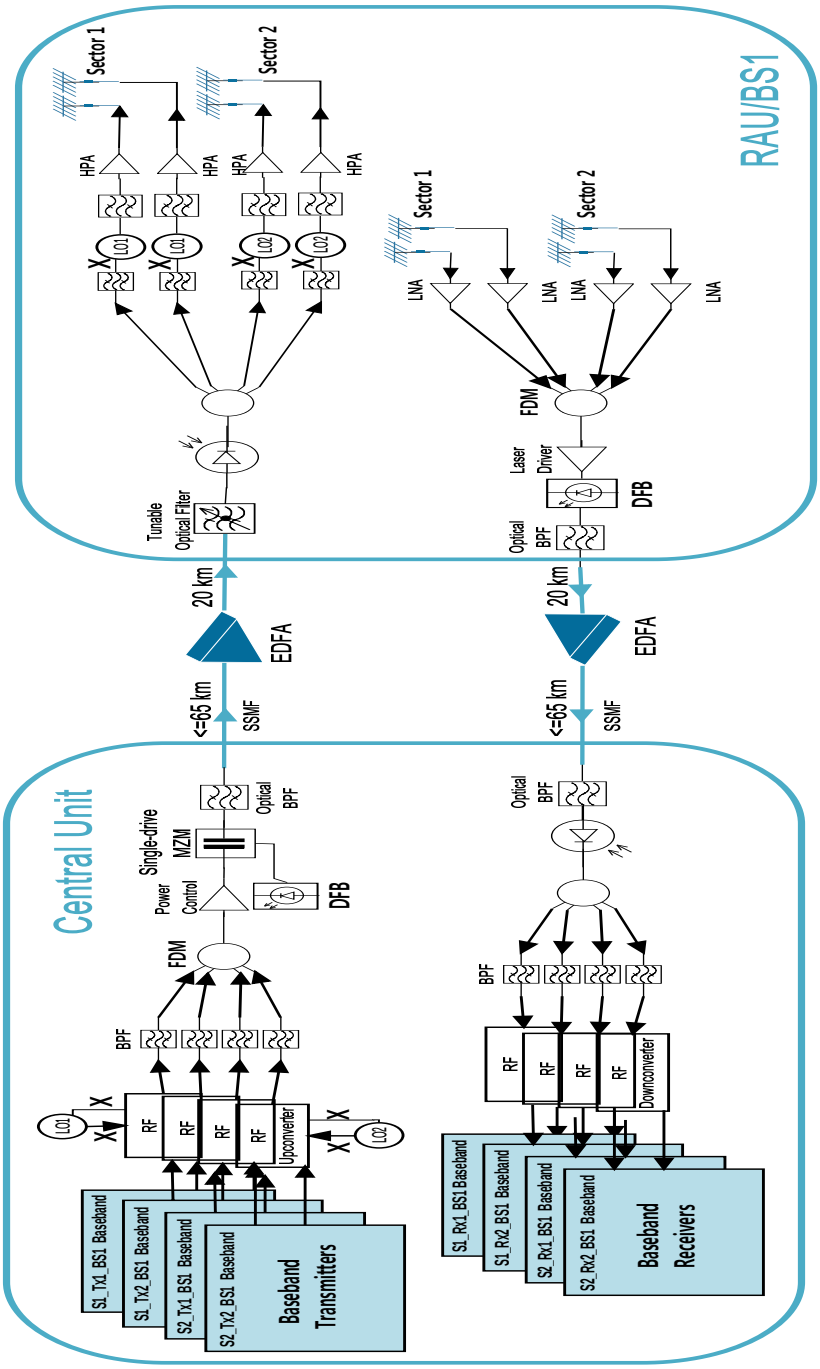

Figure 4.4: RoF Transmission System for Current C-RAN

the RF receiver side of CU, the optical signal from BS is firstly filtered by an optical BPF to suppress image noise. Its output is detected by a photodiode for converting optical signals into electrical signals. After the splitter, BPFs and RF down-converter, the electrical signals on desired RF channel are down-converted to baseband signals for further baseband processing.

At the receiver side of RAU/BS, after the passive splitter for broadcasting downstream signals and the optical circulator for bidirectional transmission, a tunable optical filter (or add/drop multiplexer) is used to select pre-determined wavelength for each RAU/BS. Then, the optical signal is detected by a photo detector, followed by splitter for multiple transmission branches. Multiple BPFs and local oscillators (LOs) are used to select pre-assigned RF channel for each transmission branch supporting a single antenna. After applying HPAs, RF signals are transmitted over the AWGN and multi-path wireless channels. At the transmitter side of RAU/BS, multiple RF broadband signals from antennas are multiplexed into a combined spectrum, which are then modulated onto pre-assigned wavelength by laser driver and tunable laser. To achieve symmetrical link length in both downstream and upstream, an optical BPF is added at the output of laser in the RAU to discard the image-band for generating OSSB signal in the upstream.

4.4.3 Proposed RoF Transmission System for Next-generation C-RAN

The scheme is Fig. 4.4 was demonstrated to support distribution range up to 85 km using 64-QAM and 20 MHz channel bandwidth for downstream (up to 65 km using 16-QAM and 10 MHz channel bandwidth for upstream) [76], which is not enough for next generation wireless systems requiring wider channel bandwidth (100 MHz) and higher level modulation schemes (256-QAM). In Fig. 4.5, RoF transmission system is designed

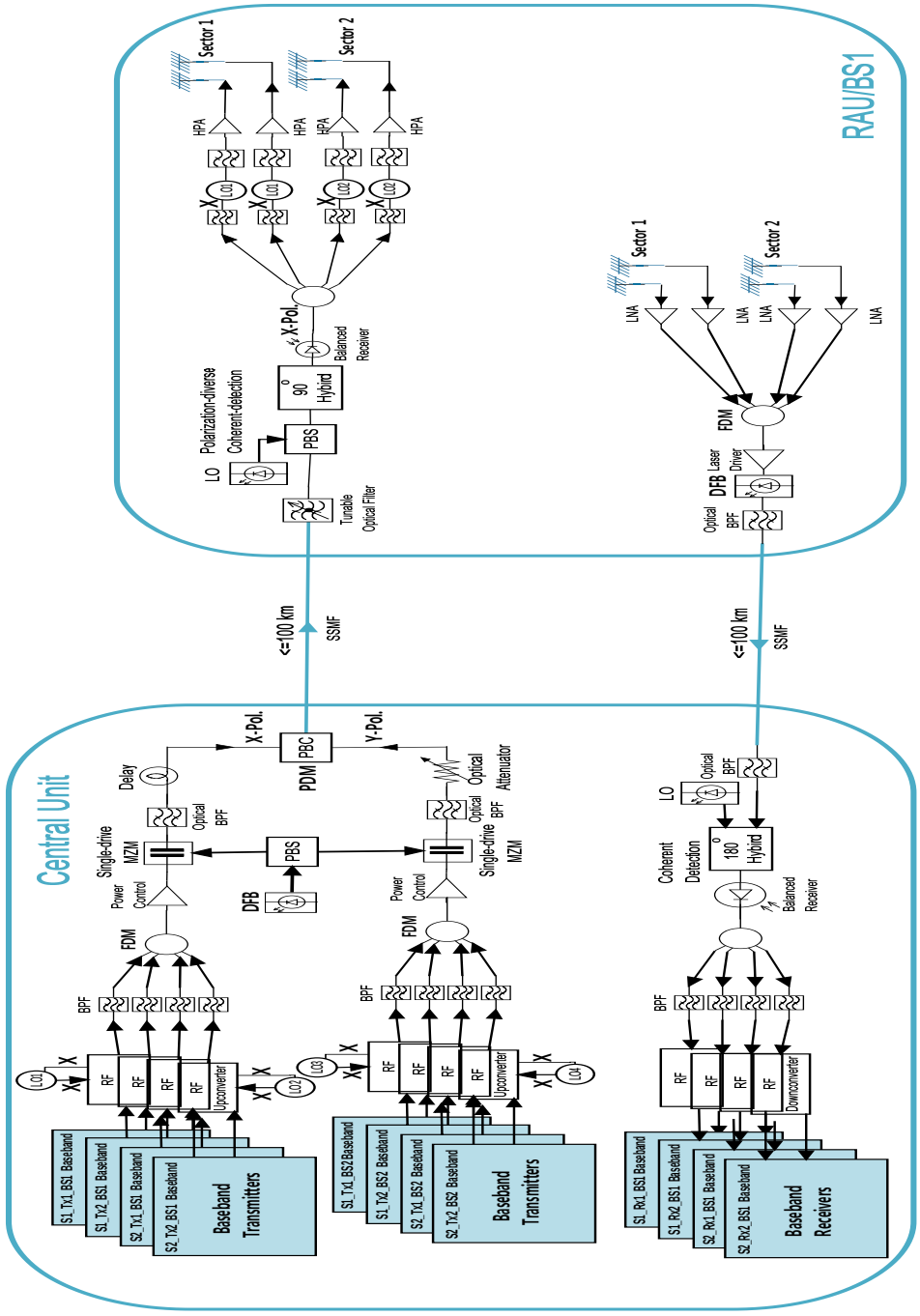

Figure 4.5: Proposed RoF Transmission System for Next-generation C-RAN

for future C-RAN with high capacity per wavelength (DS rate more than 100 Gbps, up to 256-QAM) and large distribution range (up to 100 km). To support more RAUs with higher data rate, polarization division multiplexing (PDM) is used to expand the capacity of a single wavelength.

To improve chromatic dispersion (CD) and polarization mode dispersion (PMD) tolerance, coherent optical (CO) detection is employed for high data rate and long distance transmission. Since coherent receiver without using EDFA for pre-amplification still can achieve sensitivity of -45.9 dBm in LR-PON with 10 Gbit/s transmission over 100 km SSMF [99], while the APD direct receiver only has sensitivity of -30 dBm [98], the EDFA at local exchange (LE) can be exempted for saving power or cost by using PDM-CO receiver with low level of modulation.

To realize polarization multiplexing, one path is equipped with polarization maintaining fiber (PMF) and one symbol delay to emulate PDM, and the other path uses a SSMF optical attenuator to balance power difference of the two paths. The two paths are then combined on orthogonal polarization by a polarization beam combiner. After transmitting through fiber link, the polarization de-multiplexing and coherent detection are conducted. The polarization beam splitter (PBS) splits the optical signal into two different polarization components, which are combined with polarization components of LO together as the inputs of 90 degree hybrid that embedded with 3-dB optical coupler. Each two outputs of 90 degree hybrid are applied on one balanced receiver (including two photo detectors) [100] for extracting optical signal on each polarization. After the optical-to-RF down-conversion, the electrical signal is split and filtered for each antenna. For receiver side of upstream, the optical coherent detection only needs one balanced receiver and the 180 degrees optical hybrid for detecting one side of LO spectrum. Particularly, in RF receiver, TSs can also enable MIMO processing unit to rectify rotation of polarization [101]. To coordinate the TSs of different PDM path, one OFDM symbol

delay is required, and an empty OFDM symbol is inserted before and after the TS for recognizing the TS by the system.

For some sub-channels impaired by side-modes of the local oscillator laser or In-phase and quadrature (IQ) imbalance of the electrical IQ-mixers at RF up-converter, the electrical SNR (ESNR) is not good enough to support higher modulation format. And, different modulation format would require different power consumption. For both ESNR requirement and energy efficiency, the RAU/BS can send a signal back to the CU such that the corresponding transmitters would transmit the data by using different modulation format. That is, the transmitters in CU can adaptively choose candidate modulation levels for energy efficiency. Given data rate requirement, the higher modulation level is corresponding to the lower bandwidth consumption.

4.5 Power Consumption Analysis

In this section, the relation between required ESNR and OSNR is provided based on some assumptions. The OSNR is further analyzed to calculate the required output power of laser source. Then, we analyze the power consumption for the optical part of RoF transmission system.

4.5.1 Optical SNR Calculation

By assuming an ideal detection of optical OFDM-MIMO system and the line-widths of the transmit/receive lasers to be zero, the study takes the relation between the SNR in the optical domain (OSNR) and the electrical SNR (ESNR) at ideal coherent receiver as follows [34]:

$$OSNR(M) \;=\; ESNR(M)\frac{D}{2B_{ref}\cdot m_{sys}} \tag{4.4}$$

where B_{ref} is the reference bandwidth used for the OSNR measurement ($\approx$ 12.5 GHz for 0.1-nm bandwidth around 1550 nm); M is the constellation size of M-ary quadrature amplitude modulation (QAM); m_{sys} is the system margin $\approx$ 12 dB [35]; D Gb/s is the total system symbol transmission rate. And, this relationship is independent of whether using polarization multiplexing or not [34].

As RoF downstream transmission line in Fig. 4.4, the available OSNR of a 0.1 nm band at around 1550 nm at the optical receiver can be given by:

$$\begin{aligned} OSNR &= P_{out} - L_{MZM} - 2L_{Cir} - L_{AWG} - L_{Split} \\ &\quad - L_{Pol} - L_{OBPF} - L_{TOF} - \alpha_{span} \\ &\quad - F_{EDFA} + G_{EDFA} - G_{Rx} \end{aligned} \tag{4.5}$$

where P_{out} is output power of distributed feedback laser (DFB) laser source up to 16 dBm [102]. L_{MZM} is optical excess loss of MZM with a typical value 7.75 dB for 4 channels multiplexing; L_{Cir} is circulator loss with a typical value 1 dB; L_{Pol} is polarization control loss with a typical value 1 dB; L_{AWG} is AWG loss with a typical value 3.76 dB; L_{Split} is passive splitter loss (1:16) with a typical value 14 dB [76]; L_{OBPF} is optical band-pass filter loss with a typical value 3 dB; L_{TOF} is tunable optical filter (or add/drop multiplexer) loss with a typical value 5 dB [98]; $\alpha_{span} = 17$dB is the loss of 85km SSMF span (0.2 dB/km) [98]. For a typical EDFA, F_{EDFA} is the EDFA noise figure due to the ASE noise with a typical value of 6 dB; G_{EDFA} is the EDFA gain up to 20 dB. G_{Rx} is receiver sensitivity no better than -30 dBm for the APD [98].

As PDM-based RoF downstream transmission line in Fig. 4.5, the available OSNR of a 0.1 nm band at around 1550 nm at the coherent receiver can be given by:

$$\begin{aligned} OSNR &= P_{out} + P_{LO} - L_{PDM} - 2L_{Cir} - L_{Split} \\ &\quad - L_{OBPF} - L_{TOF} - \alpha_{span} - G_{Co-Rx} \end{aligned} \tag{4.6}$$

where P_{LO} is output power of LO (DFB laser) at coherent receiver with value up to 16

dBm. G_{Co-Rx} can achieve a sensitivity of -45.9 dBm in LR-PON over 100 km SSMF by using coherent receiver without amplification [99]. L_{PDM} is the PDM loss with a typical value 24.9 dB, including laser power splitter, MZM loss, AWG loss, polarization beam splitter, variable attenuator, and polarization beam combiner [35].

4.5.2 Power Consumption Analysis

The general power consumption of optical transmitter P_{Tx} (in Watt) is given by

$$\begin{aligned} P_{Tx} = \gamma_{DC}^{-1}(&P_{laser} + P_{map} + 2P_{P/S} + n_{DAC} \cdot P_{DAC} \\ &+ n_{MZM} \cdot P_{MZM} + P_{IFFT-CP-TS}) \end{aligned} \tag{4.7}$$

where γ_{DC} is the power conversion efficiency of converting the +12 V DC power supply for transceiver modules with a value 93%; $P_{map} \approx (0.019 \cdot D)/log_2(M)$ is the power consumption for signal mapping by different modulation level M; $P_{P/S} = 0.02 \cdot D$ is the power consumption for parallel-to-serial (or serial-to-parallel) conversion; $P_{DAC} \approx (0.008 \cdot D)/log_2(M)$ is the power consumption for a single digital-to-analog converter (DAC); $P_{MZM} \approx 0.017 \cdot D$ is the power consumption for a single-drive MZM; $P_{IFFT-CP-TS} \approx (0.16 \cdot D)/log_2(M)$ is the power consumption for the IFFT, CP and TS modules for 512 OFDM subcarriers [35]. n_{DAC} and n_{MZM} are the number of required DACs and MZMs by different RoF systems, respectively.

The general power consumption of optical receiver P_{Rx} (in Watt) is given by

$$\begin{aligned} P_{Rx} = \gamma_{DC}^{-1}(&P_{LO} + P_{TIA} + n_{PD} \cdot P_{PD} \\ &+ n_{ADC} \cdot P_{ADC} + P_{Rx-DSP}) \end{aligned} \tag{4.8}$$

where P_{LO} is the power consumption for the local oscillator (LO) at coherent receiver equals to the P_{laser}; $P_{TIA} = (0.0188 \cdot D)/log_2(M)$ is the power consumption of trans-impedance amplifier with automatic gain control for current-to-voltage conversion; $P_{PD} \approx$

$0.0028 \cdot P_{CW} \cdot D$ is the power consumption for a single photodiode (PD); $P_{ADC} \approx (0.0175 \cdot D)/log_2(M)$ is the power consumption for a single analog-to-digital converter (ADC); $P_{Rx-DSP} \approx (0.36 \cdot D)/log_2(M)$ is the power consumption for the DSP module of signal post-processing at receiver for 100 km distance and 512 OFDM subcarriers [35]. n_{ADC} and n_{PD} are the number of required ADCs and photodiodes by different RoF systems, respectively.

The power consumption of the laser P_{laser} (in Watt) for downlink in CU is calculated by:

$$\begin{aligned} P_{laser} &= E_{Laser} \cdot 10^{-3} \cdot D_{down} + P_{CW} \\ &= E_{Laser} \cdot 10^{-3} \cdot D_{down} + 10^{(P_{out}-30)/10} \end{aligned} \tag{4.9}$$

where P_{CW} (in Watt) derived from P_{out} (in dBm) is the laser continuous wave (CW) output power; D_{down} is downstream data rate; E_{Laser} is the DFB laser energy consumption with a typical value as 1.5 pJ per bit for supporting up to 40 Gb/s [22]. For a $ESNR$ value, P_{out} is calculated based on Eq. 4.4, 4.5 or 4.6 by taking M as variables.

The power consumption of laser equipped with driver (instead of MZM) $P_{laserDr}$ (in Watt) for uplink in BS is calculated by:

$$\begin{aligned} P_{laserDr} &= E_{LaserDr} \cdot 10^{-3} \cdot D_{up} + P_{CW} \\ &= E_{LaserDr} \cdot 10^{-3} \cdot D_{up} + 10^{(P_{out}-30)/10} \end{aligned} \tag{4.10}$$

where D_{up} is upstream data rate; $E_{LaserDr}$ is the energy consumption of DFB laser equipped with driver, and the typical value is 37 pJ per bit for supporting up to 40 Gb/s [22].

The power consumption of a link EDFA P_{EDFA} per wavelength is given by [35]

$$\begin{aligned} P_{EDFA} = \gamma_{EDFA}^{-1} &(ESNR(M) \cdot 1.58 \cdot (e^{\alpha_{span}} - 1) \\ &\cdot (1 - e^{-\alpha_{span}}) h\nu) \cdot 10^9 \cdot D \\ &+ (P_{EDFAoh} \cdot D)/100 \end{aligned} \tag{4.11}$$

where γ_{EDFA} is the conversion efficiency of EDFA power with a value 2%; P_{EDFAoh} is the power consumption of EDFA overhead with a value 0.69 W; h is the Planck's constant with a value 6.626×10^{-34}, and ν is the optical frequency constant with a value 1.93×10^{14} Hz.

4.6 Preliminary Results

Case study is conducted to demonstrate the power consumption improvement by using the proposed RoF system for supporting a single BS. For simulating next-generation C-RAN, we set $D_{down} = 30$ Gbps for downstream data transmission from CU to a single BS, and $D_{up} = 10$ Gbps for upstream data transmission from a single BS to CU. In this case study, each RAU/BS supports 2 sectors, and each sector are equipped with 2 antennas using 2×2 MIMO configuration. So, each BS requires 4 radio channels per link direction, which are corresponding to 4 RF transmitters and 4 RF receivers in CU. For simulating required ESNR in baseband of each scenario, V-BLAST for improving capacity gain and STBC for maximizing spatial diversity are implemented in MIMO processing unit. Each radio channel includes 512 subcarriers, and candidate modulation levels include QPSK ($M = 4$), 16-QAM ($M = 16$), 64-QAM ($M = 64$) and 256-QAM ($M = 256$). For calculating OSNR, the distribution range is 85 km for current C-RAN, and 100 km for future C-RAN. The required voltage difference V_π applied to a electrode of a single-drive MZM is in the range of $6.5 \sim 10$ due to the upper bound of available OSNR. The BER requirement without using FEC at the receiver is 10^{-6}. The channel is assumed to be subject to AWGN and Rayleigh fading with maximum of 5 paths.

When V_π of MZM is small as shown in Fig. 4.6, the 256-QAM modulation suffers more signal distortion from RoF downlink than that from uplink, while the lower modulation levels of downlink suffer about the same distortion as that of uplink. When V_π of MZM

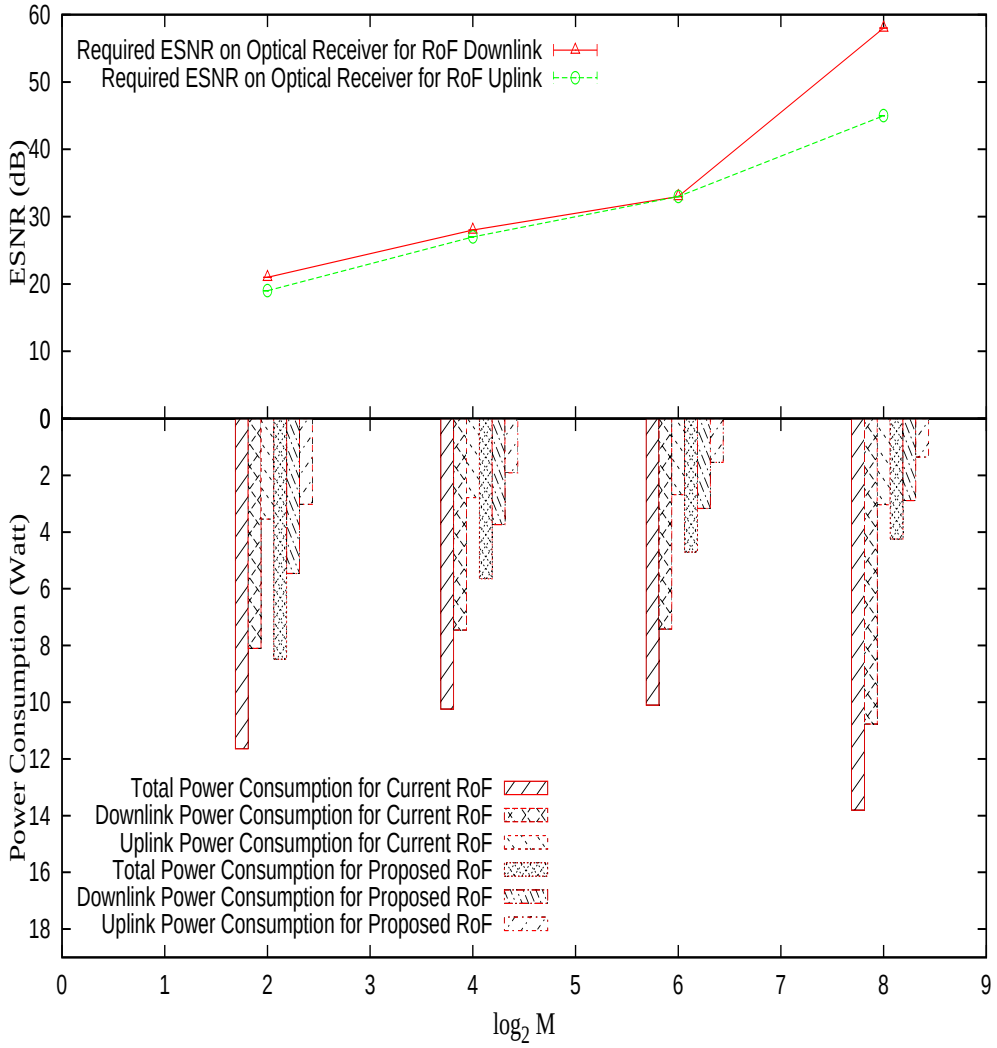

Figure 4.6: Required ESNR on Optical Receiver and Power Consumption of RoF system for supporting a single BS with $V_\pi = 6.5$ VS Modulation level

is large as shown in Fig. 4.7 and Fig. 4.8, the 64-QAM and 256-QAM modulation suffer more signal distortion from RoF uplink than that from downlink. For lower modulation levels, although most of the signals in time-domain have small amplitudes, the so called

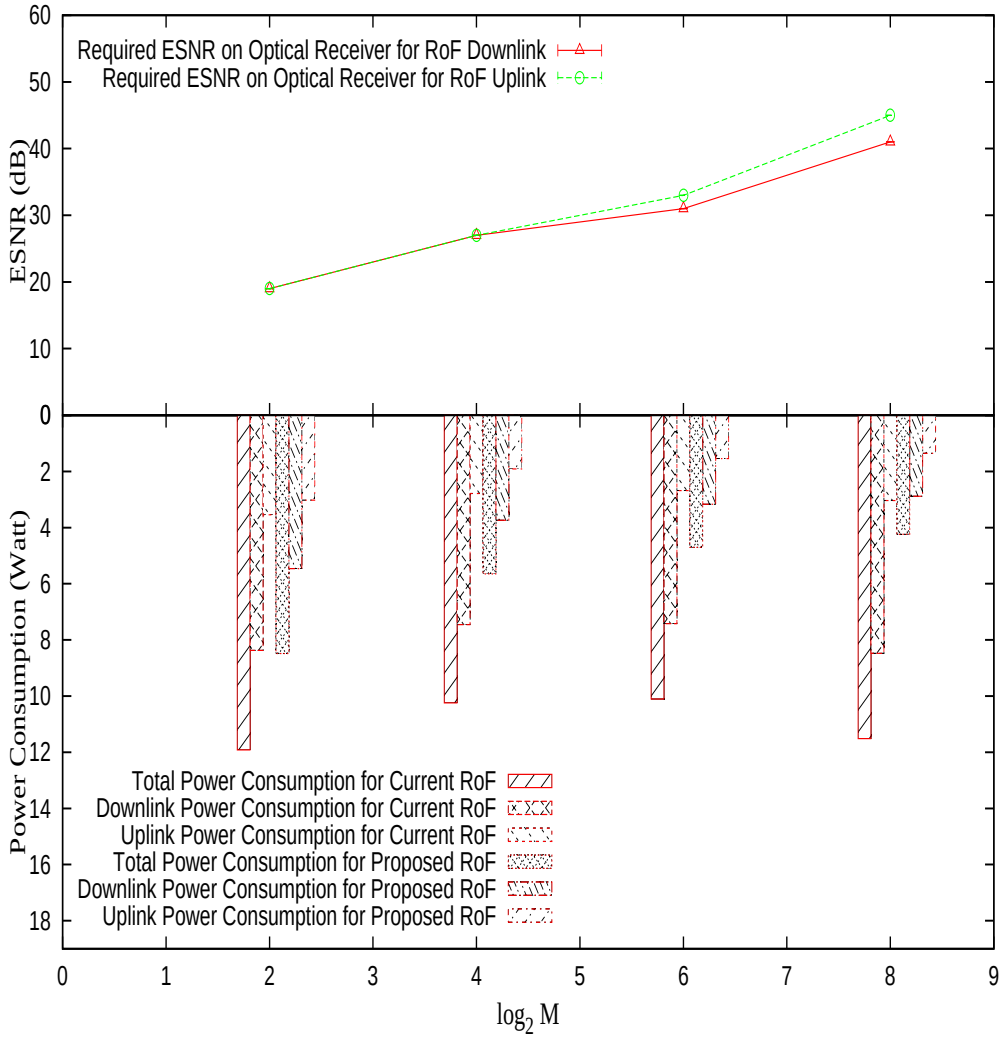

Figure 4.7: Required ESNR on Optical Receiver and Power Consumption of RoF system for supporting a single BS with $V_\pi = 7.5$ VS Modulation level

"linear region" of MZM is not strictly as linear as HPA. So, the required ESNR of lower modulation levels is not reduced too much for large V_π.

For current RoF system with small V_π as in Fig. 4.6, 256-QAM modulation format

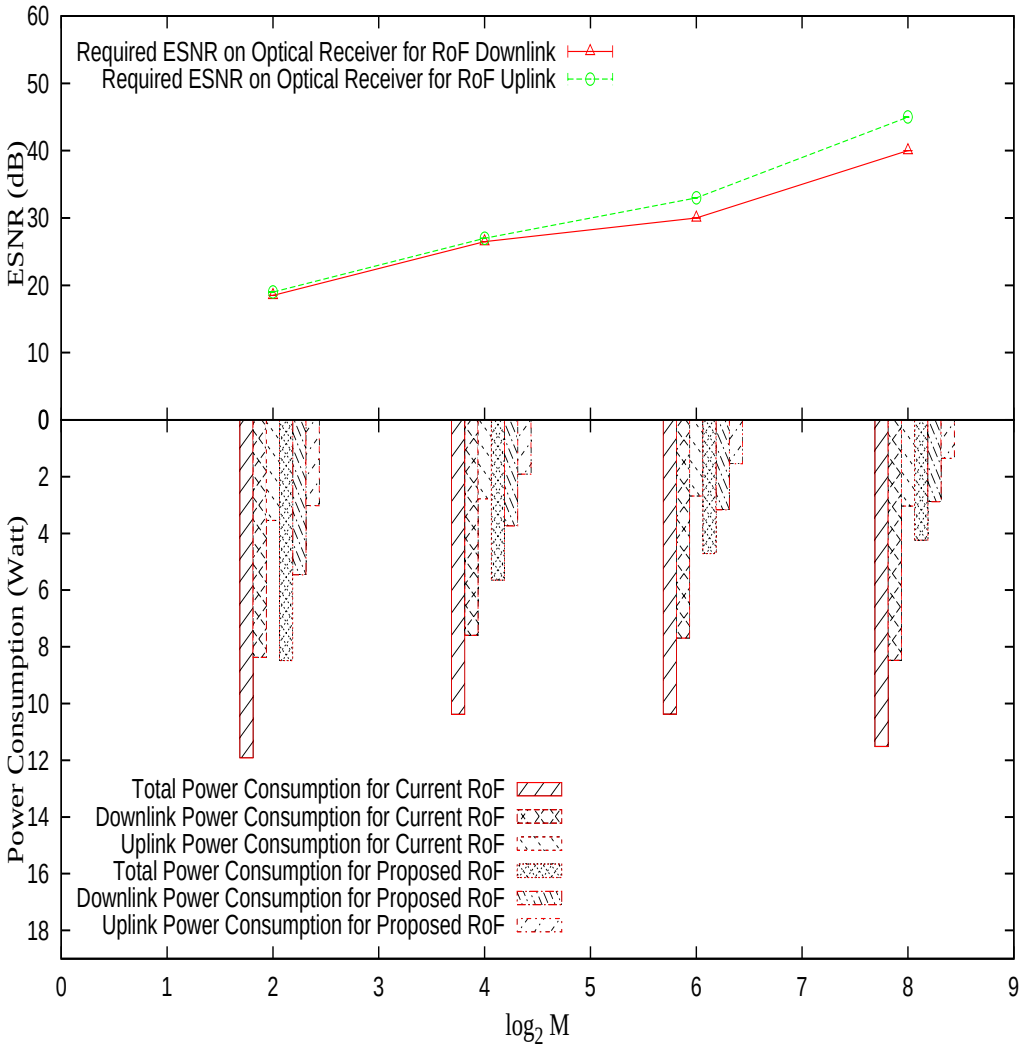

Figure 4.8: Required ESNR on Optical Receiver and Power Consumption of RoF system for supporting a single BS with $V_\pi = 10$ VS Modulation level

consumes highest power, while the lowest power is reached by a moderate modulation format (16-QAM or 64-QAM). However, for large V_π as in Fig. 4.7 and Fig. 4.8, the highest power is consumed by QPSK, and the lowest power is also achieved by 16-QAM

or 64-QAM. For proposed RoF system, 256-QAM modulation consumes not only lowest power, but also lowest bandwidth for given data rate in all three cases. Meanwhile, proposed RoF system can save $27\% - 69\%$ power consumption, comparing to current RoF system.

4.7 Summary

In this chapter, we proposed a novel adaptive radio-over-fiber (RoF) transmission system for next-generation C-RAN in which both energy consumption, capacity per wavelength, and distribution range are considered. By considering nonlinear distortion from both Mach-Zehnder modulator (MZM) and high power amplifier (HPA), we first developed a 2×2 MIMO-OFDM baseband model for simulating the required ESNR of end-to-end RoF transmission system under different scenarios. Then, we introduced the RoF system for current C-RAN, and proposed a novel RoF system for future (i.e. 5G) C-RAN. The OSNR analysis and its relation with ESNR are also provided. Based on the above, we proposed the model to analyze the power consumption for the optical part of the RoF transmission system. Case studies were performed, where we demonstrated that a moderate modulation level (16-QAM or 64-QAM) consumes the lowest power but not lowest spectrum, while proposed RoF system can reach both lowest power and spectrum consumption by using highest candidate modulation formats (256-QAM). Meanwhile, proposed RoF system consumes considerably less power than current RoF system.

Chapter 5

Conclusions

5.1 Conclusions

In this thesis, we have

- developed an analytical model of end-to-end BER performance for OFDM-based elastic optical transmission systems by considering nonlinear effect of Mach-Zehnder modulator and optical amplified spontaneous emission (ASE) noise, where the effect of high PAPR in both electrical and optical domains is jointly considered. We investigated the performance improvement when a PAPR reduction mechanism is equipped. For this purpose, we developed PAPR reduction scheme to the scenario of optical transmission, namely simplified null shifting (SNS), which is featured as subject to less dependence on CSI and better performance. An optimization framework is formulated for determining laser transmit power, bandwidth, and modulation level of a single transmission request under a given transmission data rate, such that a least-cost transmission can be achieved in the considered elastic optical systems.

- investigated routing and bandwidth allocation (RBA) solution for energy saving corresponding to a set of connection requests upon network node pairs. The proposed RBA problem optimizes the consumed power at each node, where the logical topology corresponding to the static and dynamic traffic demand of each node pair, as well as the laser transmit power, modulation level, number of subcarriers, and routing path of each node pair, are jointly determined. By solving the formulated problem via a heuristic method based on simulated annealing (SA) and K shortest paths, the proposed strategy is demonstrated to achieve better performance than using a single modulation level with shortest path routing only. Further, we propose an iterative flipping (IF) method to solve the problem, which maintains better power saving performance than SA scheme while keeping very low computational complexity.

- introduced a novel adaptive radio-over-fiber (RoF) transmission system for next-generation C-RAN, where a 2×2 MIMO-OFDM baseband model for simulating the required ESNR of end-to-end RoF transmission system is developed by considering nonlinear distortion from both Mach-Zehnder modulator (MZM) and high power amplifier (HPA). We also proposed the model to analyze the power consumption for the optical part of RoF transmission system. By using 256-QAM, proposed RoF system can achieve both lowest power and lowest spectrum consumption. Proposed RoF system is also demonstrated to consume considerably less power than current RoF system.

5.2 Further Work

The following issues could be further investigated:

- In current BER analysis model, we assume that chromatic dispersion (CD) and polarization mode dispersion (PMD) can be completely removed in an ideal coherent detection of CO-OFDM system where the line-widths of the transmit/receive lasers are assumed to be zero, which can not be realized in lab by now. In future research, the degradation due to CD and line-width of laser for OFDM-based analog signal propagation is simulated by using software like Virtual Photonic Inc. (VPI). To model wireless systems integrating with optical systems, co-simulation between VPI and MATLAB is required. For example, OFDM transceiver model including symbol formation, serial/parallel conversion, IFFT/FFT, cyclic prefix addition/removal, and channel equalization is built in MATLAB. The following point-to-point RoF link is modeled in VPI to perform quantization, signal shaping and optical modulation of FDM multiplexed OFDM-RF channels. The error vector magnitude (EVM) of the received signal after transmission over optical fiber with different length can also be estimated in VPI.

- In current RoF research, we focus on energy efficiency. The network operational cost includes not only energy consumption, but also facility expenditure. Proposed RoF system with higher facility cost is designed for BS with high capacity per wavelength (DS rate more than 100 Gbps, up to 256-QAM) and large distribution range (up to 100 km). Since not all BSs would require such high capacity and large distribution range, proposed RoF system collaborating with current RoF system will be a solution for minimizing the C-RAN costs in terms of both energy and expenditure.

- Current version only investigates power consumption for optical part of the RoF system. Further involving power consumption of wireless facilities including HPAs and antennas, will also be in future research.

- In the C-RAN, a critical issue is how to adaptively allocate subcarriers under different modulation formats for different user with different service requests. By multiplexing available subchannels to individual users in both time and frequency domain, the multiple-access technique (OFDMA) based on OFDM technique allocates different subsets of OFDM subcarriers to different users. So, upcoming work extends current research of OFDM-RoF systems to adaptive OFDMA-RoF systems.

Bibliography

[1] W. Shieh and I. Djordjevic, *Orthogonal Frequency Division Multiplexing for Optical Communication*, Amsterdam, The Netherlands: Elsevier, pp. 38-39, 2010.

[2] J. Armstrong, "OFDM for Optical Communications," *Journal of Lightwave Technology*, vol. 27, no. 3, February 1, 2009.

[3] M. Jinno, H. Takara, B. Kozicki, Y. Tsukishima, Y. Sone, and S. Matsuoka, "Spectrum-efficient and scalable elastic optical path network: Architecture, benefits, and enabling technologies," *IEEE Communications Magazine*, vol. 47, no. 11, pp. 66-73, 2009.

[4] K. Christodoulopoulos, I. Tomkos, and E. A. Varvarigos, "Elastic Bandwidth Allocation in Flexible OFDM-Based Optical Networks," *Journal of Lightwave Technology*, vol. 29, no. 9, MAY 1, 2011.

[5] A. Klekamp, R. Dischler, and F. Buchali, "Limits of Spectral Efficiency and Transmission Reach of Optical-OFDM Superchannels for Adaptive Networks," *IEEE Photonics Technology Letters*, vol. 23, no. 20, pp. 1526-1528, Oct., 2011.

[6] J. E. Mitchell, "Integrated Wireless Backhaul Over Optical Access Networks," *Journal of Lightwave Technology*, vol. 32, no. 20, pp. 3373-3382, Oct. 15, 2014.

[7] A. Lometti, C. Colombo, S. Frigerio, and V. Sestito, "Network architectures for CPRI backhauling," in *14th International Conference on Transparent Optical Networks*, Coventry, England, 2012.

[8] Z. S. Jia, J. J. Yu, G. Ellinas, and G. K. Chang, "Key enabling technologies for optical-wireless networks: Optical millimeter-wave generation, wavelength reuse, and architecture," *Journal of Lightwave Technology*, vol. 25, no. 11, pp. 3452-3471, Nov. 2007.

[9] G. L. Stuber, *Principles of Mobile Communication*, 2nd ed.: Kluwer Academic Publishers, 2001.

[10] B. X. Chen and W. Shieh, "Closed-form expressions for nonlinear transmission performance of densely spaced coherent optial OFDM systems," *Opt. Express*, vol. 18, no. 18, 2010.

[11] C. R. Borkowski, F. Karinou, M. Angelou, V. Arlunno, D. Zibar, D. Klonidis, N. G. Gonzalez, A. Caballero, I. Tomkos, and I. T. Monroy, "Experimental Study on OSNR Requirements for Spectrum-Flexible Optical Networks," *J. Opt. Commun. Netw.*, vol. 4, no. 11, pp. B85-B96, Nov. 2012.

[12] T. Jiang and Y. Wu, "An Overview: Peak-to-Average Power Ratio Reduction Techniques for OFDM Signals," *IEEE Transactions on Broadcasting*, vol. 54, no. 2, pp. 257-268, June 2008.

[13] B. Goebel, S. Hellerbrand, N. Haufe, and N. Hanik, "PAPR reduction techniques for coherent optical OFDM transmission," in *Proc. ICTON 2009*, Jul. 2009.

[14] Y. Tang, K. P. Ho, and W. Shieh, "Coherent optical OFDMtransmitter design employing predistortion," *IEEE Photonics Technology Letters*, vol. 20, no. 11, pp. 954-956, Jun. 2008.

[15] Y. London and D. Sadot, "Nonlinear Effects Mitigation in Coherent Optical OFDM System in Presence of High Peak Power," *Journal of Lightwave Technology*, vol. 29, no. 21, pp. 3275-3281, Novenmber 1, 2011.

[16] R. S. Tucker, R. Parthiban, J. Baliga, K. Hinton, R. W. A. Ayre, and W. V. Sorin, "Evolution of WDM optical IP networks: A cost and energy perspective," *Journal of Lightwave Technology*, vol. 27, no. 3, pp. 243-252, Feb. 2009.

[17] J. Baliga, R. Ayre, K. Hinton, W. V. Sorin, and R. S. Tucker, "Energy consumption in optical IP networks," *Journal of Lightwave Technology*, vol. 27, no. 13, pp. 2391-2403, Jul. 2009.

[18] S. Aleksic, "Power consumption issues in future highperformance switches and routers," *IEEE International Conference on Transparent Optical Networks*, pp. 194-198, June 2008.

[19] B. Sedighi, H. Khodakarami, B. S. G. Pillai, and W. Shieh, "Power-Efficiency Considerations for Adaptive Long-Haul Optical Transceivers," *Journal of Optical Communications and Networking*, vol. 6, no. 12, pp. 1093-1103, Dec. 2014.

[20] G.-H. Gho and J. M. Kahn, "Rate-adaptive modulation and low-density parity-check coding for optical fiber transmission systems," *Journal of Optical Communications and Networking*, vol. 4, no. 10, pp. 760-768, Oct. 2012.

[21] B. T. Teipen, M. H. Eiselt, K. Grobe, and J. P. Elbers, "Adaptive data rates for flexible transceivers in optical networks," *Journal of Networks*, vol. 7, no. 5, pp. 776-782, May 2012.

[22] R. Tucker, "Green optical communicationsPart I: Energy limitations in transport," *Journal of Selected Topics in Quantum Electronics*, vol. 17, no. 2, pp. 245-260, Mar./Apr. 2011.

[23] R. Tucker, "Green optical communicationsPart II: Energy limitations in networks," *Journal of Selected Topics in Quantum Electronics*, vol. 17, no. 2, pp. 261-274, Mar./Apr. 2011.

[24] T. Okoshi and K. Kikuchi, *Coherent optical fiber communications*, Springer, 1988.

[25] M. G. Taylor, "Coherent detection method using DSP for demodulation of signal and subsequent equalization of propagation impairments," *IEEE Photonic Technology Letters*, vol. 16, no. 2, pp. 674-676, 2004.

[26] A. J. Lowery, "Fiber nonlinearity pre- and post-compensation for longhaul optical links using OFDM," *Optical Express*, vol. 15, no. 20, Oct. 2007.

[27] E. Ip, A. P. T. Lau,D. J. F. Barros, and J. M. Kahn, "Coherent detection in optical fiber systems," *Optical Express*, vol. 16, no. 2, pp. 753-791, Jan. 2008.

[28] G. P. Agrawal, *Fiber-Optic Communication Systems*, 3rd ed., Wiley, 2002.

[29] G. L. Li and P. K. L. Yu, "Optical intensity modulators for digital and analog applications," *Journal of Lightwave Technology*, vol. 21, no. 9, pp. 2010-2029, September, 2003.

[30] K.P. Ho, *Phase-modulated optical communication systems*, Springer, Ed., 2005.

[31] V. A. Bohara and S. H. Ting, "Theoretical analysis of OFDM signals in nonlinear polynomial models," in *Proceedings of the International Conference on Information, Communications and Signal Processing*, Singapore, Dec. 2007.

[32] H. Ochiai and H. Imai, "On the distribution of the peak-to-average power ratio in OFDM signals," *IEEE Transactions on Communications*, vol. 49, no. 2, pp. 282-289, Feb. 2001.

[33] K. Cho and D. Yoon, "On the general BER expression of one- and two-dimensional amplitude modulations," *IEEE Transactions on Communications*, vol. 50, no. 7, pp. 1074-1080, Jul. 2002.

[34] R. J. Essiambre, G. Kramer, P. J. Winzer, G. J. Foschini, and B. Goebel, "Capacity Limits of Optical Fiber Networks," *Journal of Lightwave Technology*, vol. 28, no. 4, Feb. 15, 2010.

[35] B. S. Pillai, B. Sedighi, K. Guan, N. P. Anthapadmanabhan, W. Shieh, K. J. Hinton, and R. S. Tucker, "End-to-End Energy Modeling and Analysis of Long-Haul Coherent Transmission Systems," *Journal of Lightwave Technology*, vol. 32, no. 18, pp. 3093-3111, Sep. 15, 2014.

[36] A. Gumaste and T. Antony, *DWDM Network Designs and Engineering Solutions*, Cisco Press, Dec. 2002.

[37] Vivek Alwayn, *Fiber-Optic Technologies*, Cisco Press, Apr. 2004.

[38] R. O'Neill and L. B. Lopes, "Envelope Variations and Spectral Splatter in Clipped Multicarrier Signals," *Proc. IEEE PIMRC '95* , Toronto, Canada, pp. 71-75, Sept. 1995.

[39] J. Armstrong, "Peak-to-Average Power Reduction for OFDM by Repeated Clipping and Frequency Domain Filtering," *Electronics Letters* , vol. 38, no. 8, pp. 246-247, Feb. 2002.

[40] X. Li and L. J. Cimini, "Effect of Clipping and Filtering on the Performance of OFDM," *IEEE Communication Letter*, vol. 2, no. 5, May 1998, pp. 131-133.

[41] R. W. Bauml, R. F. H. Fisher, and J. B. Huber, "Reducing the Peak-to-Average Power Ratio of Multicarrier Modulation by Selected Mapping," *Electronics Letters*, vol. 32, no. 22, Oct. 1996, pp. 2056-2057.

[42] S. H. Muller and J. B. Huber, "A Comparison of Peak Power Reduction Schemes for OFDM," *Proc. IEEE GLOBECOM '97*, Phoenix, AZ, Nov. 1997, pp. 1-5.

[43] S. H. Muller and J. B. Huber, "OFDM with Reduced Peak-to-Average Power Ratio by Optimum Combination of Partial Transmit Sequences," *Electronics Letters*, vol. 33, no. 5, Feb. 1997, pp. 368-369.

[44] S. H. Muller and J. B. Huber, "A Novel Peak Power Reduction Scheme for OFDM," *Proc. IEEE PIMRC '97*, Helsinki, Finland, Sept. 1997, pp. 1090-1094.

[45] G. R. Hill, M. Faulkner and J. Singh, "Reducing the Peak-to-Average Power Ratio in OFDM by Cyclically Shifting Partial Transmit Sequences," *Electronics Letters*, vol. 36, no. 6, Mar. 2000, pp. 560-561.

[46] P. Van Eetvelt, G. Wade and M. Tomlinson, "Peak to Average Power Reduction for OFDM Schemes by Selective Scrambling," *Electronics Letters*, vol. 32, no. 21, Oct. 1996, pp. 1963-1964.

[47] A. D. S. Jayalath and C. Tellambura, "Reducing the Peakto- Average Power Ratio of Orthogonal Frequency Division Multiplexing Signal through Bit or Symbol Interleaving," *Electronics Letters*, vol. 36, no. 13, June 2000, pp. 1161-1163.

[48] J. Tellado, *Peak to Average Power Reduction for Multicarrier Modulation*, Ph.D dissertation, Stanford University, 2000.

[49] B. S. Krongold and D. L. Jones, "PAR Reduction in OFDM via Active Constellation Extension," *IEEE Transaction on Broadcasting* , vol. 49, no. 3, Sept. 2003, pp. 258-268.

[50] A.E. Jones, T.A. Wilkinson and S.K. Barton, "Block Coding Scheme for Reduction of Peak to Mean Envelope Power Ratio of Multicarrier Transmission Scheme," *Electronics Letters*, vol. 30, no 22, pp. 2098-2099, Dec 1994.

[51] M. Golay, "Complementary Series," *IEEE Transaction on Information Theory*, vol. 7, no. 2, Apr. 1961, pp. 82-87.

[52] A. D. S. Jayalath, C. Tellambura and H. Wu , "Reduced complexity PTS and new phase sequences for SLM to reduce PAP of an OFDM signal ," *IEEE Vehicular Technology Conference*, VTC 2000, pp. 1914-1917, May 2000.

[53] C. Tellambura, "Phase Optimisation Criterion for Reducing Peak-to-Average Power Ratio in OFDM," *Electronics Letters*, vol. 34, no. 2, pp. 169-170, January 22, 1998.

[54] T. Jiang, W.D. Xiang, P.C. Richardson, J.H. Guo and G.X. Zhu, "PAPR Reduction of OFDM Signals Using Partial Transmit Sequences With Low Computational Complexity," *IEEE Transactions on Broadcasting*, vol. 53, no. 3, pp. 719-724, Sep. 2007.

[55] N. N. Feng, S. Liao, D. Feng, et al., "High Speed Silicon Carrier-Depletion Mach-Zehnder Modulator with 1.4 V-cm V_{π}L," *Opt. Express*, vol. 18, no. 8, pp. 7994-7999, 2010.

[56] A. Nag, T. Wang, and B. Mukherjee, "Robust Design of Spectrum-Efficient Green Optical Backbone Networks," *Journal of Lightwave Technology*, vol. 31, no. 7, April 1, 2013.

[57] K. Christodoulopoulos, I. Tomkos, and E. A. Varvarigos, "Elastic Bandwidth Allocation in Flexible OFDM-Based Optical Networks," *Journal of Lightwave Technology*, vol. 29, no. 9, pp. 1354-1366, May 1, 2011.

[58] S. Kirkpatrick, C. D. Gelatt and M. P. Vecchi, "Optimization by simulated annealing," *Science*, vol. 220, no. 4598, pp. 671-680, May 1983.

[59] C. Tsallis, "Possible generalization of boltzmann-gibbs statistics," *Journal of Statistical Physics*, vol. 52, no. 1-2, pp. 479-487, July 1988.

[60] J. Lopez Vizcaino, Y. Ye, V. Lopez, F. Jimenez, R. Duque, F. Musumeci, A. Pattavina, and P. Krummrich, "Differentiated Quality of Protection to Improve Energy Efficiency of Survivable Optical Transport Networks," *Optical Fiber Communication Conference (OFC) 2013*, paper OM3A, March 2013.

[61] H. Khodakarami, B.S.G. Pillai, B. Sedighi, and W. Shieh, "Flexible Optical Networks: An Energy Efficiency Perspective," *Journal of Lightwave Technology*, vol. 32, no. 21, pp. 3356-3367, Nov. 1, 2014.

[62] P. Chowdhury, M. Tornatore, A. Nag, E. Ip, T. Wang, and B. Mukherjee, "On the design of energy-efcient Mixed-Line-Rate (MLR) optical networks," *Journal of Lightwave Technology*, vol. 30, no. 1, pp. 130C139, Jan. 2012.

[63] K. Zhu and B. Mukherjee, "Traffic grooming in an optical WDM mesh network," *IEEE Journal on Selected Areas in Communications*, vol. 20, no. 1, pp. 122-133, Jan., 2002.

[64] B. Ramamurthy and B. Mukherjee, "Wavelength Conversion in WDM Networking," *IEEE Journal on Selected Areas in Communications*, vol. 16, no. 7, pp. 1061-1073, Sep., 1998.

[65] S. Aleksic, "Analysis of power consumption in future high-capacity network nodes," *IEEE/OSA Journal of Optical Communications and Networking*, vol. 1, no. 3, pp. 245-258, Aug., 2009.

[66] Jin Y. Yen, "Finding the K Shortest Loopless Paths in a Network," *Management Science,*, vol. 17, no. 11, pp. 712-716, Jul. 1971.

[67] D. J. F. Barros, *Orthogonal Frequency-Division Multiplexing for Optical Communications*, Phd Thesis, Stanford University, September 2011.

[68] J. L. Vizcaino, P. Soto, Y. Ye, F. Jimenez, and P. Krummrich, "Energy-efficient and Low Blocking Probability Differentiated Quality of Protection Scheme for Dynamic Elastic Optical Networks," *IEEE International Conference on Software, Telecommunications and Computer Networks (Softcom)*, September 2013.

[69] D. Bojic, E. Sasaki, N. Cvijetic, W. Ting, J. Kuno, J. Lessmann, S. Schmid, H. Ishii, and S. Nakamura, "Advanced wireless and optical technologies for small-cell mobile backhaul with dynamic software defined management," *IEEE Communications Magazine*, vol. 51, no.9, pp. 86-93, Sep. 2013.

[70] B. Haberland, F. Derakhshan, H. Grob-Lipski, R. Klostsche, W. Rhem, P. Schefczik, and M. Soeliner, "Radio base station in the cloud," *Bell Labs Technical Journal*, vol. 18, no. 1, pp. 129-152, 2013.

[71] C. T. Lin, A. Ng'oma, W.-Y. Lee, C. C. Wei, C-Y. Wang, T.-H. Lu, J. Chen, W. Jiang, and C.-H. Ho, "22 MIMO radio-over-fiber system at 60 GHz employing frequency domain equalization," *Optical Express*, vol. 20, no. 1, pp. 562-567, 2012.

[72] D. Wake, S. Pato, J. Pedro, E. Lopez, N. Gomes, and P. Monteiro, "A comparison of remote radio head optical transmission technologies for next generation wireless

systems," in *Proceedings of IEEE Photonic Society Annual Meeting*, pp. 442-443, Oct. 2009.

[73] V. Jungnickel, K. Manolakis, S. Jaeckel, M. Lossow, P. Farkas, M. Schlosser, and V. Braun, "Backhaul requirements for inter-site cooperation in heterogeneous LTE-advanced networks," in *Proceedings of IEEE International Workshop on Optical-wireless Integrated Technology for Systems and Networks*, pp. 905-910, Jun. 2013.

[74] *Common Public Radio Interface: Interface Specification v4.1, 2009* [Online].

[75] D. Wake, A. Nkansah, and N. J. Gomes, "Radio over fiber link design for next generation wireless systems," *Journal of Lightwave Technology*, vol. 28, no. 16, pp. 2456-2464, Aug. 2010.

[76] M. Milosavljevic, M. P. Thakur, P. Kourtessis, J. E. Mitchell, and J. M. Senior, "Demonstration of Wireless Backhauling Over Long-Reach PONs," *Journal of Lightwave Technology*, vol. 30, no. 5, pp. 811-817, Mar. 2012.

[77] G. L. Stuber, J. R. Barry, S. W. McLaughlin, L. Ye, M. A. Ingram, and T. G. Pratt, "Broadband MIMO-OFDM Wireless Communications," *IEEE Proceedings*, vol. 92, no. 2, pp. 271-294, Feb. 2004.

[78] G.L. Stuber, J.R. Barry, S.W. McLaughlin, Y. Li, M.A. Ingram, and T.G. Pratt, "Broadband MIMO-OFDM wireless communications," *Proceedings of the IEEE*, vol. 92, no. 2, pp. 271-294, Feb. 2004.

[79] H. Lee, B. Lee, and I. Lee, "Iterative detection and decoding with an improved V-BLAST for MIMO-OFDM systems," *IEEE Journal on Selected Areas in Communications*, vol. 24, no. 3, pp. 504-513, Mar. 2006.

[80] V. Tarokh, H. Jafarkhani, and A. R. Calderbank, "SpaceCtime block codes from orthogonal designs," *IEEE Transactions on Information Theory*, vol. 45, no. 5, pp. 1456-1467, July 1999.

[81] C. W. Chow, C. H. Yeh, C. H. Wang, F. Y. Shih, Y. M. Lin, and S. Chi, "Demonstration of High Spectral Efficient OFDM-QAM Long Reach Passive Optical Network," in *Proceedings of European Conference on Optical Communications (ECOC)*, vol. 4, pp. 125-126, Brussels, Belgium, Sep. 2008.

[82] C. W. Chow, C. H. Yeh, C. H. Wang, F. Y. Shih, Y. M. Lin, and S. Chi, "Rayleigh Backscattering Performance of OFDM-QAM in Carrier Distributed Passive Optical Networks," *IEEE Photonics Technology Letters*, vol. 20, pp. 1848-1850, Nov. 2008.

[83] P. J. Winzer and G. J. Foschini, "MIMO Capacities and Outage Probabilities in Spatially Multiplexed Optical Transport Systems," *Optical Express*, vol. 19, no. 17, pp. 16680-16696, 2011.

[84] P. P. Mitra and J. B. Stark, "Nonlinear limits to the information capacity of optical fiber communications," *Nature*, vol. 411, pp. 1027-1030, 2001.

[85] C. H. Ho, W. J. Jiang, R. Sambaraju et al., "Performance Evaluation of a 60 GHz Radio-over-Fiber System Employing MIMO and OFDM Modulation," *IEEE Journal on Selected Areas in Communications/Supplement-Part 2*, vol. 31, no. 12, pp. 780-787, Dec. 2013.

[86] H. Takahashi, A. A. Amin, S. L. Jansen, I. Morita, and H. Tanaka, "Highly Spectrally Efficient DWDM Transmission at 7.0 b/s/Hz Using 8x65.1-Gb/s Coherent PDM-OFDM," *Journal of Lightwave Technology*, vol. 28, no. 4, pp. 406-414, Feb. 15, 2010.

[87] S. L. Jansen, I. Morita, T. C. W. Schenk, and H. Tanaka, "121.9-Gb/s PDM-OFDM TransmissionWith 2-b/s/Hz Spectral Efficiency Over 1000 km of SSMF," *Journal of Lightwave Technology*, vol. 27, no. 3, pp. 177-188, Feb. 1, 2009.

[88] R. Ryf, S. Randel, A. H. Gnauck et al., "Mode-division multiplexing over 96 km of few-mode fiber using coherent 6x6 MIMO processing," *Journal of Lightwave Technology*, vol. 30, no. 4, pp. 521-531, Feb. 15, 2012.

[89] M. Fabbri and P. Faccin, "Radio over fiber technologies and systems: New opportunities," in *Proceedings of International Conference on Transparent Optical Networks*, vol. 3, pp. 230-233, Jul. 2007.

[90] "C-RAN: The road towards green ran," *China Mobile Research Insititute*, October 2011.

[91] S. Dahlfort and K. Laraqui, "Exploring the antenna lambda connection," in *Optical Fiber Communication Conference Exposition*, Los Angeles, USA, 2012.

[92] F. Diehm, J. Holfeld, G. Fettweis, N. J. Gomes, D. Wake, A. Nkansah, and E. L. Casariego, "The FUTON prototype: Broadband communication through coordinated multi-point using a novel integrated optical/wireless architecture," in *Proceedings of IEEE GLOBECOM Workshops*, pp. 757-762, 2010.

[93] N. Ghazisaidi, M. Maier, and C. Assi, "Fiber-wireless (FiWi) access networks: Asurvey," *IEEE Communications Magazine*, vol. 47, no. 2, pp. 160-167, Feb. 2009.

[94] K. Kanonakis, I. Tomkos, T. Pfeiffer, J. Prat, and P. Kourtessis, "ACCORDANCE: A novel OFDMA-PON paradigm for ultra-high capacity converged wireline-wireless access networks," in *12th International Conference on Transparent Optical Networks (ICTON)*, 2010.

[95] S. Litsyn, *Peak Power Control in Multicarrier Communications*, Cambridge, U.K.: Cambridge University Press, 2007.

[96] Y. Tang, W. Shieh, X. Yi, and R. Evans, "Optimum design for RF-to-optical up-converter in coherent optical OFDM systems," *IEEE Photonic Technology Letter*, vol. 19, no. 7, pp. 483-485, April 1, 2007.

[97] J. I. Kani, F. Bourgart, A. Cui, A. Rafel, M. Campbell, R. Davey, and S. Rodrigues, "Next-generation PON-Part I: Technology roadmap and general requirements," *IEEE Communication Magazine*, vol. 47, no. 11, pp. 43-49, Nov. 2009.

[98] *Gigabit-Capable Passive Optical Networks (GPON): Physical Media Dependent (PMD) Layer Specification*, ITU-T G.984.2, 2003.

[99] D. Lavery, E. Torrengo, and S. J. Savory, "Bidirectional 10 Gbit/s long-reach WDM-PON using digital coherent receivers," in *Optical Fiber Communication Conference and Exposition (OFC/NFOEC)*, 2011.

[100] Calvin C. K. Chan, *Optical Performance Monitoring Advanced Techniques for Next-Generation Photonic Networks*, Elsevier, 2010.

[101] S. L. Jansen, I. Morita, T. C. W. Schenk, and H. Tanaka, "Long-haul transmission of 16×52.5-Gb/s polarization division multiplexed OFDM enabled by MIMO processing," *OSA Journal of Optical Networking*, vol. 7, pp. 173-182, Feb. 2008.

[102] "Optilab DFB-1550-PM-40 DFB laser," *http://www.optilab.com.*